# Delft University of Technology

Master Thesis

# Ammonium recovery with energy consumption using ammonium sulfate salt with varied current densities and BPMED cell arrangements

by

Hiteshree Mithaiwala
Student no.: 5564131

Graduation committee:
Prof. Dr. Ir. Henri Spanjers
Prof. Dr. Ir. Jules van Lier
Ir. Dhavissen Narayen
Prof. Dr. Ir. David Vermaas

## Abstract

One of the methods to recover ammonium is Bipolar Membrane Electrodialysis (BPMED), a chemical-free technology that enables recovery and purification of the corresponding acid and base by the application of electrical energy. This thesis aims to evaluate five different BPMED cell configurations using the ammonium sulfate ($(NH_4)_2SO_4$) salt. Experiments are based on evaluating operational parameters including flow rate, feed volume, base volume, and current density to achieve the maximum ammonium recovery using ammonium sulfate salt with efficient electrochemical energy consumption. Additionally, the optimum experiment was carried out with the best results of operational parameters to understand the impact on ammonium recovery and electrochemical energy consumption. However, other operational parameters including the impact of varied salt concentration in the feed and base compartment, the varied ERS concentration, and volume were not tested in this research and need to be studied further.

Stimulated wastewater with feed conc. 50 g ammonium sulfate salt in 1 L demineralized water, with acid and base conc. etc., and with a temperature of 25 ± 0.5 °C was treated with BPMED. The influence of current density, flow rate, base volume, feed volume, and different BPMED Cell configurations was researched independently in experiments of 120 minutes, after which ammonium recovery, $NH_4^+$ current efficiency, and electrochemical energy consumption were assessed.

From the experiments with increasing current densities (CD), ammonium recovery in the base increased, and thus, less back-diffusion from the base to the acid compartment was observed. The highest ammonium recovery in the base was observed at the highest 100% current density. With electrochemical energy consumption, there was an increasing trend with increasing current density. The lowest average energy consumption was noted at 24.2 ± 0.4 MJ/kg-$NH_4^+$ for 25% current density. Average $NH_4^+$ current efficiency decreased from 54.8% to 26.4 % when the current density decreased from 100% to 25%.

For the second research question, increasing flow rates showed a fall in the ammonium recovery in the base but a rise in electrochemical energy consumption. The highest average ammonium recovery in the base was observed at a flow rate of 7.6 L/h (1 cm/s, crossflow velocity) of 4.8 g, and the lowest average energy consumption was observed at a 7.6 L/h flow rate with a value of 39.5 ± 1.1 MJ/kg- $NH_4^+$. However, it was found that very low flow rates caused concentration polarization on the membranes, and very high flow rates caused ions to move out of the stack too soon, which resulted in increased back-diffusion in the acid compartment. The highest average $NH_4^+$ current efficiency was observed at a 7.6 L/h flow rate with a value of 27.8%.

The third research question focused on investigating various base volumes, which showed that with increasing base volumes, the ammonium recovery increased (causing less back-diffusion of ammonium in the acid) and the electrochemical energy consumption decreased. The highest

average mass of ammonium in the base at the end of the experiment was 6.8 g at 3 L base volume with the lowest average energy consumption of 29.8 ± 1.3 MJ/kg-$NH_4^+$. The lowest average ammonium current efficiency of 26.6 % was observed with the lowest base volume of 0.5 L, whereas the highest average $NH_4^+$ current efficiency of 39.6% was observed with a base volume of 3 L.

Regarding different BPMED cell configurations, five different BPMED setups namely, a two-compartment cation, a two-compartment anion, a three-compartment, a multi-chamber cation, and a multi-chamber anion cell were assessed. Three-compartment cell and cation configurations gave the highest ammonium recovery. The rise in average $NH_4^+$ mass recovery was observed from 3.7 g in a two-compartment cation cell to 4.2 g in a multi-chamber cation cell. Three-compartment required the highest average energy to transport ammonium in the base i.e., 43.1 ± 0.3 MJ/kg-$NH_4^+$, whereas the lowest energy consumption was observed with anion configurations.

With increasing feed volumes, it was observed that ammonium recovery increased leading to a decreased energy consumption because of larger concentration gradients between compartments. The highest average ammonium mass in the base was observed to be 6.8 g with the highest feed volume of 3 L with the lowest average energy consumption of 23.6 ± 1.5 MJ/kg-$NH_4^+$. The highest average $NH_4^+$ current efficiency i.e., 39.6% and 39.4% was observed in the highest feed volumes of 2 L and 3 L.

Lastly, for the optimum experiment, the best operational parameters were chosen considering both the ammonium recovery in the base and the electrochemical energy consumption. The operational parameters were a 75% CD (i.e., 0.96 A), a 7.6 L/h flow rate, a 3 L base volume, a 2 L feed volume, and a multi-chamber cation cell. It was observed that the experiment recovered the highest average ammonium mass of 8 g in the base with an electrochemical energy consumption of 12.7 ± 0.6 MJ/kg-$NH_4^+$. However, all the operational parameters were tested on a three-compartment BPMED cell, the impact of those parameters including flow rate, feed volume, base volume, and salt concentration on other configurations, especially multi-chamber cell configurations are yet to be investigated, and need further studies on understanding its impact on ammonium and sulfate recovery.

To address the gap between lab-scale data and large-scale execution, thorough modeling and simulations, as well as pilot-scale investigations, are important. When scaling up from the lab scale, the membrane area and operation time become larger and thus, it becomes more essential to test the operating parameters to balance energy consumption, scaling mitigation, and removal/recovery efficiency.

## Acknowledgments

I would like to express my gratitude to all the people without whom this thesis journey wouldn't have been so fun and joyful.

Firstly, I would like to thank my daily supervisor, Ir. Dhavissen Narayen, who has been the biggest critic of my thesis journey and then, at the same time motivates me to always think out of the box. The topic wouldn't have been more interesting without his continuous comments and then, also hinting me on how to solve those problems. A major thanks to you for always being there whether you were on campus or on-call; whenever there were problems with multimeters or power box, you were always the one whom I called and you provided me with back-ups. Thanks for answering my questions and also, for being patient with me whenever the experiments didn't work out.

I would also like to thank my chief supervisor, Dr. Ir. Henri Spanjers for his constant guidance throughout my thesis. I would also like to thank you for providing me with important feedback for my thesis writing, which helped me learn a lot and improved my writing skills. Thanks to you for keeping a constant check on my thesis work, which keeps me in check and helps me maintain my progress and schedule. I would also like to thank Prof. Dr. Ir. Jules van Lier and Dr. Ir. David Vermaas for always guiding me when I felt stuck on some results, especially during my mid-term meeting.

Besides that, I would also like to thank Armand from the Waterlab community for always providing me with technical support, helping me in solving Ion Chromatography issues, and providing me an exception for weekend access when I needed it. I would also like to express my gratitude to Bokure, and Bright from the Waterlab community who always provided me in urgency with different multimeters or cables or any other lab supplies.

Apart from this, my fellow mates, seniors, and juniors were constantly making my lab journey fun by always providing me with suggestions and snacks, and also staying late with me in the lab. Thank you Iosif and Gladys for always providing me with suggestions and also, for helping me discuss weird results and how it can be further optimized. It helped me a lot to come up with a good discussion. I would also like to thank Akhilesh, Tejas, and Ragashree for listening to me whenever I felt frustrated and then, taking me out to distract from the problems.

My hearty gratitude goes to my family and friends from India who even though stayed miles away from me yet supported me regardless of day or night. I would like to thank my mom, dad, and Khushi for always inspiring me to go on and never give up. Thank you for always loving me, inspiring me, and having faith in me. Of course, my thanks also go to friends like family, Rajvi, Aneri, and Parth for always being there and cheering me.

Last but not least, I would also like to say my special thanks to Yash Bhavsar, and his family, who were always there with me through thick and thin. Thank you, Yash, for always sharing a smile, keeping a cool mind, and motivating me to work even harder the next day.

# Contents

# List of Figures

# List of Tables

# 1. Introduction

## 1.1 Ammonia recovery from residual waters:

Many developed countries such as The Netherlands, are now seriously concerned about ammonia nitrogen pollution, and there is a significant demand for efficient ammonia nitrogen recovery methods. In previous times, ammonium in wastewater was simply seen as a pollutant that needed to be removed by turning it into $N_2$ via biological processes (such as nitrification-denitrification or anammox)(D. Yang et al., 2023). However, since ammonium is a crucial nutrient for the cultivation and growth of vegetation, ammonium-enriched wastewater (such as domestic wastewater, and industrial ammonium rich-effluent) can be viewed as a valuable resource for producing ammonium-based fertilizer from a circular economy and sustainable development perspective (Cruz et al., 2019; Xiang et al., 2020; D. Yang et al., 2023; Ye et al., 2018).

It is essential to have a reliable supply of ammonia and an effective ammonium removal system. Due to the considerable energy and cost requirements of traditional ammonium removal technologies, ammonium recovery in wastewater treatment appears to be more valuable than ammonia removal(Foley et al., 2010; Ledezma et al., 2015; Ye et al., 2018). In addition, ammonium recovery can improve resource management and serve as a supplement to the manufacture of fertilizer(Ye et al., 2018). Ammonium recovery has been discussed in some studies on wastewater treatment(Barbera et al., 2018; J. Huang et al., 2018; Iskander et al., 2016; Ye et al., 2018). Thus, it becomes important to comprehend the methods of ammonia recovery from residual water as it is used in subsequent applications of recovered ammonia in large-scale industries(Ye et al., 2018). There are major industrial ammonia recovery technologies that are widely used, one being ammonia stripping and scrubbing (Bousek et al., 2016) with the disadvantage that it needs chemicals to treat ammonia rich-effluents; and the other being membrane concentration i.e., electrodialysis (H. Huang et al., 2014; Sotres et al., 2015; Xie et al., 2016; T. Yan et al., 2018), which is energy-efficient technology and does not involve the use of chemicals.

## 1.2 Membrane technology:

The most popular chemical-free membrane technologies to recover ammonium in today's life are electrodialysis and then, bipolar membrane electrodialysis (Ye et al., 2018).

In the ED process, cation and anion exchange membranes were used. Cations such as ammonium ions diffuse through cation membranes toward the cathode to move to the base compartment and vice versa for anions (Ye et al., 2018).

**Bipolar Membrane Electrodialysis:**

Membrane water-dissociation technology is a process that uses bipolar membranes for converting soluble salts to their corresponding acids and bases (Pourcelly, 2002). Bipolar membrane electrodialysis (BPMED) is an alternate method of electrodialysis because it

generates $H^+$ and $OH^-$ ions. This can be used to manufacture the corresponding acid and base from salts without the production of oxygen and hydrogen gasses.

The application of the BPMED cell determines how the bipolar membrane electrodialysis method was configured (Franken, 2000; Mani, 1991; Pourcelly, 2002). The method is currently used to produce bases and acids from a concentrated salt stream, such as $Na_2SO_4$, and to recover concentrated acids, such as $H_2SO_4$ and NaOH. Bipolar membranes have applications in chemical processing in addition to environmental control (Franken, 2000; Mani, 1991; Pourcelly, 2002).

In theory, treating an ammonium sulfate waste stream from the stripper/scrubber process using BPMED can remove $NH_4^+$ from industrial reject water sustainably and produce acid that can be used again in the stripper/scrubber system. When used in conjunction with BPMED, the stripper/scrubber process can effectively remove ammonium sulfate $(NH_4)_2SO_4$ from industrial reject waters, thereby yielding long-term financial benefits.

## 1.3 NoChemNAR Project:

From the flowchart below (fig. 1), it can be seen that this process works like a cycle. Here, the stripping and scrubbing column uses sulfuric acid which is in turn an effluent from BPMED along with ammonia water. To use ammonium salts like ammonium sulfate as an influent in the BPMED technology, is an effluent of stripping/scrubbing process. This combination of technologies prevents the addition of external or extra chemicals and enables the removal of ammonium salts from municipal and industrial wastewater, leading to the formation of a valuable ammonium-rich stream.

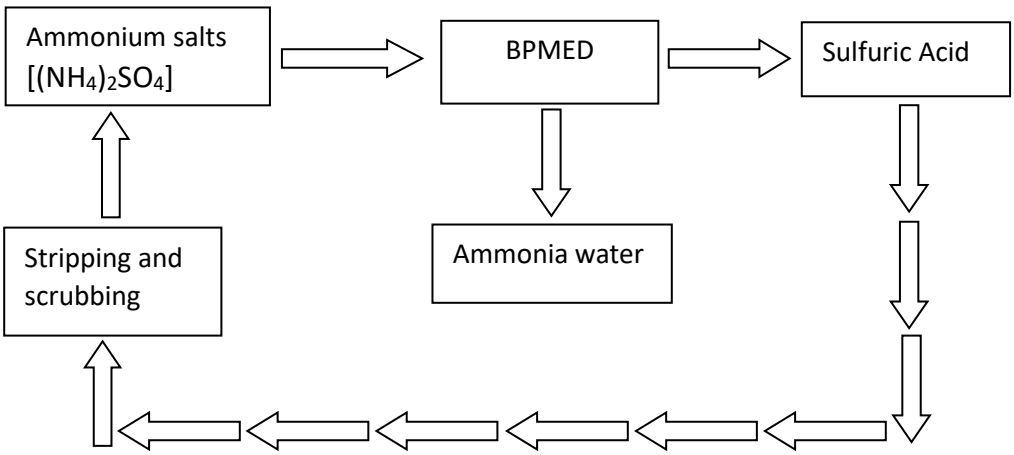


*Figure 1 The cyclic process between ammonia stripping-scrubbing and BPMED i.e., the influent for stripping-scrubbing comes out from BPMED and the influent for BPMED comes out from the stripping-scrubbing process.*

## 1.4 Knowledge gaps:

### 1.4.1 Current density:

Previous study by (Ali et al., 2004), it was known that increased current density leads to increased ammonium recovery efficiency and a shorter experimental time (section 2.4). However, previous studies by (Ali et al., 2004; D. Yang et al., 2023) focused on changing the current and keeping the time constant. In this study, the number of coulombs applied for each experiment was kept constant, thus, resulting in a shorter experimental time, which might result in higher ammonium recovery than the mass of ammonium recovered in the base obtained in previous studies (Ali et al., 2004; D. Yang et al., 2023). Therefore, it would be interesting to research ammonium recovery, energy consumption, and ammonium diffusion with different current densities while keeping the coulombic efficiency for each experiment the same.

### 1.4.2 Flow rate:

There were quite a few studies (H. Guo et al., 2021; Lee et al., 2006) on flow rate has already been done on BPMED and one study by (De Jaegher et al., 2020) where 2 to 3.5 cm/s crossflow velocities were optimized. Here, the flow rate of the pump is calculated based on the crossflow velocity of the compartment, c/s area of spacers, thickness of spacer, void fraction, and no. of cell triplicates in a three-compartment stack. Note that an increased flow rate may also increase Limiting Current Density, which can eventually result in decreased ammonia recovery efficiency (Lee et al., 2006). However, there was no comprehensive research done on the entire range of flow rates to know the effect of flow rate on ammonium recovery and energy consumption. Therefore, efficient ammonium recovery and energy consumption using ammonium sulfate salt with distinct flow rates (section 4.2) were investigated in this research.

### 1.4.3 Base volume:

Most of the studies focused on evaluating feed volume to get higher efficiency and recovery (as known from sections 2.6 and 1.4.5). However, the effect of varying base volume on the ammonium recovered in the base has yet to be investigated. Thus, this study involves varying base volumes to see the effect of ammonium recovery concerning energy consumption on BPMED.

### 1.4.4 Cell arrangement configurations:

Very few studies (Mani, 1991; Pourcelly, 2002) have been done where different cell configurations were investigated. In a study by Pourcelly, 2002, it was discussed that while working with organic acids or bases from the equivalent salts that exhibit poor conductivity, a two-compartment cation cell (for acidification) and a two-compartment anion cell (for base) should be used. To treat concentrated salt solutions to produce their respective acid and base, a three-compartment cell was recommended (Pourcelly, 2002). When a larger acid-to-base ratio must be achieved given the product's salt level, a multi-chamber configuration was required where the effluent from the chamber between two cation membranes or two anion membranes goes to their dedicated chamber for efficient transport of cations/ anions

(Pourcelly, 2002). However, there were no significant research studies where all configurations were measured on the same conditions and compared based on energy consumption and ammonium recovered in the base. Thus, it would be interesting to investigate all the different BPMED cell configurations to achieve efficient ammonium recovery along with ammonium back-diffusion and energy consumption.

### 1.4.5 Feed Volume:

Li et al., 2016 focused on the hydrochloric acid efficiency by comparing the effect of varied diluate to acid/base volume ratios from simulated ammonium chloride wastewater. A recent study by Yang et al., 2023 focused on the ammonium concentration efficiency by evaluating diluate to concentrate ratios in the electrodialysis. However, the impact and direct link of feed volume on recovery with the diffusion was missing in the previous research. In this study, the effect of varying feed volumes on BPMED for efficient ammonium recovery along with energy consumption was evaluated.

## 1.5 Research approach:

Considering Section 1.4 Knowledge gaps, the research involves different operational parameters that can affect ammonium recovery in the base with the impact on energy consumption of BPMED. Therefore, the main objective of the research is to test parameters including varied flow rates, feed and base volumes, BPMED cell configurations, and current density to understand its impact on the ammonium recovery in the base with the energy consumption.

**Main research question:**

"What is the effect of operational parameters on the overall ammonium recovery in the base and energy consumption of BPMED?"

**Sub-research questions:**

1. What is the effect of varying current densities on ammonium recovery and energy consumption?
2. What is the effect of varying flow rates on ammonium recovery and energy consumption?
3. What is the effect of varying base volumes on ammonium recovery and energy consumption?
4. Which cell arrangement among the five BPMED configurations gives efficient ammonium recovery, purity of ammonium in the base, and energy consumption?
5. What is the effect of varying feed volumes of the BPMED stack on the $NH_4^+$ recovery and energy consumption?

**Optimum Experiment:** What is the effect of the optimum experiment on ammonium recovery in the base and electrochemical energy consumption?

# 2. Literature review

## 2.1 Ammonia stripping and scrubbing:

Ammonium recovery through the stripping adsorption process is mainly attributed to the fact that at high reaction temperatures and/or pH, the ammonium can be converted to volatile ammonia (Ye et al., 2018)(EL-Bourawi et al., 2007). Shifting equilibrium toward the gaseous phase and then removing ammonia from the solution is a way to recover ammonium from wastewater (Bousek et al., 2016). Typically, the stripping gas enters from the bottom. In a counter-current system, ammonia is thus transported from the liquid to the gaseous phase (Bousek et al., 2016).

In this case, the scrubber works in a way that stripped ammonia can be aided by a sulfuric acid solution to create ammonium salts like ammonium sulfate [$(NH_4)_2SO_4$] by adsorbing by acid solutions as shown in Fig. 2. As an alternative solution, it can be harvested as an ammonia-rich solution in liquid ammonia (Ye et al., 2018). Also, it was observed in a study by Wu & Vaneeckhaute, 2022) that more than 90% of ammonium nitrogen was recovered through ammonium stripping from wastewater.

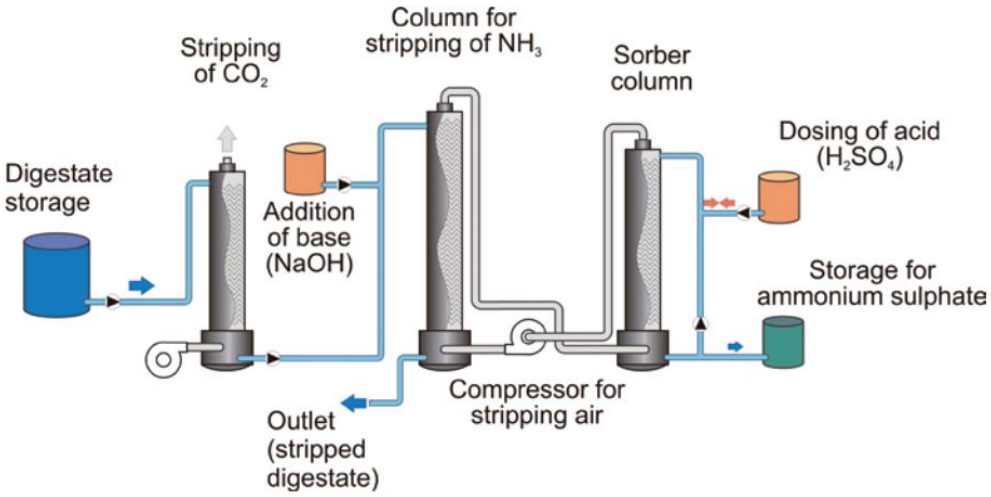


*Figure 2 Ammonia air stripping including CO2 removal and ammonia recovery by sulfuric acid scrubbers* (Drosg et al., 2020)

When compared to less concentrated streams, ionic strength was higher in high-concentration waste streams like scrubbing effluents, which raises the ammoniacal nitrogen pH value (van Linden et al., 2020). For the same quantity of ammonia recovery, this requires introducing more chemicals to streams with higher concentrations to raise the pH to pHa (van Linden et al., 2020).

## 2.2 Bipolar membrane electrodialysis:

Being a new type of electrodialysis technology, BPMED has received intensive research attention due to its high efficiency in producing acid and base from the neutral salt under the direct electric field, in which the bipolar membrane with the interface layer can split water into $H^+$ and $OH^-$ ions under the direct electric field (Mafé et al., 1998). Salt, for example, ammonium

sulfate was pumped into the space between the cation and anion-selective membranes (Fig. 3). The cations ($NH_4^+$) and anions ($SO_4^-$) migrate through the monopolar membranes and interact with the hydroxide and hydrogen ions produced at the bipolar membrane to form the base and acid when an electrical potential was applied across the electrodes (Mani, 1991).

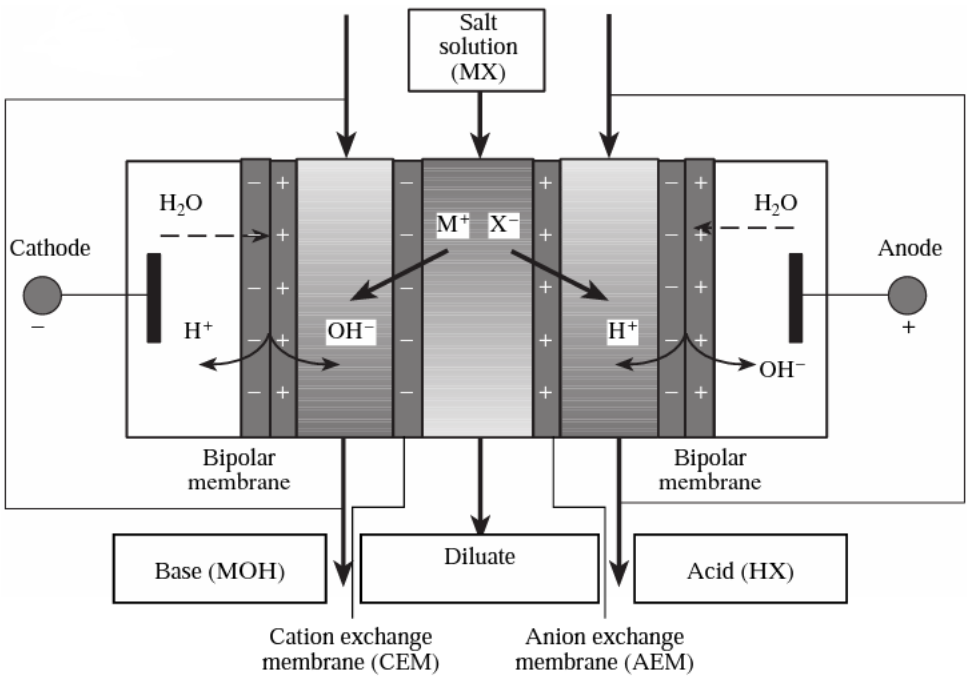


*Figure 3 The three-compartment BPMED cell configuration* (Pourcelly, 2002)

There are different cell arrangements in electrodialysis suitable for appropriate solutions. The main five cell arrangements are: Two-compartment cation cell, Two-compartment anion cell, Three-compartment cell, multi-chamber cation cell, and multi-chamber anion cell (Mani, 1991).

### 2.2.1 Two-compartment cation cell:

Previously, the most popular configuration was a two-compartment design with a cation-exchange membrane since it is less complicated and more energy-efficient than a three-compartment design (Jaime-Ferrer et al., 2009). For converting ammonium sulfate into a mixed acid/salt stream and a relatively pure, but lowly, concentrated ammonium hydroxide product, a two-compartment cell design (Fig. 4) was suitable (Kroupa et al., 2015). Only when $NH_4^+$ ions are transported does ammonium hydroxide form; when $H^+$ ions move through CEM and recombine with $OH^-$ in the base chamber, the current utilization is decreased (Kroupa et al., 2015). For salts of weak acids, a two-compartment cation cell works best to produce effluents as mixed salt/acid stream and base stream. (Mani, 1991). The cell had a BPMED membrane stack with ten cell duplicates, in which one cell duplicate consisted of a bipolar membrane in conjunction with a cation membrane. Two Anion exchange end membranes (AEEM) were placed adjacent to the cathode and anode electrodes (Nosova et al., 2022).

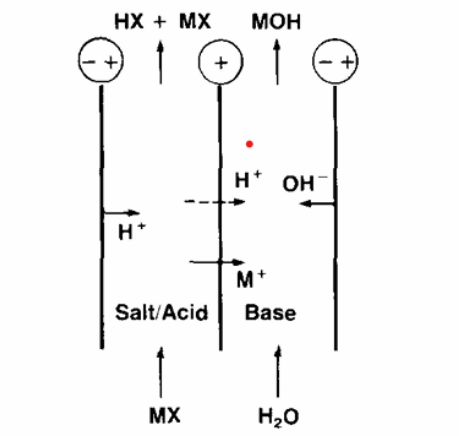


*Figure 4 Two-compartment cation cell, where MX is the salt formed by $M^+$ and $X^-$ ions* (Mani, 1991).

### 2.2.2 Two-compartment anion cell:

For salts of weak bases, a two-compartment anion cell works best to produce effluents as mixed base/salt stream and acid stream (Fig. 5) (Mani, 1991). The product liquid was converted into an alkaline ammonia solution in the two-compartment setup, while ammonium sulfate contributed to a higher conductivity. This was opposed to a system using a three-compartment stack, where ammonium will become the only cation resulting in the (inherently low) conductivity (Koivisto et al., 2023). Fewer membranes will be needed in a two-compartment stack, which was advantageous in terms of cost and maintenance (Koivisto et al., 2023). With energy values in the range of 3630–4844 kJ/kg of ammonium sulfate, it had been demonstrated that a two-compartment stack was more energy-efficient than a three-compartment stack, which needs 5102–7223 kJ/kg of ammonium sulfate (Koivisto et al., 2023). The cell had a BPMED membrane stack with ten cell duplicates, in which one cell duplicate consisted of a bipolar membrane in conjunction with an anion membrane. Two Anion exchange end membranes (AEEM) were placed adjacent to the cathode and anode electrodes.

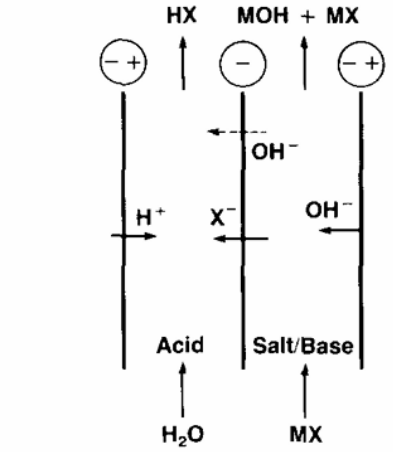


*Figure 5 Two-compartment anion cell, where MX is the salt formed by $M^+$ and $X^-$ ions* (Mani, 1991)

### 2.2.3 Three-compartment cell:

When compared to the two-compartment system, the acid and hydroxide were obtained in the three-compartment arrangement (Fig. 6) with concentrations that were more than twice as high (Kroupa et al., 2015). It is the standard purpose unit that can work efficiently over a wide range of different salts and can also generate and recover relatively pure, concentrated acid and base streams (Mani, 1991). A three-compartment stack's overall current density was constrained when the base (or acid) compartment produced a low-conductivity solution (Koivisto et al., 2023). The cell had a BPMED membrane stack with ten cell triplets, in which one cell triplet consisted of a bipolar membrane, an anion membrane, and a cation membrane. Two Anion exchange end membranes (AEEM) were placed adjacent to the cathode and anode electrodes. Feed was passed between the cation and anion membranes.

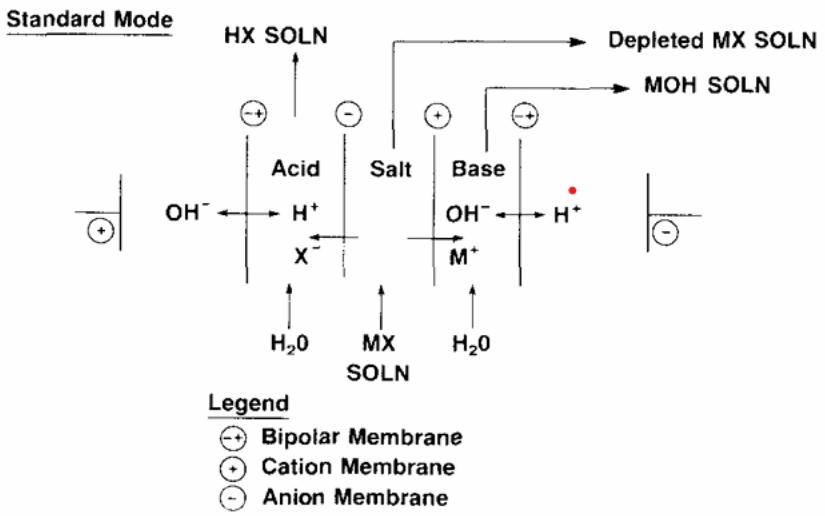


*Figure 6 Three-compartment standard cell, where MX is the salt solution formed by $M^+$ and $X^-$ ions* (Mani, 1991).

### 2.2.4 Multi-chamber cation cell:

The salt solution was fed between two cation membranes and then passed through the acid stream, resulting in high conc. of the acid in the acid/salt stream than two-compartment cation cell whereas base output remains the same as two-compartment cation cell (Fig. 7) (Mani, 1991). In other words, the cell had a BPMED membrane stack with ten cell duplicates, in which one cell duplicate consisted of two cation membranes in conjunction with a bipolar membrane. Two Cation exchange end membranes (CEEM) were placed adjacent to the cathode and anode electrodes.

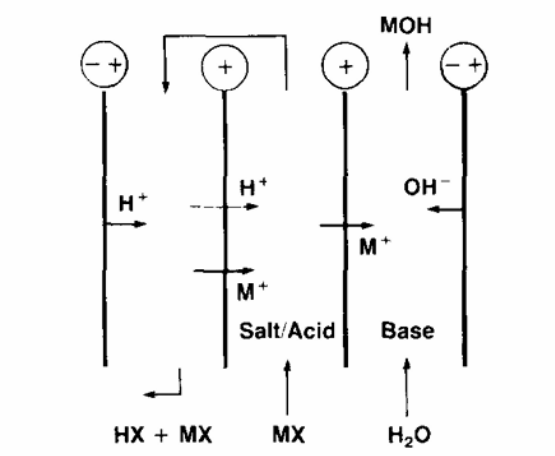


*Figure 7 Multi-chamber cation cell, where MX is the salt formed by $M^+$ and $X^-$ ions* (Mani, 1991)

### 2.2.5 Multi-chamber anion cell:

The salt solution was fed between two anion membranes and then passed through the base stream, resulting in high conc. of the base in base/salt stream than two-compartment anion cell whereas acid output remains same as two-compartment anion cell (Fig. 8) (Mani, 1991). The cell had a BPMED membrane stack with ten cell duplicates, in which one cell duplicate consisted of two anion membranes in conjunction with a bipolar membrane. Two Anion exchange end membranes (AEEM) were placed adjacent to the cathode and anode electrodes.

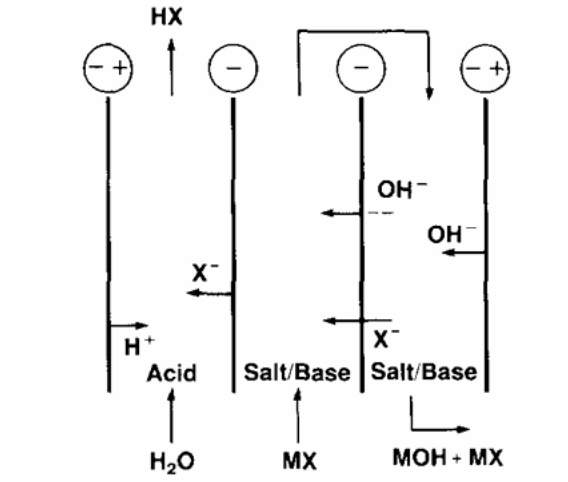


*Figure 8 Multi-chamber anion cell, where MX is the salt formed by $M^+$ and $X^-$ ions* (Mani, 1991)

## 2.3 Ammonia and sulfuric acid recovery with BPMED:

A BPMED stack was manufactured by joining no. of CEM, AEM, and spacers (Bauer et al., 1988; Simons, 1993). Many studies reported ammonium recovery through the BPMED stack (H. Guo et al., 2021; Y. Li et al., 2016; Shi et al., 2018; van Linden et al., 2020).

The study by Graillon et al., 1996, was the first-time attention arose to understanding the recovery of ammonia from a nitrogen-rich water source. The maximum current efficiency of

ammonium achieved in that experiment was limited to 70% because of ammonia gas diffusion (Graillon et al., 1996).

Other studies were conducted to achieve ammonium concentration from different water effluents such as van Linden et al., 2020 the study investigated ammonium recovery through BPMED from $NH_4HCO_3$ in batch cycles; Li et al., 2016 study experimented with different operational parameters like initial ammonium concentration (110 g/L) from simulated ammonium chloride wastewater; Shi et al., 2018 also investigated the effect of recovery of nutrients in two experimental BPMED stages.

Previous studies by Ye et al., 2018; Wang et al., 2020; Zhou et al., 2016, this was known that sulfuric acid was widely used in scrubber systems. Thus, with the help of BPMED, it was possible to achieve recovery and purity of acid to be used in scrubber systems.

From the studies of Zhou et al., 2016, and Wang et al., 2020, it was seen that a greater recovery of sulfuric acid was achieved when the current density, flow rate, and salt concentration were increased.

## 2.4 Current Density:

For Limiting current density (LCD), as shown in the figure below, the y-axis denotes current density in terms of A/cm$^2$ and the x-axis denotes voltage. It is important to define LCD which is when an ion is depleted at the membrane surface (Fig.9) due to concentration polarization and thus, ion concentration reaches 0 (Strathmann, 1995). Further increase in voltage does not help in increasing current density (Strathmann, 1995).

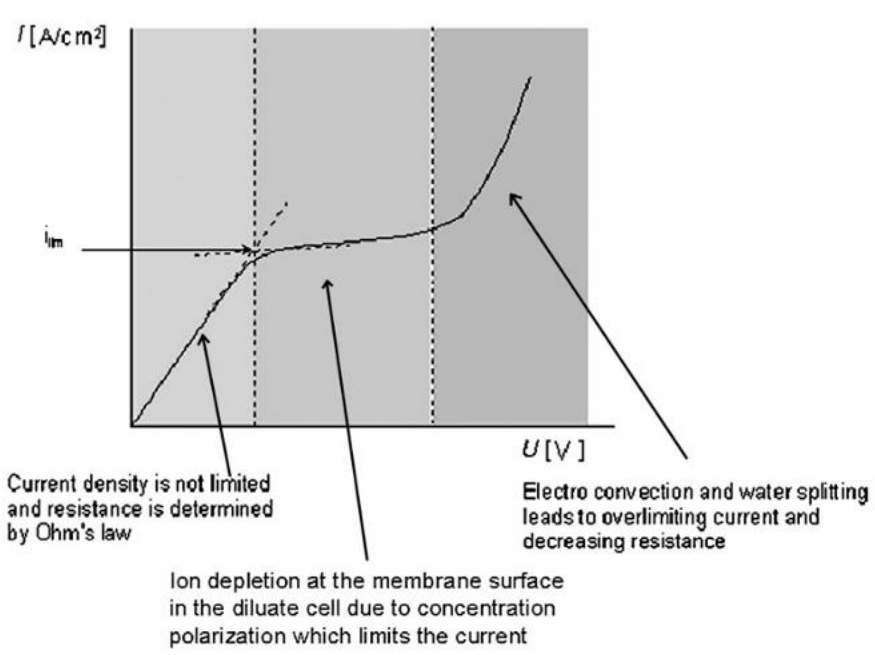


*Figure 9 LCD-voltage curve in ED* (Strathmann, 1995)

A study by Zhang et al., 2019, it was reported that the salt stream reached a pH value of 4 quickly when the current density was increased from 40 to 70 mA/cm$^2$. Also, a study by Ali et al., 2004, showed that in terms of ammonia recovery efficiency and concentration in the base compartment, an application of high current density (i.e., 50 mA/cm$^2$) worked out very well.

Yang et al., 2023 proved that increasing current density under LCD showed a more significant increment in ammonia recovery. It was observed that with 2 mA/cm$^2$ current density, the ammonia concentration in the base increased from 48 to 145 mg/L whereas with 1 mA/cm$^2$, ammonia concentration reached only 67 mg/L (D. Yang et al., 2023). It was also observed by Yang et al., 2023 that with higher current density also resulted in slightly higher ammonium leakage (from 59.6 mg/L to 67.6 mg/L) from diluate to electrode solution.

In a study by Li et al., 2016, showed an increase in current efficiency and a decrease in energy consumption when the current efficiency increased from 38 mA/cm$^2$ to 58 mA/cm$^2$. Moreover, higher current density means a higher membrane stack voltage which eventually helps to prevent back diffusion of ions especially when there is a large concentration gradient between diluate and acid/base (Y. Li et al., 2016). In addition, the higher current density could shorten the reaction time to decrease the loss of ammonia due to ammonia volatilization and improve the production efficiency (Y. Li et al., 2016). Thus, higher current density leads to higher ammonia recovery and increased energy consumption in the base compartment with a shorter experimental time (Y. Li et al., 2016).

The high ammonia recovery results were consistent with the high electric current density at the high flow rate (H. Guo et al., 2021). The decreased mass-transfer limitation close to the membrane surfaces can be used to explain the enhanced electric current density (H. Guo et al., 2021). This result was in line with earlier research by (Kim et al., 2011; Walker et al., 2014), which found that a high flow rate enhanced the degree of mixing conditions and raised the electric current (H. Guo et al., 2021).

## 2.5 Flow rate:

It was known from the study of Guo et al., 2021, that the higher flow rate (i.e., water flow velocity in the BMED stack) resulted in higher ammonia recovery. The ammonia recovery of 88.4% was observed at the flow rate of 180 mL/min (water flow velocity of 1.40 cm/s) while the ammonia recovery was 76.1% at 120 mL/min (0.93 cm/s) and 68.7% at 60 mL/min (0.47 cm/s) (H. Guo et al., 2021). Additionally, When the flow rate was raised from 60 mL/min to 120 mL/min, the $NH_4^+$ removal efficiency went up from 84.6% to 89.7% (H. Guo et al., 2021). However, the removal of $NH_4^+$ increased somewhat (0.1%) when the flow rate was raised from 120 to 180 mL/min (H. Guo et al., 2021). Therefore, it was observed that there was a back-diffusion of ammonium but was not calculated.

It should be noted that the increase in the ammonia recovery was significant when the flow rate increased from 60 to 120 mL/min for the first 60 min (H. Guo et al., 2021). However, there was a subtle increase in the ammonia recovery when the flow rate increased from 120 to 180 mL/min.

Therefore, a further increase in the flow rate above 180 mL/min (1.40 cm/s) was not expected to improve ammonia recovery using the BMED system (H. Guo et al., 2021). The membrane stack's electric energy consumption dropped as the flow rate increased, demonstrating that high flow rate conditions were more advantageous for BMED's energy-efficient ammonia generation (H. Guo et al., 2021). De Jaegher et al., 2020 evaluated flow rate by varying crossflow velocities, namely 2, 2.5, 3, and 3.5 cm/s with varying current densities.

Zoungrana & Çakmakci, 2021 experimented with different flow rates ranging between 15 to 75 ml/min. It was observed that it reached the power density (0.54 $W/m^2$) at 60 ml/min and a further increase in flow rate showed a very low or almost zero increment in power density. Therefore, when the flow rate is too high, the solutions escape the membrane stack too quickly and don't give the ions enough time to migrate properly, which results in a decline in the electrical energy, which lowers the voltage and energy consumption (Zoungrana & Çakmakci, 2021). Also, a study by Kang et al., 2017, showed similar results to Zoungrana & Çakmakci, 2021 when it was observed that at very high flow rates, the pressure inside the stack increases which causes most ions to move at a faster rate which eventually contributes to lower power density.

## 2.6 Base Volume:

It was found from a study by Li et al., 2016, that an increase in $V_{salt}$ : $V_{base}$ ratio could cause an increase in current efficiency and also a reduction in energy consumption. It was known that diffusion takes place from a region of high concentration to a region of low concentration. Similarly, when the base volume is increased, it becomes more diluted, and thus, ions will transport easily from diluate to base and help in less back diffusion from the base.

## 2.7 Feed Volume:

In a recent study by Yang et al., 2023, it was observed that out of three Diluate/Concentrate volume ratios i.e., 20:1, 10:1, and 5:1, ammonium concentration in the concentrate for D/C of 20:1 was slightly higher than the other two volume ratios (i.e., more recovery with higher D/C volume ratios).

It was also observed from the study by Yang et al., 2023 that the slopes of concentrate conductivity-time curves for D/C of 10:1 and followed by D/C of 5:1 were lower than 20:1 which ultimately indicates that for the ratios of 10:1 and 5:1, concentration efficiencies were lower. Thus, high volume ratios were favorable for higher ammonium recovery when the experimental time was long (in this case, the time was 270 min) (D. Yang et al., 2023).

Moreover, ammonium concentration in the diluate for D/C of 5:1 reduced to 9.5 g/L which was lower than the other two D/C ratios (D. Yang et al., 2023). Hence, it can be concluded from the study by Yang et al., 2023 that with higher Diluate/concentrate volume ratios, there can be less ammonia back diffusion.

# 3. Research design and methods

## 3.1 Materials and Methods:

A bench-size PC-Cell 64004 ED cell (Heusweiler, Germany), which had an 8 cm x 8 cm stainless steel cathode and a Pt/Ir-MMO coated and Ti-stretched metal anode was employed (Heusweiler, Germany). 450 µm spacers were used in the stack between membranes. Spacers were made of the material Silicon/Polypropylene as mentioned in the manual from the manufacturer: PC Cell (Heusweiler, Germany). PC 100D AEMs, PC-SK CEMs, and PC Bip BPMs were used in this research. The main features of PCCell's (Heusweiler, Germany) ion exchange membranes are presented in Table 1 below:

*Table 1 The main characteristics of membranes purchased from PC Cell (Heusweiler, Germany) for this study*

| Membranes | Thickness (µm) | Area resistance ($\Omega$ cm$^2$) | Water content (wt%) | Ion exchange capacity (meq. g$^{-1}$) | | Transport number (–) |
|---|---|---|---|---|---|---|
| | | | | Strong basic | Weak basic | |
| AEM (PC 100D) | 100–160 | ~5 | ~ 50 | ~ 1.2 | ~ 0.7 | >0.94 |
| CEM (PC-SK) | 100–120 | ~ 2.5 | ~ 9 | – | | >0.95 |
| BPM (PC Bip) | ~120 | – | ~ 30 | – | | – |

Magnetic stirrers were used to continuously mix the solutions on a mixing plate with a temperature setting of 25 ± 0.5 °C. The reagents used in this research are ammonium sulfate $(NH_4)_2SO_4$ salt (≥99 %), sodium sulfate ($Na_2SO_4$) salt (≥99 %), $H_2SO_4$ (2.5 M), and $NH_4OH$ (25 %). These reagents were used to prepare the initial solutions used in the acid, base, diluate, and ERS compartments. All the reagents were supplied by Sigma Aldrich (Zwijndrecht, The Netherlands). The solutions were stored in different borosilicate bottles.

The electric current and voltage were constantly logged in the computer to assess the electrochemical energy consumption with the help of a TENMA 72-1330 power supply. The solutions were pumped through a Peristaltic Watson-Marlow 520S pump with separate Watson-Marlow 313 pump heads into the BPMED membrane stack. The pump was calibrated before starting the experiment as shown in Appendix A. Solution volumes, mass, pH, and EC were measured manually at the beginning and the end. To analyze the pH and EC of the compartments, there were calibrated multimeters for each compartment. Furthermore, pH and EC were constantly recorded every 5 seconds with the help of multimeters to check the performance of compartments throughout the cycle. For pH, IDS SenTix 940 pH meters and WTW Multi 3620 IDS multimeters, and for EC, TetraCon 925 EC meters and WTW Multi 3620 IDS multimeters. The ions from samples (taken from each solution bottle) were measured using ion chromatography (IC).

## 3.2 Methods per experimental phases

Phase 0: Preliminary information

The operational run time of the experiments was determined to be kept for 2 hours. The limiting current density (LCD) of the system was determined.

Initially, the diluate, acid, and base contained 50 g, 0.66 g, and 0.66 g ammonium sulfate salt ($(NH_4)_2SO_4$) (≥ 99%) in 1 liter, 0.5 liters, and 0.5 liters demi water respectively, which were stirred on mixing plate with the help of magnetic stirrers. It means that the diluate contained an ammonium concentration of 13.6 g/L; the acid and base contained an ammonium concentration of 0.18 g in 0.5 liters. The Electrode Rinse Solution (ERS) contained 71 g sodium sulfate salt ($Na_2SO_4$) (≥ 99%) in 0.5-liter demi water. The pump was set to a constant flow rate of 15.3 L/h. The electric current and potential were initially set to 1.28 A and 60 V. The samples were taken every 15 minutes for a whole experimental time of 120 minutes.

Phase 1: Different current density

This phase studied the effect of varying current densities (taking 2400 coulombs) in the BPMED. The same number of coulombs was applied for all the experiments, resulting in the shortest experimental time for 100% current density and vice-versa for 25% current density, as shown in Table 2:

*Table 2 Varying current densities with their calculated current, total experimental time, and the sampling interval period*

| Sr. No. | CD (%) | Current (A) | Experimental time | Sampling time |
|---|---|---|---|---|
| 1 | 100 | 1.28 | 31 mins 15 secs | 3 mins 54 secs |
| 2 | 75 | 0.96 | 41 mins 40 secs | 5 mins 12.5 secs |
| 3 | 50 | 0.64 | 1 hour 2 mins 30 secs | 7 mins 48.75 secs |
| 4 | 25 | 0.32 | 2 hours 5 mins | 15 mins 37.5 secs |

Triplicates with each current density were carried out to increase the reliability of the results.

The diluate, acid, base, and ERS contained the same concentration of salts and volumes as mentioned in Phase 0. The electric potential was kept at 60 V. The flow rate was 15.3 l/h.

The current density that gives the highest ammonium recovery will be taken into account for the next phases (i.e., Phases 2, and 3).

Phase 2: Flow rate variation for best current density

This phase studied the effect of varying flow rates in the BPMED with the best current density (in terms of highest ammonium recovery). Thus, four varied flow rates based on their corresponding crossflow velocity were tested as mentioned below (table 3):

*Table 3 Flow rate and their corresponding crossflow velocities*

| Sr. No. | Flow rate (L/h) | Crossflow velocity (cm/s) |
|---|---|---|
| 1 | 3.8 | 0.5 |

| | | |
|---|---|---|
| 2 | 7.6 | 1 |
| 3 | 15.3 | 2 |
| 4 | 30.6 | 4 |

Triplicates with each flow rate were carried out to increase the reliability of the results. The samples were taken every 15 minutes.

The diluate, acid, base, and ERS contained the same concentration of salts and volumes as mentioned in Phase 0. The electric potential was kept at 60 V.

Phase 3: Variation in base volume for best current density

This phase studied the effect of varying base volumes for the best current density in the BPMED. Thus, four varied base volumes (i.e., B = 0.5 L, B = 1 L, B = 2 L, and B = 3 L) were tested. Triplicates with each base volume were carried out to increase the reliability of the results. The samples were taken every 15 minutes.

The diluate, acid, and ERS contained the same concentration of salts as mentioned in Phase 0. The volumes of diluate, acid, and ERS were similar as mentioned in Phase 0. The electric potential was also kept the same as mentioned in Phase 0 (i.e., 60 V). The flow rate was 15.3 L/h.

Phase 4: Different cell configurations

Different cell configurations were built up as stated in the materials (2.2.1-2.2.5). Triplicates were carried out with each BPMED cell configuration to increase the reliability of the results.

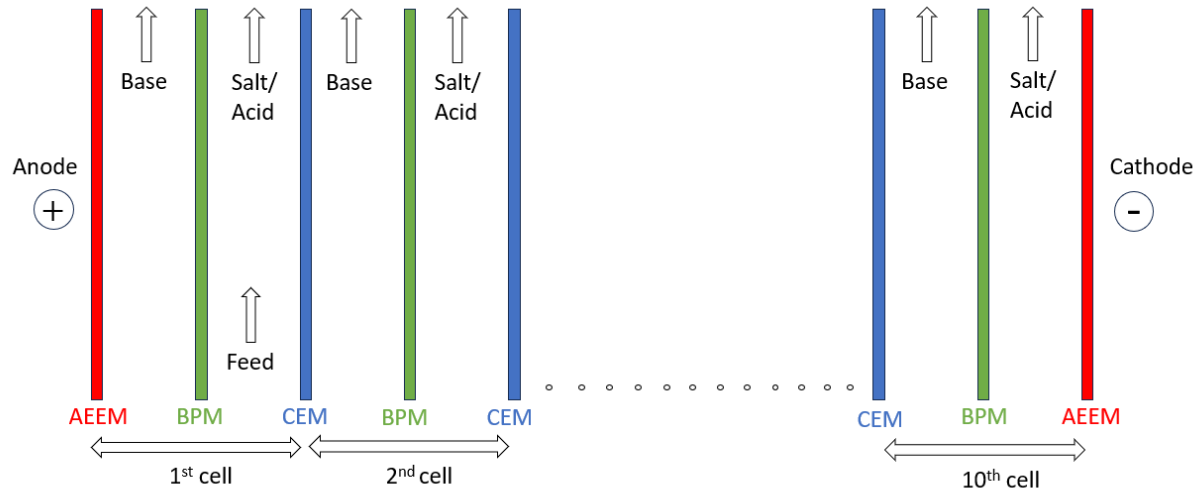


*Figure 10 Two-compartment cation cell with ten cell duplicates, in which one cell duplicate consisted of a bipolar membrane in conjunction with a cation membrane.*

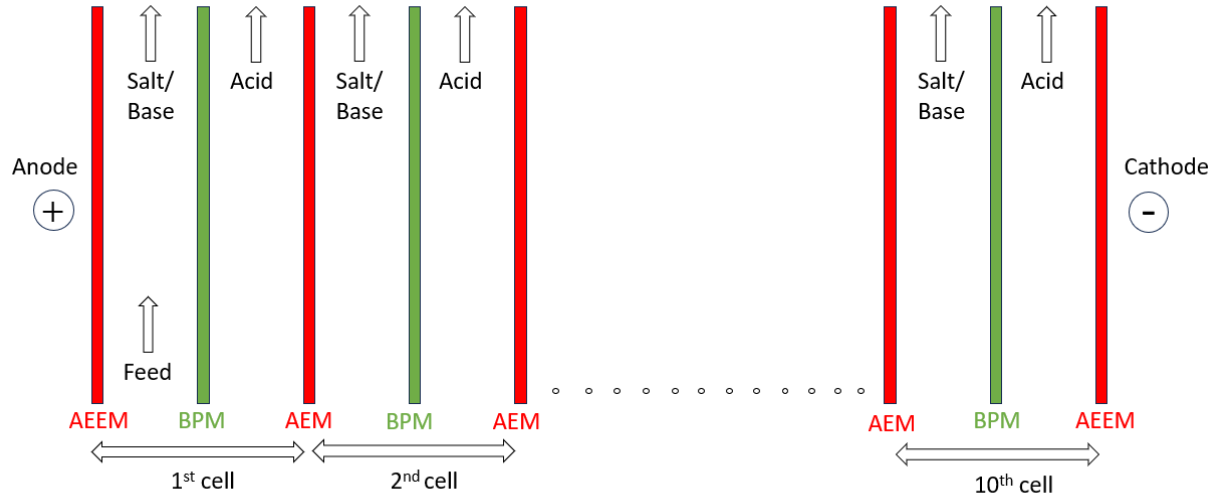


*Figure 11 Two-compartment anion cell with ten cell duplicates, in which one cell duplicate consisted of a bipolar membrane in conjunction with an anion membrane.*

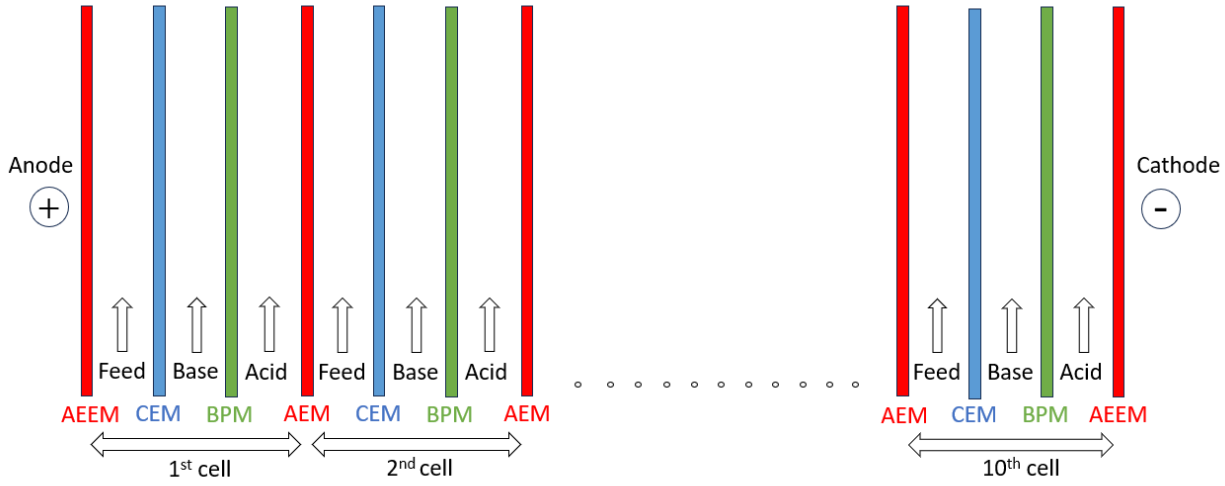


*Figure 12 Three-compartment cell with ten cell triplets, in which one cell triplet consisted of a bipolar membrane, an anion membrane, and a cation membrane*

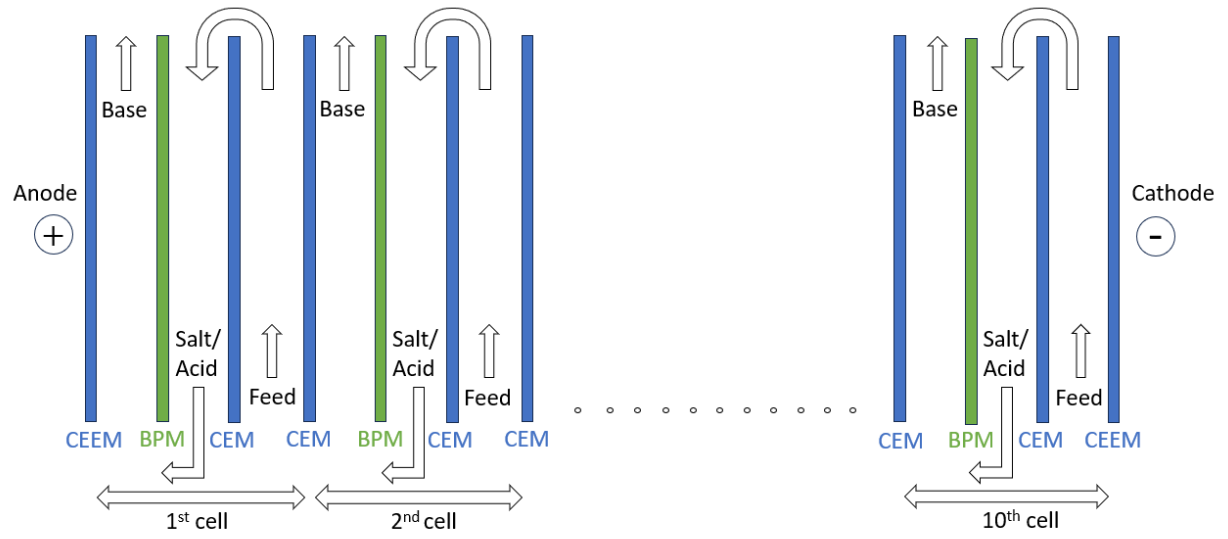


*Figure 13 Multi-chamber cation cell with ten cell duplicates, in which one cell duplicate consisted of two cation membranes in conjunction with a bipolar membrane.*

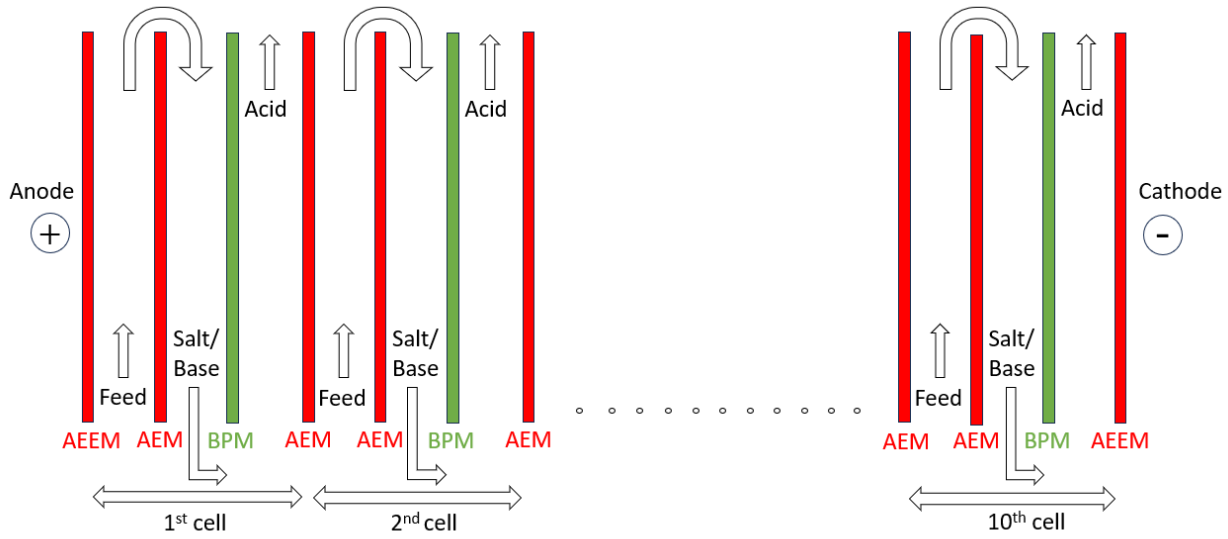


*Figure 14 Multi-chamber anion cell with ten cell duplicates, in which one cell duplicate consisted of two anion membranes in conjunction with a bipolar membrane*

The concentrations and volume (for diluate, acid, base, and ERS), flow rate, electric current, and potential were the same as in mentioned in Phase 0.

<u>Phase 5: Feed volumes of BPMED</u>

This phase studied the effect of varying feed volumes (i.e., diluate volumes) in the BPMED. Thus, four varied feed volumes (i.e., D = 0.5 L, D = 1 L, D = 2 L, and D = 3 L) were tested. Triplicates with each feed volume were carried out to increase the reliability of the results. The samples were taken every 15 mins and the total experimental time was 120 minutes.

The diluate, acid, base, and ERS contained the same concentration of salts as mentioned in Phase 0. The volumes of acid, base, and ERS were similar as mentioned in Phase 0. The electric current and potential were also kept the same as mentioned in Phase 0 (i.e., 1.28 A, and 60 V respectively). The flow rate was 15.3 L/h.

Phase 6: Optimum Experiment

This phase aims to study the effect of the experiment with parameters that provide efficient ammonium recovery and electrochemical energy consumption. The parameters for the experiment were discussed based on the results from all the previous research questions.

## 3.3 Performance Indicators:

Performance indicators for this experiment were energy consumption, ammonium recovery in the base (g), mass of ammonium in the base (%), and ammonium current efficiency (%).

### 3.3.1 Electrochemical energy consumption:

$$E_{\mathrm{NH4+,b}} = \frac{\sum_{t=0}^{t}(U_{\Delta t}.I_{\Delta t}.\Delta t) * 0.0036}{m_{\mathrm{NH4+,b}}}$$

Here, E = electrochemical energy in MJ/kg-$NH_4^+$,

$U_{\Delta t}$ . $I_{\Delta t}$ = Power during each time interval in W,

Δt = time interval in hours and

0.0036 to convert Wh to MJ

$m_{\mathrm{NH4+,b}}$ = amount of ammonium that was transferred to base in kg-$NH_4^+$.

### 3.3.2 Ammonium recovery in the base:

$$r_{(NH4+)}(t) = \frac{C_b(t).V_b(t) - C_b(i).V_b(i)}{C_f(i).V_f(i)}$$

Here, $r_{(NH4+)}$ (t) = recovery of ammonium in the base at time t (in g)

$C_b$ (t) = the concentration of ammonium in the base solution at time t (in g/L)

$V_b$ (t) = the volume of the base solution at time t (in L)

$C_b$ (i) = the concentration of ammonium in the base solution at time 0 (in g/L)

$V_b$ (i) = the volume of the base solution at time 0 (in L)

$C_f$ (i) = the concentration of ammonium in the feed solution at time 0 (in g/L)

$V_f$ (i) = the volume of the feed solution at time 0 (in L)

### 3.3.3 Mass of ammonium in the compartment (%):

$$M_c(\%) = \left(\frac{M_{c,NH4+}(t = \text{mins } at\ the\ end\ of\ experiment)}{M_{D,NH4+}(t = 0\ \text{min})}\right) * 100$$

Here, $M_c$ = Mass of ammonium in the compartment (diluate, acid, and base) in %,

$M_{c,\ NH4+}$ = Mass of ammonium in the compartment at t (min) = end of the experiment (g),

$M_{D,\ NH4+}$ = Mass of ammonium in the diluate at t = 0 min (g)

### 3.3.4 $NH_4^+$ Current efficiency:

$$\eta_{NH_4^+} = \frac{z \cdot F \cdot n_{NH_4^+,b}}{N \cdot \sum_{t=0}^{t}(I_{\Delta t} \cdot \Delta t)} \cdot 100\%$$

Here, $\eta_{NH4+}$ = the $NH_4^+$ current efficiency (unitless)

z = the ion valance (z = 1, unitless),

F = the Faraday's constant (F = 96,485 C/mol),

$n_{NH4+,b}$ = the amount of $NH_4^+$ transported to the base (in mol),

N = the number of repeated cell units (N=10, unitless),

$I_{\Delta t}$ = the average electric current in time interval Δt (in A = C/s),

Δt = the time interval (in s).

# 4. Results and discussion

## 4.1 Current density:

The effect of different current densities (CD) in a three-compartment BPMED cell on ammonium recovery and energy consumption was tested in this research topic. The experimental time and current were different as shown in section 3.2 Methods per experimental phases: Phase 1. The number of coulombs applied (i.e., 2400 Coulombs) was the same for all current densities. The concentration and volumes for diluate, acid, base, and ERS were the same as mentioned in section 3.2 Methods per experimental phases: Phase 0. The pH and EC graphs for diluate, acid, base, and ERS can be found in Appendix B.2. The avg. $NH_4^+$ concentration graphs over time can also be found in Appendix B.1.

### 4.1.1 Ammonium mass distribution

The average mass of ammonium transported from diluate to base and acid is shown in Table 4 below. The transport of average $NH_4^+$ mass from diluate into acid and base is depicted in Fig. 15. It was observed that with increasing current density, the amount of $NH_4^+$ mass recovered in the base also increased. The highest average ammonium recovery of 2.5 g in the base was observed at the highest current density of 100% with 1.28A and the least, 1.2 g in the base was observed at the lowest current density of 25% with 0.32A. The reason for the increased ammonium recovery is the accelerated migration velocity of ions due to increased current (X. Guo et al., 2023). Therefore, with increasing current density, the increase in ion removal from diluate was observed in Fig. 15 and 16. This is in line with previous studies by (X. Guo et al., 2023; Y. Liu et al., 2023), where they found that with increasing current density, recovery in the concentrate compartment increases.

Moreover, with low current density, it was observed that back diffusion increases in the acid compartment as observed in a previous study by (van Linden et al., 2019). This is probably because there is a higher concentration gradient at lower current densities due to the slower migration of ions, which leads to back diffusion. Thus, with decreasing current density back-diffusion becomes dominant.

*Table 4 CD: Average $NH_4^+$ mass in the diluate at the end of the experiment; Average $NH_4^+$ mass diff. in acid, and base at the end of the experiment*

| Current Density | Avg. Diluate mass (g) | Avg. Acid mass diff. (g) | Avg. Base mass diff. (g) |
|---|---|---|---|
| 100% CD | 10.1 | 0.6 | 2.5 |
| 75% CD | 9.9 | 0.6 | 2.4 |
| 50% CD | 10.5 | 0.9 | 2.0 |
| 25% CD | 10.7 | 1.2 | 1.2 |

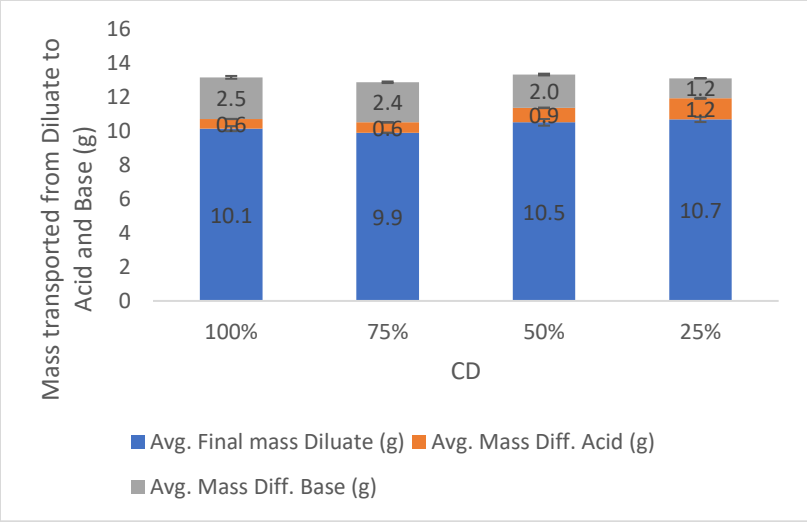


*Figure 15 Average $NH_4^+$ mass transported from diluate to acid and base with decreasing current density. Error bars represent the deviation between triplicates.*

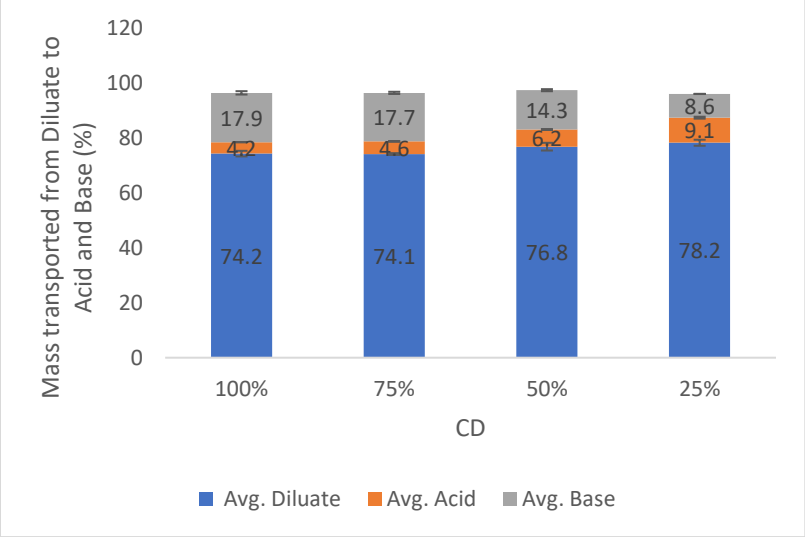


*Figure 16 Average $NH_4^+$ mass transported from diluate to acid and base in % with decreasing current density. Error bars represent the deviation between triplicates.*

### 4.1.2 Electrochemical Energy Consumption and $NH_4^+$ Current Efficiency

The average electrochemical energy consumption based on $NH_4^+$ transported in the base for varied current densities is shown in Fig. 17(left). It was found that average electrochemical energy consumption decreased with decreasing current density, which in turn, leads to increased average current efficiency as shown in Fig. 17(right). Average current efficiency ranged from 54.8% to 26.4 % when the current density decreased from 100% to 25%. It was thus, observed that increased current density could speed up ion transmembrane migration and $H_2O$ dissociation into $H^+$ and $OH^-$ ions. This is similar to the results reported by by Li et al., 2016.

The highest average energy consumption of 28.1 ± 1.4 MJ/kg-$NH_4^+$ was calculated at the highest current density of 100%, followed by a decreasing trend of average energy consumption with the lowest of 24.2 ± 0.4 MJ/kg-$NH_4^+$ for 25% current density. The increased energy consumption with increasing current densities showed that a large part of energy was consumed as current density increased, to overcome the electrical resistance to migrate ions from diluate to acid and base. This is also found in earlier research by (Choi et al., 2003; Shen et al., 2013).

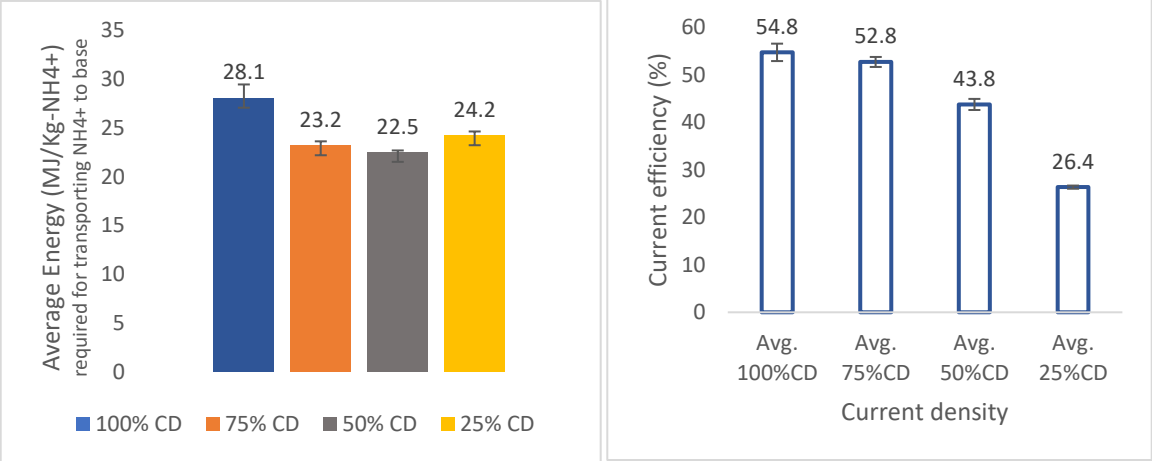


*Figure 17 Left: Graph of Average electrochemical energy consumption to transport $NH_4^+$ mass to base in MJ/kg-$NH_4^+$ with decreasing current density. Right: Graph of Average $NH_4^+$ current efficiency with decreasing current density. Error bars represent the deviation between triplicates.*

A large part of electrical energy consumption comes from having a higher electrical resistance of the stack. The higher average electrical resistance can be understood when observing a higher voltage as can be seen in Fig. 18. The highest average electric potential of 28.7 ± 1.1 V was observed at the highest current density of 100%, with other current densities having a lower potential development over time i.e., 22.8 ± 0.8 V, 18.4 ± 0.6 V, and 11.9 ± 0.2 V for 75 %, 50 %, and 25 % respectively. The higher electrical resistance can also be understood from the electrical conductivity in diluate (Appendix B.2.6). The lower the conductivity, the higher the resistance in transporting ammonium from the diluate and thus, the higher the voltage. The higher voltage/electric potential thus, contributes to the fact that the higher energy was consumed to overcome the higher electrical resistance of the stack. This relationship between energy consumption, electrical resistance, and electric potential was also observed in research by (Y. Liu et al., 2022; Shen et al., 2013).

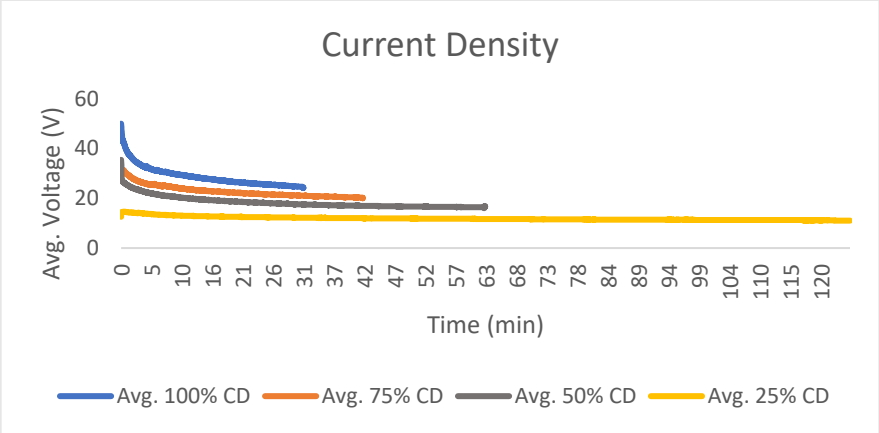


*Figure 18 Average electric potential/voltage (V) over time (min) for varied current densities.*

## 4.2 Flow rate:

In this topic, different flow rates in a three-compartment BPMED cell were optimized to obtain efficient ammonium recovery and energy consumption. The flow rates were decided based on crossflow velocity, where 0.5 cm/s was 3.8 L/h, 1 cm/s was 7.6 L/h, 2 cm/s was 15.3 L/h, and 4 cm/s was 30.6 L/h as mentioned in 3.2 Methods per experimental phases: Phase 2. The L/h flow rates were calculated based on the calibration of the pump. The experimental time was 120 min. The concentrations, electric potential, current, and volumes for all the compartments were the same as mentioned in 3.2 Methods per experimental phases: Phase 0 The pH and EC for diluate, acid, base, and ERS can be found in Appendix C.2. The avg. $NH_4^+$ concentration graphs over time can also be found in Appendix C.1.

### 4.2.1 Ammonium mass distribution

The average mass (g) of $NH_4^+$ migrated from diluate into acid and base is shown in Table 5 and Fig. 19. It is shown in the graph below that the highest average ammonium recovery in the base was observed at a flow rate of 7.6 L/h (1 cm/s, crossflow velocity) of 4.8 g, also with the highest removal from diluate of 3.6 g. As the flow rate increases, the recovery in the base (i.e., 4.6 g for 15.3 L/h and 4.1 g for 30.6 L/h), and removal from the diluate (i.e., 4 g for 15.3 L/h and 4.1 g for 30.6 L/h) also decreases. The decreased ammonium recovery is a result of decreased residence time of ions in the compartment. Decreased residence time of ions eventually results in the enhanced turbulence of flow which diminishes the concentration gradient and increases ion migration. The higher the flow rate, the more no. of cycles completed within a period in a stack, and thus, more no. of ions migrated. The result is similar to the observation by (Omran et al., 2023; J. Yang et al., 2024).

*Table 5 Flow rate: Average $NH_4^+$ mass in the diluate at the end of the experiment; Average $NH_4^+$ mass diff. in acid, and base at the end of the experiment*

| Flow rate | Avg. Diluate mass (g) | Avg. Acid mass diff. (g) | Avg. Base mass diff. (g) |
|---|---|---|---|
| 3.8 L/h | 4.8 | 4.6 | 4.6 |

| | | | |
|---|---|---|---|
| 7.6 L/h | 3.6 | 4.5 | 4.8 |
| 15.3 L/h | 4.0 | 4.8 | 4.6 |
| 30.6 L/h | 4.1 | 5.0 | 4.1 |

However, it is important to note that a low flow rate such as 3.8 L/h can cause ions to retain too long in the stack causing thick boundary layers near the membrane surface and a concentration profile. This eventually raises the voltage and affects the membranes of the stack (Omran et al., 2023; Zoungrana & Çakmakci, 2021). Also, a very high flow rate such as 30.6 L/h causes ions to leave the stack too soon without having proper contact with the surface of the membrane, which reduces the ammonium recovery efficiency in the base and thus, more back-diffusion in the acid compartment. Thus, the higher the flow rate, the more the back-diffusion of ions. This can be seen in the average mass (%) graph in Fig. 20. The highest average back-diffusion in the acid compartment of 36.1% was observed with a flow rate of 30.6 L/h and the lowest of 33.1 % with a flow rate of 7.6 L/h.

Note: Too high flow rates such as 38.2 L/h and 45.8 L/h (which corresponds to 5 cm/s and 6 cm/s crossflow velocity, respectively) were tested too but due to higher leakage from base to diluate, within 30 mins of experimental time, base volume reduced from 0.5 L to 200 ml and 100 ml, respectively. Therefore, no results were obtained.

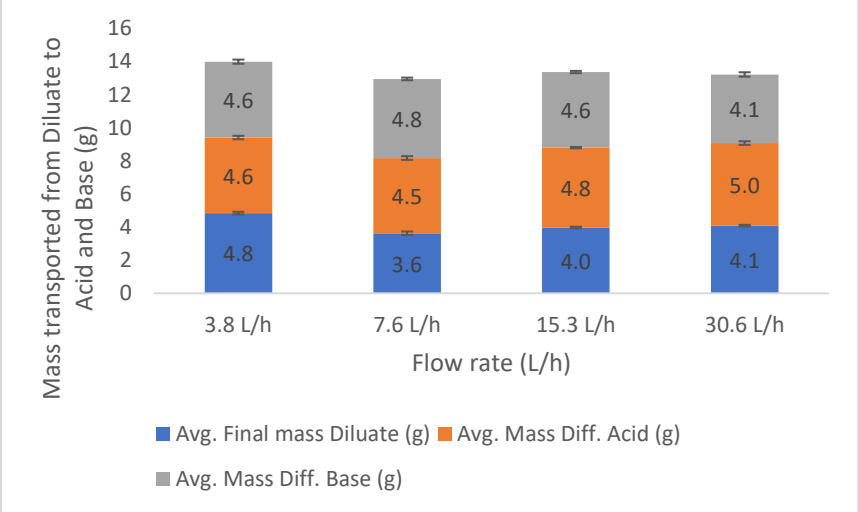


*Figure 19 Average $NH_4^+$ mass transported from diluate to acid and base with increasing flow rate. Error bars represent the deviation between triplicates.*

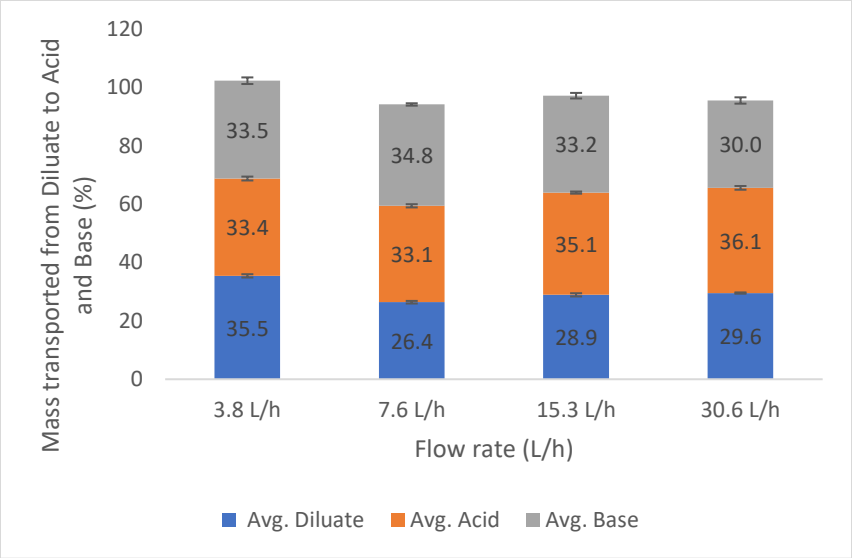


*Figure 20 Average $NH_4^+$ mass transported from diluate to acid and base in % with increasing flow rate. Error bars represent the deviation between triplicates.*

### 4.2.2 Electrochemical Energy Consumption and $NH_4^+$ Current Efficiency

The average electrochemical energy required for transporting ammonium in the base is presented graphically in Fig. 21(left) below. The average current efficiency for transporting $NH_4^+$ in the base is shown in Fig. 21(right). The average energy consumption increased from 39.5 ± 1.1 MJ/kg-$NH_4^+$ to 44.7 ± 2.5 MJ/kg-$NH_4^+$ as the flow rate increased from 7.6 L/h to 30.6 L/h. With increasing flow rate, the resistance to transport more ions in the base increases, and thus, the energy required to recover ammonium in the base also increases, which causes decreased average current efficiency of ammonium from 27.8 %, followed by 26.6 %, and 24.1%. Increased vertical flow velocity and intense flow turbulence have an impact on lateral ion migration, which raises the specific energy required for ion recovery. Higher feed flow rates greatly increase the membrane stack's processing capability, but they also run the danger of overloading the pump and mechanically damaging the membranes (J. Yang et al., 2024).

However, this is not in line with 3.8 L/h flow rate. This is because when the flow rate is too low, flow between the spacers may behave as laminar (Reynolds number may be low). Spacers in the stack direct the flow through the membrane and the cross straps within the spacers enable this flow (Sonu Vinay et al., 2016). The laminar flow between the spacers' cross strips leads to increased resistance and thus, higher energy consumption. Similar results were obtained with lower flow rates when observed by (Min et al., 2021; Zoungrana & Çakmakci, 2021). A too-low flow rate can cause a drastic drop in process efficiency, potentially decreasing current efficiency (Min et al., 2021).

In electrodialysis operations, it is crucial to optimize the flow rate of the solutions to increase the generation of energy while avoiding extremely low flow rates that might degrade system efficiency and very high flow rates that may harm the membranes (Zoungrana & Çakmakci, 2021).

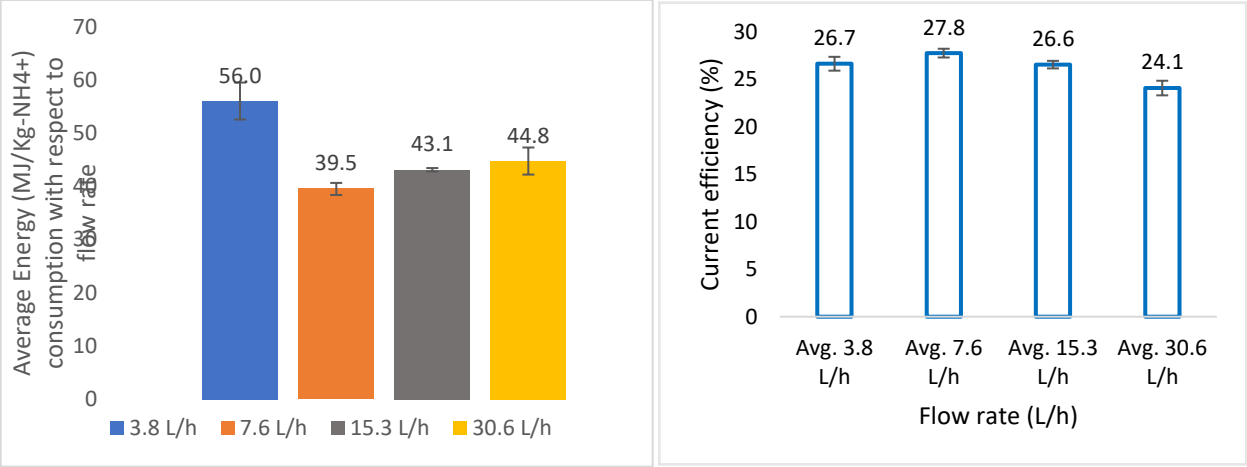


*Figure 21 Left: Graph of Average electrochemical energy consumption to transport $NH_4^+$ mass to base in MJ/kg-$NH_4^+$ with increasing flow rate. Right: Graph of Average $NH_4^+$ current efficiency with increasing flow rate. Error bars represent the deviation between triplicates.*

As can be seen from Fig. 22, the average electric potential ranges from 28. 5 ± 1.7 V to 20 ± 0.8 V for the flow rates ranging from 3.8 L/h to 30.6 L/h. The highest average electric potential was seen in the lowest flow rate which was typically because of the highest electrical resistance observed due to concentration polarization. This is because the depleted boundary layer has a higher electrical resistance of the compartment. The lower the conductivity of diluate (Appendix C.2.6), the higher the electrical resistance of the stack and thus, the higher the electric potential. This was observed in previous studies by (Omran et al., 2023; Zoungrana & Çakmakci, 2021). The noise in the graph of the average voltage of 3.8 L/h flow rate was mainly due to the depleted boundary causing a concentration profile.

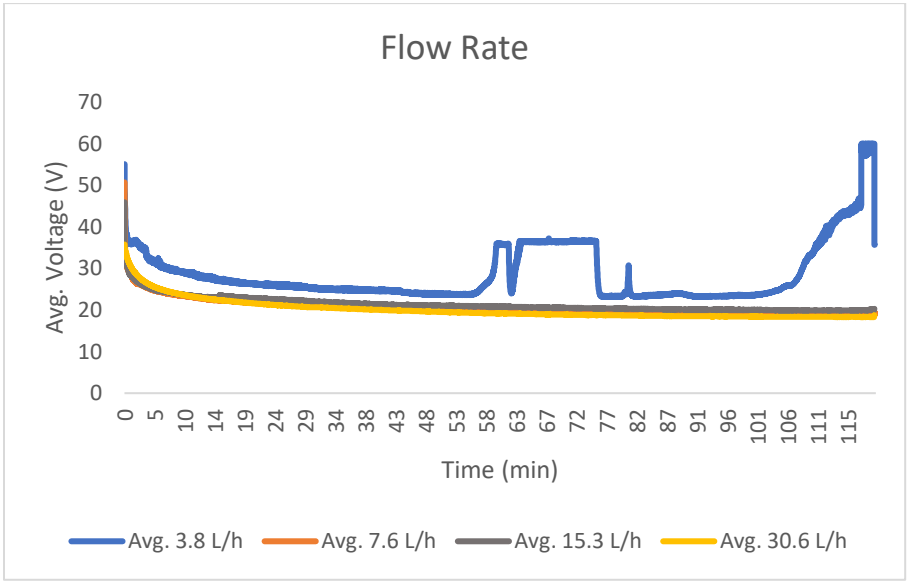


*Figure 22 Average electric potential/voltage (V) over time (min) for increased flow rate*

## 4.3 Base Volume:

The study covers varying base volumes in a three-compartment BPMED cell ranging from 0.5 L to 3 L to optimize the effect of $NH_4^+$ recovery efficiency and electrochemical energy consumption. The initial ammonium sulfate salt concentration was kept the same but the volume of the base was varied (i.e., 0.66 g in 0.5 L, 1.32 g in 1 L, 2.64 g in 2 L, and 3.96 g in 3 L). The concentration, and volume for diluate, acid, and ERS were the same as mentioned in in 3.2 Methods per experimental phases: Phase 0. The other details of the flow rate, current, and electric potential were also mentioned in 3.2 Methods per experimental phases: Phase 0. The pH and EC for diluate, acid, base, and ERS can be found in Appendix D.2. The avg. $NH_4^+$ concentration graphs over time can also be found in Appendix D.1.

### 4.3.1 Ammonium mass distribution

The average $NH_4^+$ mass transfer values from diluate to acid and base are shown in Table 6. The graphical representation of average mass transfer is shown in Fig. 23. Ions moved easily from a highly concentrated solution to a lower concentrated solution. So, as the base volume increases, the generated alkali concentration becomes larger, which means the ions concentration gradient increases, and thus, ions migrate faster from diluate to base. The highest average mass of ammonium in the base at the end of the experiment was 6.8 g at 3 L base volume, followed by 6.2 g, 4.9 g, and 4.6 g at 2 L, 1 L, and 0.5 L, respectively. The faster the ions were migrated, the more $NH_4^+$ ions were recovered in the base. Similar research by (Dong et al., 2023) observed that as the volume ratio of the acid-to-base compartment increased, the ion content gradient increased, causing the faster ions to migrate between the two compartments. In another research by (Cui et al., 2024), it is shown that larger volumes resulted in wider concentration gaps, which prompted active concentration diffusion from diluate to base, faster ion migration, and a more rapid approach to the endpoint of the reaction (Cui et al., 2024).

*Table 6 Base Volume: Average $NH_4^+$ mass in the diluate at the end of the experiment; Average $NH_4^+$ mass diff. in acid, and base at the end of the experiment*

| Base Volume | Avg. Diluate mass (g) | Avg. Acid mass diff. (g) | Avg. Base mass diff. (g) |
|---|---|---|---|
| 0.5 L | 4.0 | 4.8 | 4.6 |
| 1 L | 4.1 | 3.7 | 4.9 |
| 2 L | 3.8 | 2.3 | 6.2 |
| 3 L | 4.3 | 1.8 | 6.8 |

With increasing base volumes, the concentration gaps are enhanced which causes less back-diffusion in the acid. The average back diffusion is observed in Fig. 24. The maximum average back diffusion of $NH_4^+$ in the acid of 35.1 % was seen at the lowest base volume of 0.5 L and, as base volumes increased, it showed lower back diffusion in the acid compartment (i.e., 27.1 %, 17.5 %, and 13.5% for 1 L, 2 L, and 3 L, respectively) due to a more uniform concentration profile in the end. This is shown in the previous study by Li et al., 2016 where the study

mentioned that ammonium ions easily move from diluate to base solution, resulting in less back diffusion in the acid compartment. Different studies based on the D/C ratio are done by (Abtahi Mehrjardi et al., 2023; Araji, 2019), which showed that a higher D/C ratio helps in maintaining a more uniform profile across the stack, which diminishes the driving force for back diffusion.

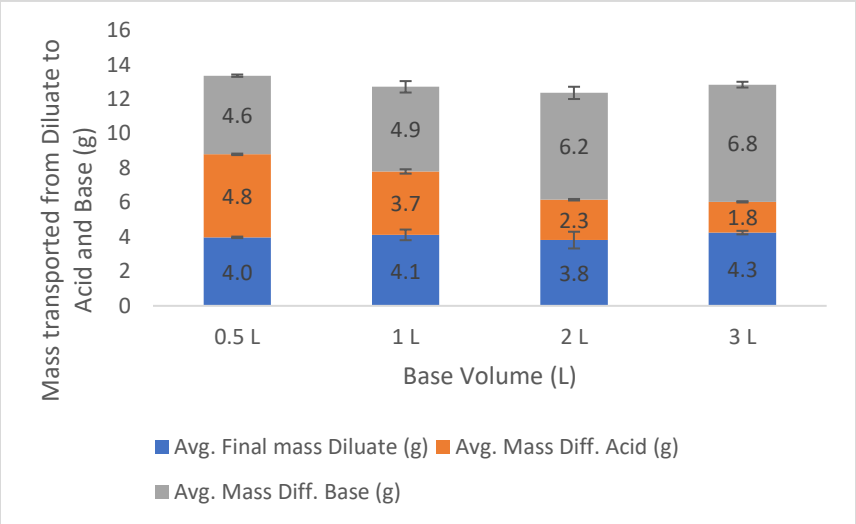


*Figure 23 Average $NH_4^+$ mass transported from diluate to acid and base with increasing base volume. Error bars represent the deviation between triplicates.*

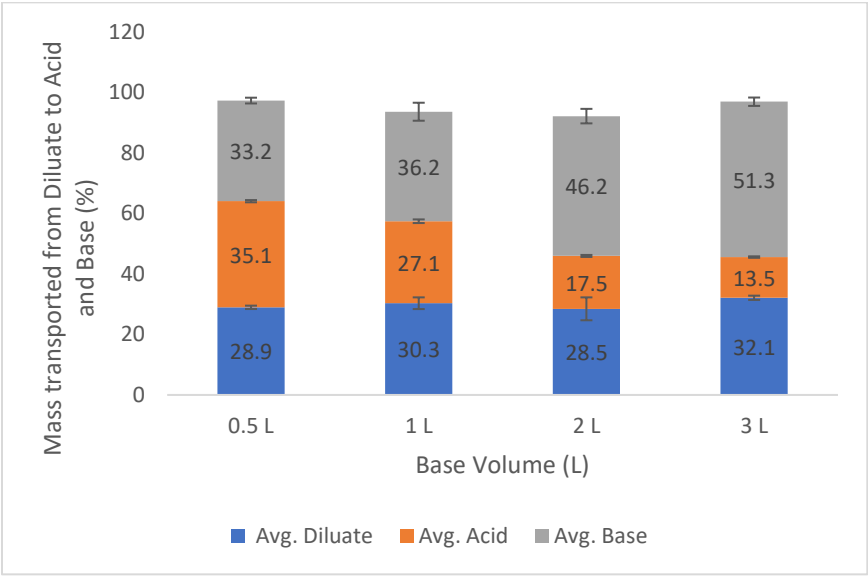


*Figure 24 Average $NH_4^+$ mass transported from diluate to acid and base in % with increasing base volume. Error bars represent the deviation between triplicates.*

### 4.3.2 Electrochemical Energy Consumption and $NH_4^+$ Current Efficiency

The graphical representation for the average electrochemical energy consumption to transport $NH_4^+$ from diluate to acid and base is shown in Fig. 25(left) and the average $NH_4^+$ current

efficiency for transporting ammonium to the base is depicted in Fig. 25(right). It was observed that with increased base volume, the energy required to transport ammonium in the base was decreased, causing an increase in ammonium current efficiency in the base. The lowest average ammonium current efficiency of 26.6 % was observed with the lowest base volume of 0.5 L, whereas the highest $NH_4^+$ current efficiency of 39.6% was observed with the base volume of 3 L. The current efficiency follows an increasing trend with increased base volume. The concentration gradient becomes larger with increasing base volume, the less the mass of ammonium back-diffused into acid from the base. Thus, increasing the volume ratio (i.e., base volume) improves the current efficiency of the process by suppressing back-diffusion effects and enhancing mass recovery in the base. This was in line with previous studies by (X. Li et al., 2024; H. Yan et al., 2019).

The maximum average energy consumed (43.1 ± 0.3 MJ/kg-$NH_4^+$) was 0.5 L as the concentration gradient was the least when compared to 1 L (38.6 ± 2.3 MJ/kg-$NH_4^+$), 2 L (32.2 ± 2.9 MJ/kg-$NH_4^+$), and 3 L (29.8 ± 1.3 MJ/kg-$NH_4^+$) as depicted in Fig. 25(left). As the volume ratio rises, the energy consumption falls. Ions find it easier to migrate from the diluate to the base due to the decreased mass transfer resistance caused by the elevated concentration gradient (Li et al., 2024).

An increased base volume leads to less electric potential over time. However, it was observed that major variation between different energy consumption comes from the variated mass transported into the base. As seen in fig. 23 and 24 above, the mass of ammonium recovered in the base varies greatly with increasing base volume. The increased $NH_4^+$ mass causes lower electrical stack resistance and thus, lower energy consumption.

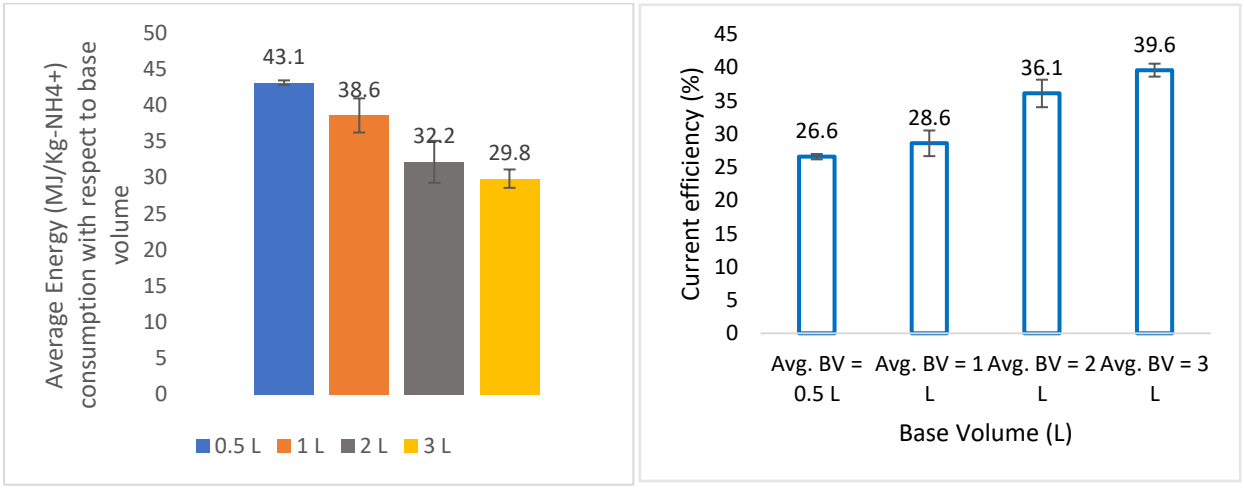


*Figure 25 Left: Graph of Average electrochemical energy consumption to transport $NH_4^+$ mass to base in MJ/kg-$NH_4^+$ with increasing base volume. Right: Graph of Average $NH_4^+$ current efficiency with increasing base volume. Error bars represent the deviation between triplicates.*

The graph for average electric potential over time for all the different base volumes is depicted in Fig. 26. It was clear that the average electric potential over time for all base volumes does not

have a very big difference between them as the electrical conductivity of diluate was almost the same (Appendix D.2.6), resulting in no significant difference in electrical resistance. Increasing the volume ratio improves the overall energy efficiency of the process by suppressing back-diffusion effects. The less the back-diffusion effect, the less is energy consumed in transporting ammonium from diluate to base.

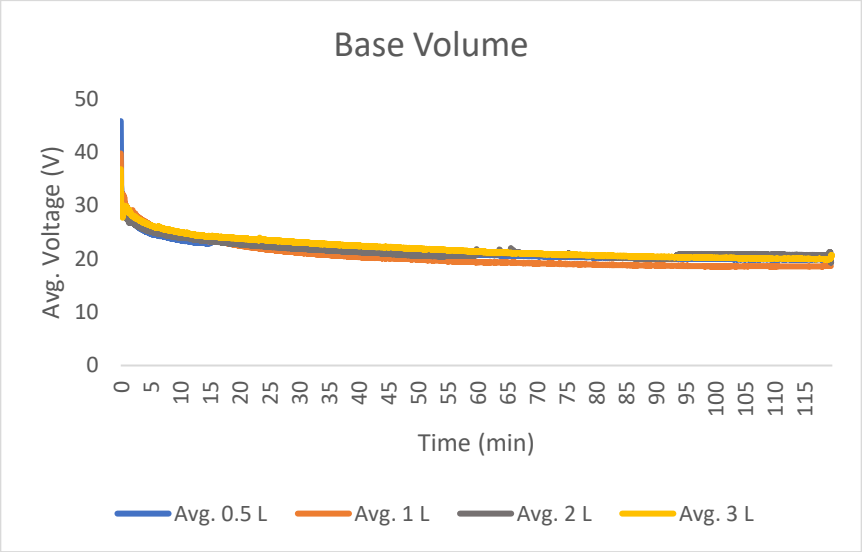


*Figure 26 Average electric potential/voltage (V) over time (min) for increased base volume*

## 4.4 BPMED Cell configurations:

The research topic covers optimizing different BPMED cell configurations to understand the impact it had on ammonium recovery efficiency and electrochemical energy consumption. The no. of cell pairs for all types of BPMED cell configurations was 10. The build-up mechanism of different BPMED cells can be understood from Fig. 10-14 in section 3.2 Methods per experimental phases: Phase 4. The electric potential, current, concentration, and volumes for diluate, acid, base, and ERS were the same as mentioned in section 3.2 Methods per experimental phases: Phase 0. The experimental time was kept for 120 minutes. The pH and EC graphs for diluate, acid, base, and ERS can be found in Appendix E.2. The avg. $NH_4^+$ concentration graphs over time and the purity of base can also be found in Appendix E.1 and E.3, respectively.

### 4.4.1 Ammonium mass distribution

Table 7 below shows the average values of ammonium in grams that were transferred from the diluate to acid and base for a three-compartment cell; from diluate to acid for a two-compartment anion cell and multi-chamber anion cell; from diluate to base for a two-compartment cation cell and multi-chamber cation cell. It can be observed from Fig. 27 that with more compartment BPMED cells, the recovery of average ammonium mass in the base also increases. The rise in average $NH_4^+$ recovery in the base was observed from 3.7 g in a two-compartment cation cell to 4.2 g in a multi-chamber cation cell. The rise in recovery is probably

because of dedicated compartments (i.e., base, and acid) available for better separation of cations and anions with a three-compartment cell than a two-compartment cell. In a three-compartment cell, the cathode compartment is specifically designated for the separation of ammonia water from $NH_4^+$ and $OH^-$ ions; whereas, with a two-compartment cation cell or multi-chamber cation cell, the separation of cations or anions is not designated in a particular compartment, which ultimately leads to a lower ammonium recovery efficiency than a three-compartment cell. Additionally, the increase in ammonium recovery in the base with multi-chamber electrodialysis compared to two-compartment cation cells was mainly due to increased compartments for salts and base, which allow multiple stages of separation of ions. This discussion is similar to some of the previous studies of (Jaime-Ferrer et al., 2009; Yasri & Gunasekaran, 2017).

*Table 7 BPMED Cell Configurations: Average $NH_4^+$ mass in the diluate at the end of the experiment; Average $NH_4^+$ mass diff. in acid, and base at the end of the experiment*

| BPMED Cell Conf. | Avg. Diluate mass (g) | Avg. Acid mass diff. (g) | Avg. Base mass diff. (g) |
|---|---|---|---|
| 3 comp. | 4.0 | 4.8 | 4.6 |
| 2 comp. anion | 8.7 | 4.3 | - |
| 2 comp. cation | 9.1 | - | 3.7 |
| Multi-chamber anion (AEEM) | 7.8 | 5.2 | - |
| Multi-chamber cation (CEEM) | 7.3 | - | 4.2 |

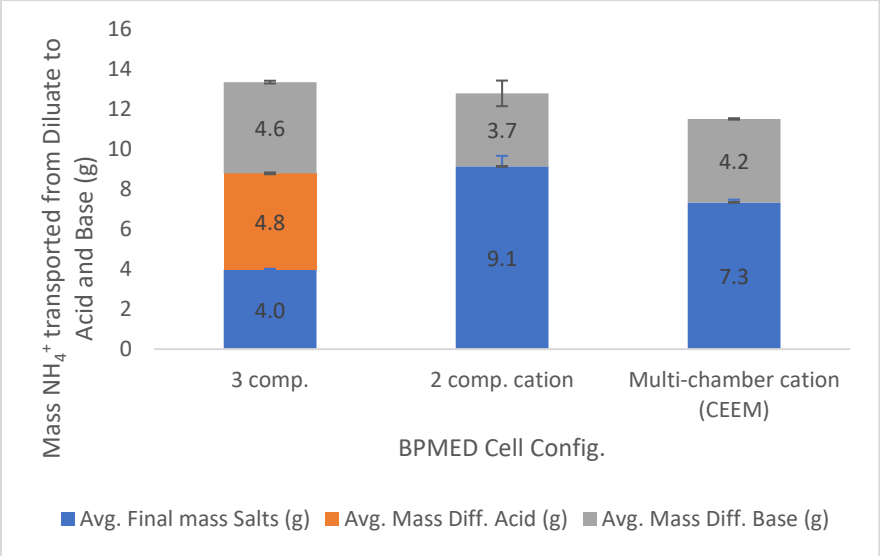


*Figure 27 Average $NH_4^+$ mass transported from diluate to acid and base with different BPMED cell configurations. Error bars represent the deviation between triplicates.*

From Fig. 28 below, it was seen that the average back-diffusion of ammonium in the acid increases with a two-compartment anion cell, followed by a three-compartment cell and a

multi-chamber anion cell. The increase in back-diffusion is the result of increased no. of compartments with two-compartment anion cells, three-compartment cells, and a multi-chamber anion cell. As the compartments increase, the diffusion path for ions from one end to another also becomes longer. This extended pathway causes ions to back-diffuse into acid from the base. Moreover, with three-compartment and multi-compartment anion cells, multiple compartments cause a larger concentration gradient between adjacent compartments, causing more no. of ions to back-diffuse. This is in line with a study by (Doornbusch et al., 2019).

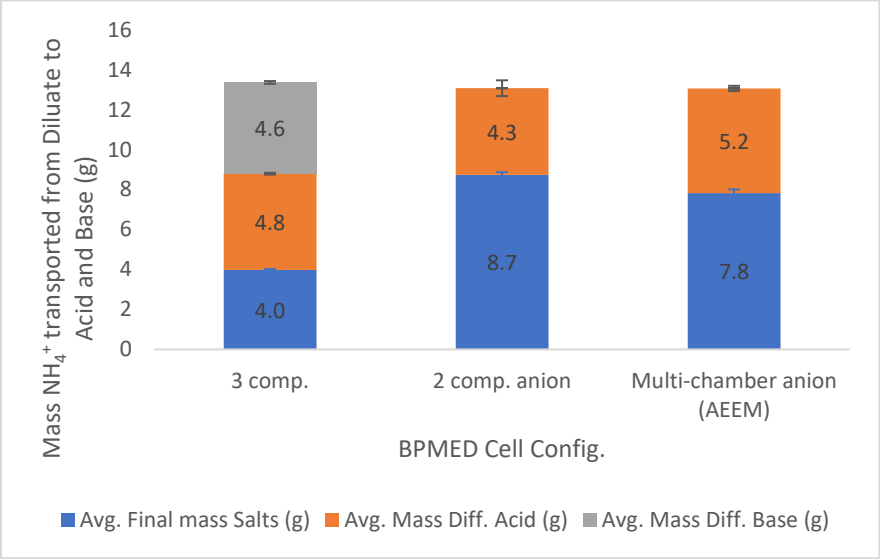


*Figure 28 Average $NH_4^+$ mass transported from diluate to acid and base with different BPMED cell configurations. Error bars represent the deviation between triplicates.*

### 4.4.2 Electrochemical Energy Consumption and $NH_4^+$ Current Efficiency

When comparing AEMs to CEMs from the earlier studies by (Rodrigues et al., 2020; van Linden et al., 2020), the ammonium transport number, which indicates the percentage of current carried by ammonium ions, is greater through AEMs. This results in increased average current efficiency and decreased average energy consumption since more ammonium ions are carried in the anion form per unit of applied current. The result can be observed in Fig. 29 (top and bottom). The highest average $NH_4^+$ current efficiency (as shown in Fig. 29(bottom)) was observed in anion configurations, i.e., a two-compartment anion cell (50.8%) and a multi-chamber anion cell (45.5%), whereas the lowest $NH_4^+$ current efficiency was observed in cation configurations, i.e., a two-compartment cation cell (21.3%) and a multi-chamber cation cell (24.3%).

As discussed in earlier sections 4.4.1, a three-compartment cell provides for the highest average ammonium recovery but from Fig. 29(top), it was also seen that three-compartment takes up the highest average energy to transport ammonium in the base i.e., 43.1 ± 0.3 MJ/kg-$NH_4^+$, whereas the least average energy consumption was observed with a two-compartment anion cell (31 ± 1.3 MJ/kg-$NH_4^+$) and a multi-chamber anion cell (30.2 ± 0.7 MJ/kg-$NH_4^+$). The highest energy consumption for a three-compartment cell is a result of the higher electric potential

observed to overcome the higher resistance of the stack, which is discussed further. For the two-compartment anion and multi-chamber anion cell, ammonium transports from salt to the base compartment through AEMs, which ultimately leads to more ammonium ions being transported per unit of applied electric current (resulting in lower energy consumption) compared to a two-compartment cation cell and a multi-chamber cation cell, where, ammonium ions pass through CEMs making ammonium transport number lower for an applied electric current. This is in line with previously discussed studies by (Georg et al., 2023; Rodrigues et al., 2020).

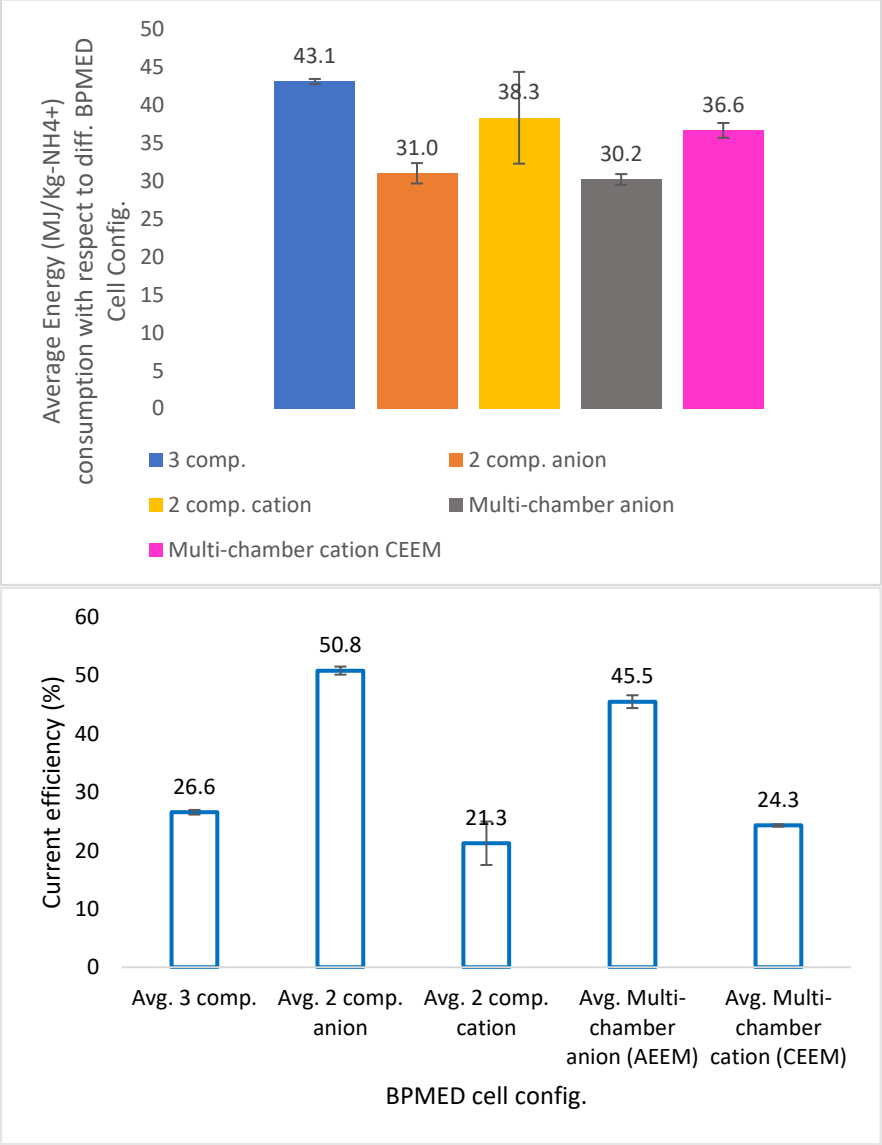


*Figure 29 Top: Graph of Average electrochemical energy consumption to transport $NH_4^+$ mass to base in MJ/kg-$NH_4^+$ with different BPMED cell configurations. Bottom: Graph of Average $NH_4^+$ current efficiency with different BPMED cell configurations. Error bars represent the deviation between triplicates.*

As can be seen from Fig. 30, the average electric potential does not have a significant difference between them except for the three-compartment cell which had the highest average electric

potential of 21.4 ± 0.1 V. The lowest average electric potential was observed for a two-compartment anion cell with a value of 15 ± 0.4 V. Higher potential differences can be generated throughout the three-compartment cell by separating cations and anions into distinct compartments, which may lower the overall resistance to ion transport and ultimately resulting in higher ammonium recovery efficiency. The highest electrical conductivity in diluate (Appendix E.2.6) was observed for the two-compartment anion and multi-chamber anion cell, which ultimately resulted in lower electrical resistance and lower electrical energy consumption compared to other BPMED configurations.

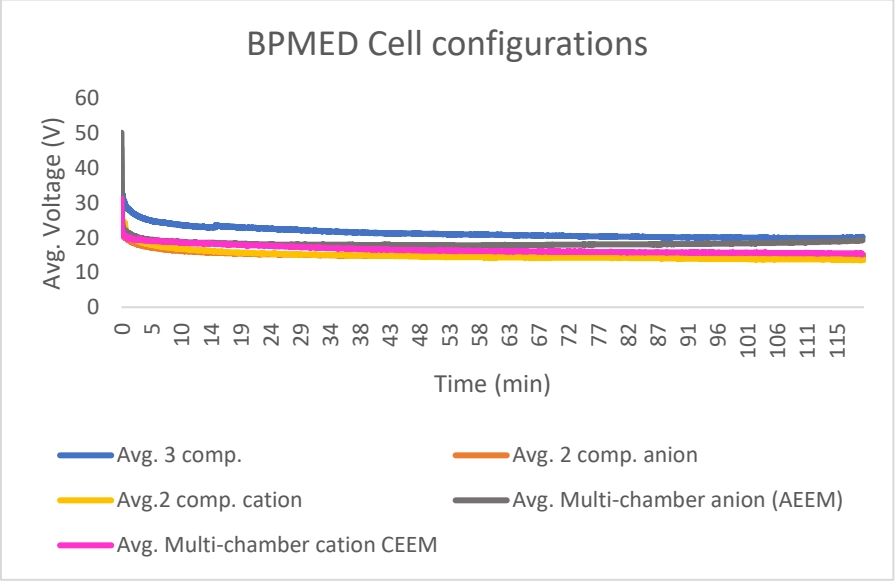


*Figure 30 Average electric potential/voltage (V) over time (min) for different BPMED cell configurations*

## 4.5 Feed Volume:

The research involves varying feed volumes in a three-compartment BPMED cell ranging from 0.5 L to 3 L to optimize the effect of $NH_4^+$ recovery efficiency and electrochemical energy consumption. The experiment was carried out in such a way that the initial ammonium sulfate salt concentration was kept the same but the volume of the feed was varied (i.e., 25 g in 0.5 L, 50 g in 1 L, 100 g in 2 L, and 150 g in 3 L). The concentration, and volume for acid, base, and ERS were the same as mentioned in in 3.2 Methods per experimental phases: Phase 0. The other necessary parameters involving the flow rate, current, and electric potential of the experiment were also mentioned in 3.2 Methods per experimental phases: Phase 0. The pH and EC for diluate, acid, base, and ERS can be found in Appendix F.2. The avg. $NH_4^+$ concentration graphs over time can also be found in Appendix F.1.

### 4.5.1 Ammonium mass distribution

As can be seen from Fig. 31 below, the average ammonium mass in the base compartment increases with an increase in feed volume. The highest average ammonium mass in the base was observed to be 6.8 g with the highest feed volume of 3 L. The increase in recovery increases with increasing feed volumes because the concentration gradient becomes larger, which causes

ions to move easily from feed to the base compartment. However, there was no significant difference in the $NH_4^+$ recovery between 2 L and 3 L. In other words, a larger feed volume allows for more ammonium ions to be brought into the system, leading to a higher number of ions to be recovered. Similarly, with a smaller feed volume (i.e., 0.5 L and 1 L), the concentration gradient between the feed and base may be maintained for a shorter duration, causing less recovery of ammonium in the base.

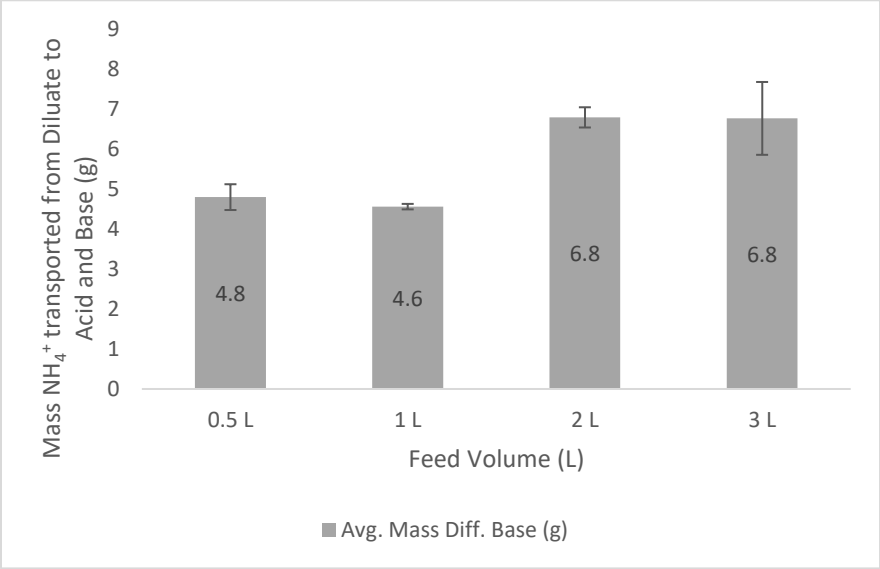


*Figure 31 Average $NH_4^+$ mass transported from diluate to acid and base with increasing feed volume. Error bars represent the deviation between triplicates.*

### 4.5.2 Electrochemical Energy Consumption and $NH_4^+$ Current Efficiency

It was observed from the fig. 32(left) that with increasing feed volume, there was a fall in the average electrochemical energy consumption to transport ammonium in the base and an increase in $NH_4^+$ current efficiency. The average $NH_4^+$ current efficiency to transport ammonium ions in the base can be explained in Fig. 32(right). The highest average $NH_4^+$ current efficiency i.e., 39.6% and 39.4% was observed in the highest feed volumes of 2 L and 3 L, respectively. The higher concentration of salts in the feed can correspond to higher recovery, which potentially can increase the driving force for transporting ammonium ions per unit of applied electric current. Moreover, the larger feed volume may correspond to a longer contact time between the solution and the membranes, leading to efficient ion transport and better ammonium current efficiency. This discussion is also observed in the study by Deckers, 2017.

The highest average energy consumption of 43 ± 2.4 MJ/kg-$NH_4^+$ was with the lowest feed volume of 0.5 L and the lowest energy consumption of 23.6 ± 1.6 MJ/kg-$NH_4^+$ was with the highest feed volume of 3 L as shown in Fig. 32(left). The reason for such energy difference is partially about the discussion in section 4.5.1. The concentration gradient is larger with larger feed volumes which leads to more space for ions to migrate and that reduces the resistance of the stack leading to lower energy consumption.

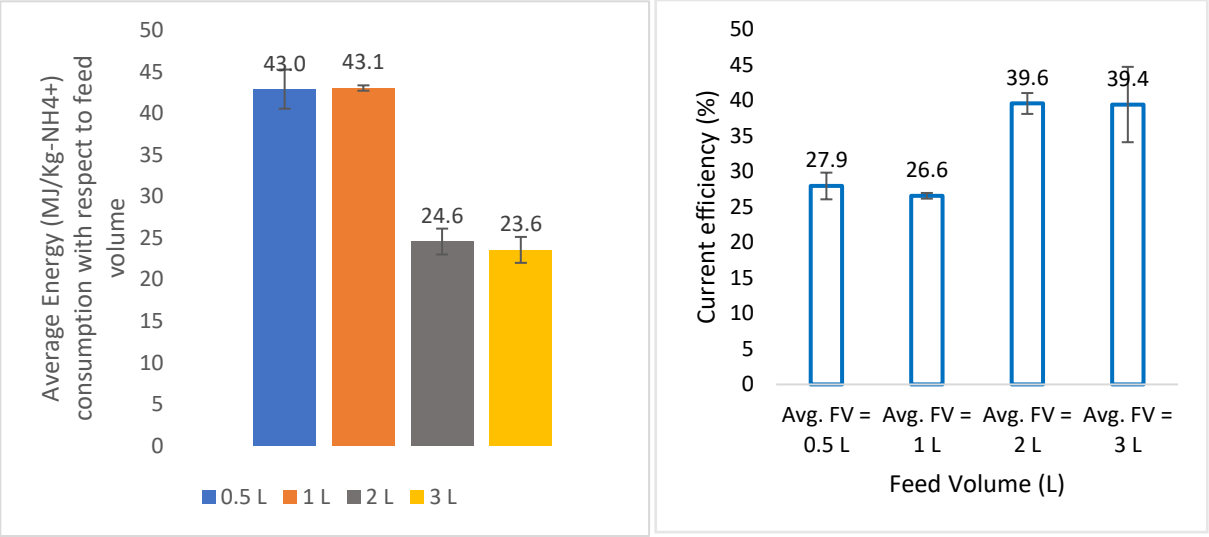


*Figure 32 Left: Graph of Average electrochemical energy consumption to transport $NH_4^+$ mass to base in MJ/kg-$NH_4^+$ with increasing feed volume. Right: Graph of Average $NH_4^+$ current efficiency with increasing feed volume. Error bars represent the deviation between triplicates.*

The other reason involves understanding the effect of feed volumes on electric potential over the whole experimental time. The two reasons together make up the total electrochemical energy consumption. Fig. 33 helps to understand that although there is no significant difference in average electric potential values of feed volume of 2 L and 3 L, however, the concentration polarization and scaling effects associated with a low feed volume consume higher potential (22.5 ± 0.4 V for 0.5 L to 17.2 ± 1 V for 3 L). It can be seen from fig. 33, that with 0.5 L there was a very high average electric potential observed at the end of the experiment probably because of the smaller concentration gradient and lower electrical conductivity (Appendix F.2.6) that caused very high resistance for the ions to migrate resulting in a very high electric potential. This causes concentration polarization at the membrane surface.

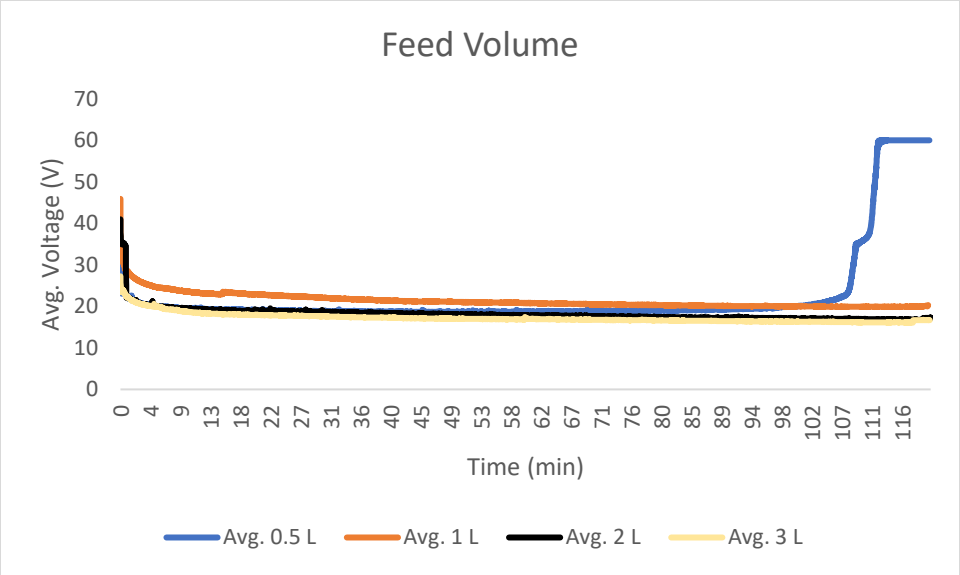


*Figure 33 Average electric potential/voltage (V) over time (min) for increased feed volume*

After discussing both the concentration gradient (from section 4.5.1) and electric potential over time, it can be made clear that the difference in energy consumption in Fig. 32, was mainly due to the concentration gradient difference for feed volumes of 1 L to 3 L. However, for 0.5 L feed volume, the higher energy consumption is mainly due to both the smaller concentration gradient difference and the higher electric potential (due to increased resistance).

## 4.6 Optimum Experiment

This research aims to experiment by taking all the parameters with the most efficient ammonium recovery and electrochemical energy consumption of previously discussed topics of the study. The concentration, and volume for acid, and ERS were the same as mentioned in in 3.2 Methods per experimental phases: Phase 0. The pH and EC for diluate, acid, base, and ERS can be found in Appendix G.2. The avg. $NH_4^+$ concentration graph over time can also be found in Appendix G.1.

### 4.6.1 Choosing Parameters for the Optimum Experiment

I. From section 4.1 Current Density, it was observed that with 100% CD, there was the highest ammonium recovery in the base of 2.5 g but it also takes up the highest energy consumption of 28.1 MJ/kg-$NH_4^+$. However, the 50% CD had the least energy consumption of 22.5 MJ/kg-$NH_4^+$ but also had a lower ammonium recovery of 2 g. Therefore, considering both the conditions of ammonium recovery and energy consumption, *75% CD* (i.e., 60 V with 0.96 A for 120 mins) was chosen with an ammonium recovery similar to 100% CD (i.e., 2.4 g) and with no significant difference in energy consumption with 50% CD (i.e., 23.2 MJ/kg-$NH_4^+$).

II. From section 4.2 Flow rate, it was observed that 7.6 L/h corresponding to a crossflow velocity of 1 cm/s gives the most efficient result among all the other flow rates, in terms of both the highest ammonium recovery in the base (i.e., 4.8 g) and the least electrochemical

energy consumption (39.5 MJ/kg-$NH_4^+$). Therefore, *a 7.6 L/h flow rate* was chosen for the optimum experiment.

III. From section 4.3 Base Volume, it was observed that the highest base volume, 3 L provides the highest ammonium recovery of 6.8 g and the least electrochemical energy consumption of 29.8 MJ/kg-$NH_4^+$. Therefore, *a 3 L base volume* (i.e., 3.96 g ammonium sulfate salt in 3 L demi-water) was chosen as the optimum parameter.

IV. From section 4.4 Different BPMED Cell Configurations, it was observed that ammonium recovery efficiency in the base was nearly the same for multi-chamber cation cell and three-compartment cell (i.e., 4.2 g and 4.6 g, respectively); however, the energy consumption for a three-compartment cell was 43.1 MJ/kg-$NH_4^+$ whereas for multi-chamber cation cell was 36.6 MJ/kg-$NH_4^+$. Therefore, considering both the conditions of ammonium recovery and energy consumption, *a multi-chamber cation cell* was chosen for the optimum experiment.

V. From section 4.5 Feed Volume, it was observed that the ammonium recovery efficiency for 2 L and 3 L of feed volume was almost the same (i.e., 6.8 g). However, for electrochemical energy consumption, 2 L and 3 L had almost no significant difference between the values (i.e., 24.6 MJ/kg-$NH_4^+$ and 23.6 MJ/kg-$NH_4^+$, respectively). Taking the experimental setup into account, if the base volume was already chosen as 3 L, it wasn't possible to set a 3 L feed volume with the setup as well. Therefore, *a 2 L feed volume* (i.e., 100 g ammonium sulfate salt in 2 L demi-water) was chosen for the optimum experiment.

### 4.6.2 Ammonium mass distribution

From Table 8 below, it was observed that with the optimum parameters, average ammonium recovery in the base had reached the highest 8 g when compared to a multi-chamber cation cell with 4.2 g (i.e., when the feed volume was 1 L and base volume was 0.5 L from Fig. 27); when compared to a three-compartment cell with average ammonium recovery of 6.8 g (i.e., when the base volume was 3 L and feed volume was 1 L from Fig. 23). Therefore, experimenting with the optimum parameters gives the highest average ammonium recovery in the base than all the other results obtained from this research.

*Table 8 Average values for the optimum experiment: $NH_4^+$ mass distribution (g), Energy consumption to transport $NH_4^+$ in the base (MJ/kg-$NH_4^+$), $NH_4^+$ Current efficiency in the base (%), and electric potential over time (V)*

| Optimum Experiment | Avg. $NH_4^+$ mass distribution (g) | Avg. Energy consumption (MJ/kg-$NH_4^+$) | Avg. $NH_4^+$ Current efficiency (%) | Avg. Electric potential over time (V) |
|---|---|---|---|---|
| Base | 8 | 12.7 ± 0.6 | 62 | 16.3 ± 0.5 |
| Salt/Acid | 19.2 | - | - | - |

### 4.6.3 Electrochemical Energy Consumption and $NH_4^+$ Current Efficiency

It was observed that the optimum experiment had the lowest average energy consumption of 12.7 ± 0.6 MJ/kg-$NH_4^+$ when compared to all the other energy consumption observed from the previous graphs and the average ammonium current efficiency reached a value of 62%. This low

energy consumption and high current efficiency are mainly due to a high concentration gradient and high electrical conductivity (Appendix G.2.4) that makes it easy to transport more ammonium ions into the base. Such lower energy consumption was never observed with any of the individual parameter analyses such as when with a multi-chamber cation cell, the average energy consumption observed was 36.6 MJ/kg-$NH_4^+$ (Fig. 29 (top)); or when the base volume was 3 L (i.e., 29.8 MJ/kg-$NH_4^+$ from Fig. 25 (left)); or when the feed volume was 2 L (i.e., 24.6 MJ/kg-$NH_4^+$ from Fig. 32 (left)). The large concentration gradient ultimately offers lower resistance as can be seen from high electrical conductivity (Appendix G.2.4), which can be further understood from the electric potential over time.

As can be seen from Table 8 above, the electric potential observed with the optimum parameters (i.e., 16.3 ± 0.5 V) was similar to a multi-chamber cation cell (i.e., 16.6 ± 0.4 V from Fig. 30). Thus, the resistance of the stack that the optimum parameters offer was the same as the resistance of the stack of a multi-chamber cation cell. Therefore, the electrochemical energy consumption difference comes majorly from the concentration gradient.

# 5. Overall discussion and recommendation

The study successfully demonstrated the usefulness of BPMED as a technique for recovering $NH_4OH$ from ammonium sulfate-rich water sources under extreme conditions. Flow rate, base volume, feed volume, current density, and different BPMED cell configurations were investigated in this study. However, other operational parameters including the impact of varied salt concentrations in the feed and base compartment (Y. Li et al., 2016), the varied ERS concentration, and volume (S. Wang et al., 2023; X. Wu et al., 2023) were not tested in this research as according to previous study by (Y. Li et al., 2016; S. Wang et al., 2023; X. Wu et al., 2023) might end up in higher recovery. Furthermore, the study used stimulated wastewater which contained pure ammonium sulfate, which may be different from industrial wastewater. Industrial wastewater contains many different cations and anions, which may lead to varied diffusion over time or distinct energy consumption due to scaling or fouling in the membranes. This eventually, will affect the efficiency of BPMED.

By increasing the current density of the three-compartment BPMED stack, the migration velocity of ions also increases, this increases the recovery of ammonium in the base along with electrochemical energy consumption. Additionally, this leads to reduced back-diffusion of ammonium in the acid from the base compartment. However, the experiments performed were for a shorter period (keeping 2400 Coulombs constant) and thus, experimenting it for a longer duration with a greater no. of coulombs applied (i.e., high current density) is further to be investigated as this can end up in high ammonium recovery (X. Guo et al., 2023; Y. Liu et al., 2023).

Since lab-scale studies are usually carried out for shorter periods, it can be difficult to properly capture the long-term scaling and fouling behavior. Large-scale scaling is more frequent due to the larger membrane area and longer operation times (Han et al., 2019; H. Liu & She, 2024; Van Geluwe et al., 2011).

Experiments with flow rate showed that by increasing flow rate, the ammonium recovered in the base increased, leading to enhanced turbulence in the stack, and thus, higher overall energy consumption. However, it was observed that at very low flow rates, there was concentration polarization near the membranes; and at very high flow rates, the solution didn't have enough time in the stack due to very high turbulence, leading to decreased ammonium recovery. This in turn affected the stability and efficiency of membranes (Omran et al., 2023; Zoungrana & Çakmakci, 2021). Therefore, the implementation of BPMED technology, which is characterized by very high flow rates or very low flow rates, will be made easier by the development of more stable membranes for varied flow rate processing. This kind of research will shed further insights on the application of flow rate on the amount of energy consumed during BPMED of $(NH_4)_2SO_4$ effluents. Moreover, the bipolar membrane stack PC 100D, designed mostly for organic acid synthesis, was employed in this study. However, with constantly new membranes being designed every day with different materials, there may exist alternative membranes (that

are selective) that work even better in this regard (Raissouni et al., 2007). Therefore, a study focusing on the impact of different parameters with different materials of membranes should be tested under extreme conditions to gain more insights into choosing the right material for membranes.

In large-scale systems, there are larger membrane areas, and maintaining a uniform flow rate along a longer flow path becomes challenging, this leads to potential drops across the stack and increases overall energy consumption, especially at higher flow rates (Al-Amshawee & Yunus, 2023; F. Li et al., 2022). Therefore, it is important to optimize the flow rate and proper flow distribution to avoid scaling issues when performing at a large-scale.

Furthermore, with increasing base and feed volumes experiments, it was observed that the mass of ammonium in the base increased but this resulted in lower energy consumption because of reduced stack resistance due to a larger concentration gradient. However, the maximum base volume that was tested was 3 L which was less compared to industrial applications (P. F. Li et al., 2022). Therefore, very high volumes for base and feed should be tested which may result in very low energy consumption leading to an increased ammonium recovery in the base.

Furthermore, for different BPMED cell configurations, it was observed that compared to anion configurations, cation configurations (i.e., two-compartment cation cell, multi-chamber cation cell) gave the maximum ammonium recovery in the base compartment. But when a multi-chamber cation cell was compared to a three-compartment cell, a three-compartment cell dominated the ammonium recovery in the base. It is also important to note that this also resulted in the highest energy consumption, followed by cation configurations, and then, the least energy consumption by anion configurations.

The purity of acid and base is not studied in this research and needs further insights. This study generated both acid and base as a result of using a three-compartment BPMED cell. According to published research by Cherif et al., 1997; Rodrigues et al., 2020, a three-chambered BPMED arrangement yields higher current efficiency than one with two compartments. A two-compartment stack, however, may help ensure that the generated acid and base are pure as mentioned in a study by Pourcelly, 2002. Thus, research into the functioning of a two-compartment BPMED stack might be helpful depending on the application.

The optimum experiment was carried out to see the impact on ammonium recovery in the base and also on energy consumption by putting forward the best of the parameters tested. It was observed that with optimum conditions, the highest mass of ammonium was recovered in the base (compared to all other individual parameter results) when tested with a multi-chamber cation cell along with the lowest energy consumption.

However, all the operational parameters were tested on a three-compartment BPMED cell, the impact of those parameters including flow rate, feed volume, base volume, and salt concentration on other configurations, especially multi-chamber cell configurations are yet to

be investigated, and need further studies on understanding its impact on ammonium and sulfate recovery.

The impact of all the above-mentioned parameters on sulfate recovery in the acid is also not measured in this research and can be further studied in depth to use it as an influent for the stripping/scrubbing process (D. Wang et al., 2020; Ye et al., 2018; Zhou et al., 2016).

To address the gap between lab-scale data and large-scale execution, thorough modeling and simulations, as well as pilot-scale investigations, are important. When scaling up from the lab scale, it becomes more essential to optimize the operating parameters to balance energy consumption, scaling mitigation, and removal/recovery efficiency. Localized low-flow rate zones can be caused by irregular flow patterns on a large scale, which can further contribute to decreased removal efficiency and higher concentration polarization (Min et al., 2021; Van Geluwe et al., 2011). Additional energy losses in large-scale systems can be brought on by non-uniform current distribution, electrode overpotentials, and solution resistance (Min et al., 2021; Van Geluwe et al., 2011). Operational difficulties with membrane replacement, cleaning techniques, and maintenance may arise in large-scale systems; these issues are not entirely present in lab-scale setups. Thus, regular monitoring and data gathering from large industrial facilities might enhance our knowledge of scaling, concentration polarization, and variations of energy consumption at larger scales.

# 6. Conclusions

This research successfully demonstrated the practicality of Bipolar Membrane Electrodialysis as a technique for treating ammonium sulfate-rich water under varying operational parameters. The technology was proven to be efficient in both ammonium recovery and energy consumption. The varying operational parameters are addressed through sub-research questions that support the main research question:

**"What is the effect of operational parameters on the overall ammonium recovery in the base and energy consumption of BPMED?"**

- *What is the effect of varying current densities on ammonium recovery and energy consumption?*

  It was observed that with increasing current density, the amount of $NH_4^+$ recovered in the base also increases. The highest average ammonium recovery of 2.5 g in the base was observed at the highest 100% current density (with 1.28A) and the lowest, 1.2 g in the base was observed at the lowest 25% current density (with 0.32A). This is because a higher current causes a higher migration velocity of ions. However, a higher concentration gradient at lower current densities due to the slower migration of ions, leads to back diffusion into the acid.

  From the study, it was also observed that the electrochemical energy consumption decreased with decreasing current density. The lowest average energy consumption observed was 24.2 ± 0.4 MJ/kg-$NH_4^+$ at 25% current density, whereas the highest average energy consumption was 28.1 ± 1.4 MJ/kg-$NH_4^+$ at the highest current density of 100%. The higher energy consumption comes from the higher electric potential required to overcome the electrical resistance.

- *What is the effect of varying flow rates on ammonium recovery and energy consumption?*

  In this topic, it was observed that as the flow rate increased, the recovery in the base, and removal from the diluate decreased. Decreased ammonium recovery in the base was a result of decreased residence time of ions in the stack, which eventually gives the enhanced turbulence of flow, increasing ion migration. The highest average ammonium recovery in the base was observed at a flow rate of 7.6 L/h (1 cm/s, crossflow velocity) of 4.8 g, along with the highest removal from diluate of 3.6 g.

  However, note that at very low flow rates such as 3.8 L/h, concentration polarization was observed near the membrane surface and a very high flow rate such as 30.6 L/h causes ions to leave the system too soon without having proper contact with the surface of the membrane, and thus, more back-diffusion into the acid compartment.

The electrochemical energy consumption increased with increasing flow rate due to the intense mixing of flow, which raised the specific energy required for ion recovery. The lowest average energy consumption of 39.5 ± 1.1 MJ/kg-$NH_4^+$ was observed at a flow rate of 7.6 L/h.

- *What is the effect of varying base volumes on ammonium recovery and energy consumption?*

From this study, it was observed that as the base volume increased, the generated alkali concentration tended to be larger, which means the ions concentration gradient between the compartments also increased, and thus, ions migrate faster from diluate to base. The highest average mass of ammonium recovered in the base was 6.8 g at 3 L base volume. Thus, this was also seen in terms of back-diffusion, i.e., when the concentration gradient was larger, there was less back-diffusion of ammonium ions noted into the acid compartment.

Regarding energy consumption, it was observed that with an increased base volume, the energy required to transport ammonium in the base decreased. The lowest average energy consumption of 29.8 ± 1.3 MJ/kg-$NH_4^+$ was observed with the highest base volume of 3 L. This was in line with the findings reported in the literature that with increasing base volume, a larger concentration gradient reduces the mass transfer resistance of the stack leading to lower energy consumption.

- *Which cell arrangement among the five BPMED configurations gives efficient ammonium recovery, purity of ammonium in the base, and energy consumption?*

For this research question, out of the five configurations, cation configurations gave the maximum ammonium recovery in the base compartment. The highest average ammonium recovery in the base of 4.6 g was observed in a three-compartment cell. This is due to dedicated compartments available for the separation of ammonium and sulfate ions. These compartments are missing in the two-compartment and multi-chamber cation cell causing lower average ammonium recovery: 3.7 g and 4.2 g, respectively. Although multi-chamber cation cells did not have dedicated compartments as three-compartment cells, ammonium recovery in the base was found to be almost similar (because of the higher number of repeated compartments available, allowing for more ions to go through multiple stages). However, the increased multiple stages for better separation of ammonium in multi-chamber anion cells causes more back-diffusion in the acid compartment due to the longer migration path of ions which elevates the back-diffusion of ions in the acid compartment.

The average electrochemical energy consumption was observed highest in a three-compartment cell, with a value of 43.1 ± 0.3 MJ/kg-$NH_4^+$, whereas the least average energy

consumption was observed in anion configurations: a two-compartment anion cell (31.0 ± 1.3 MJ/kg-$NH_4^+$) and a multi-chamber anion cell (30.2 ± 0.7 MJ/kg-$NH_4^+$)). This is because ammonium ions transported through AEMs are higher than CEMs, causing less resistance of the stack and thus, lower energy consumption compared to cation configurations.

- *What is the effect of varying feed volumes of the BPMED stack on the $NH_4^+$ recovery and energy consumption?*

The increase in feed volumes creates a larger concentration gradient, making ions move easily from a highly concentrated compartment to a low concentrated compartment. This was observed in this research question that the ammonium mass in the base compartment increases with an increase in feed volume. The highest average ammonium mass in the base was observed to be 6.8 g with the highest feed volume of 3 L. This is in line with the energy consumption due to the larger concentration gradient made, more space for ions to migrate, causing less resistance. The lowest average energy consumption of 23.6 ± 1.56 MJ/kg-$NH_4^+$ was observed with the highest feed volume of 3 L.

However, it was also observed that with very low feed volume, there was concentration polarization at the end of the experiment leading to increased resistance of the stack and thus, increased overall energy consumption to transport ammonium in the base.

- *What is the effect of the optimum experiment on ammonium recovery in the base and electrochemical energy consumption?*

The optimum experiment was carried out to put the best results together to understand the effect it offers on the overall ammonium recovery in the base and energy consumption.

The highest average ammonium recovery of 8 g was observed in the base when the experiment was performed with a multi-chamber cation cell, flow rate of 7.6 L/h, base volume of 3 L, feed volume of 2 L, and current density of 75% (i.e., 0.96 A) for 120 minutes. Neither of any individual parameters showed such high ammonium recovery in the base. This higher ammonium recovery is due to an enhanced concentration that makes it easy to transport more ammonium ions into the base. This also supports the discussion on electrochemical energy consumption. It was observed that it had the lowest average energy consumption of 12.7 ± 0.6 MJ/kg-$NH_4^+$ because of the large concentration gradient as the electric potential was almost the same as a multi-chamber cation cell without optimum parameters.

# 7. References


Abtahi Mehrjardi, S. A., Khademi, A., Said, Z., Ushak, S., & Chamkha, A. J. (2023). Enhancing latent heat storage systems: The impact of PCM volumetric ratios on energy storage rates with auxiliary fluid assistance. *Energy Nexus*, *11*. https://doi.org/10.1016/j.nexus.2023.100227

Al-Amshawee, S. K. A., & Yunus, M. Y. B. M. (2023). Electrodialysis desalination: The impact of solution flowrate (or Reynolds number) on fluid dynamics throughout membrane spacers. *Environmental Research*, *219*. https://doi.org/10.1016/j.envres.2022.115115

Ali, M. A. B., Rakib, M., Laborie, S., Viers, P., & Durand, G. (2004). Coupling of bipolar membrane electrodialysis and ammonia stripping for direct treatment of wastewaters containing ammonium nitrate. *Journal of Membrane Science*, *244*(1–2). https://doi.org/10.1016/j.memsci.2004.07.007

Araji, M. T. (2019). Surface-to-volume ratio: How building geometry impacts solar energy production and heat gain through envelopes. *IOP Conference Series: Earth and Environmental Science*, *323*(1). https://doi.org/10.1088/1755-1315/323/1/012034

Barbera, E., Bertucco, A., & Kumar, S. (2018). Nutrients recovery and recycling in algae processing for biofuels production. In *Renewable and Sustainable Energy Reviews* (Vol. 90). https://doi.org/10.1016/j.rser.2018.03.004

Bauer, B., Gerner, F. J., & Strathmann, H. (1988). Development of bipolar membranes. *Desalination*, *68*(2–3). https://doi.org/10.1016/0011-9164(88)80061-4

Bousek, J., Scroccaro, D., Sima, J., Weissenbacher, N., & Fuchs, W. (2016). Influence of the gas composition on the efficiency of ammonia stripping of biogas digestate. *Bioresource Technology*, *203*. https://doi.org/10.1016/j.biortech.2015.12.046

Cherif, A. T., Molenat, J., & Elmidaoui, A. (1997). Nitric acid and sodium hydroxide generation by electrodialysis using bipolar membranes. *Journal of Applied Electrochemistry*, *27*(9). https://doi.org/10.1023/A:1018438710451

Choi, E. Y., Choi, J. H., & Moon, S. H. (2003). An electrodialysis model for determination of the optimal current density. *Desalination*, *153*(1–3). https://doi.org/10.1016/S0011-9164(02)01134-7

Cruz, H., Law, Y. Y., Guest, J. S., Rabaey, K., Batstone, D., Laycock, B., Verstraete, W., & Pikaar, I. (2019). Mainstream ammonium recovery to advance sustainable urban wastewater management. In *Environmental Science and Technology* (Vol. 53, Issue 19). https://doi.org/10.1021/acs.est.9b00603

Cui, H., Ruan, H., Wei, H., Ang, E. H., Dong, Y., Lu, H., Liu, H., Liao, J., Xu, Y., & Shen, J. (2024). Innovative sodium acrylate wastewater resource recovery through electrodialysis with

integrated bipolar membranes. *Journal of Environmental Chemical Engineering*, *12*(2). https://doi.org/10.1016/j.jece.2024.112278

De Jaegher, B., Larumbe, E., De Schepper, W., Verliefde, A., & Nopens, I. (2020). Data on ion-exchange membrane fouling by humic acid during electrodialysis. *Data in Brief*, *31*. https://doi.org/10.1016/j.dib.2020.105763

Deckers, R. W. J. (2017). *Optimizing electrodialysis processes for concentrating ammonium rich streams*. http://repository.tudelft.nl/.

Dong, Y., Wei, H., Cui, H., Lu, H., Liao, J., Qiu, Y., & Shen, J. (2023). Techno-Economic Analysis of Bipolar Membranes Electrodialysis for the Hexacyanocobalic Acid Green Conversion. *Industrial and Engineering Chemistry Research*, *62*(49), 20996–21006. https://doi.org/10.1021/acs.iecr.3c02954

Doornbusch, G. J., Tedesco, M., Post, J. W., Borneman, Z., & Nijmeijer, K. (2019). Experimental investigation of multistage electrodialysis for seawater desalination. *Desalination*, *464*. https://doi.org/10.1016/j.desal.2019.04.025

Drosg, B., Fuchs, W., Al Seadi, T., Madsen, M., & Linke, B. (2020). Nutrient Recovery by Biogas Digestate Processing Bernhard. In *Integrated Sustainable Urban Water, Energy, and Solids Management*.

EL-Bourawi, M. S., Khayet, M., Ma, R., Ding, Z., Li, Z., & Zhang, X. (2007). Application of vacuum membrane distillation for ammonia removal. *Journal of Membrane Science*, *301*(1–2). https://doi.org/10.1016/j.memsci.2007.06.021

Foley, J., de Haas, D., Hartley, K., & Lant, P. (2010). Comprehensive life cycle inventories of alternative wastewater treatment systems. *Water Research*, *44*(5). https://doi.org/10.1016/j.watres.2009.11.031

Franken, T. (2000). Bipolar membrane technology and its applications. *Membrane Technology*, *2000*(125). https://doi.org/10.1016/S0958-2118(00)80212-8

Georg, S., Puari, A. T., Hanantyo, M. P. G., Sleutels, T., Kuntke, P., ter Heijne, A., & Buisman, C. J. N. (2023). Low-energy ammonium recovery by a combined bio-electrochemical and electrochemical system. *Chemical Engineering Journal*, *454*. https://doi.org/10.1016/j.cej.2022.140196

Graillon, S., Persin, F., Pourcelly, G., & Gavach, C. (1996). Development of electrodialysis with bipolar membrane for the treatment of concentrated nitrate effluents. *Desalination*, *107*(2). https://doi.org/10.1016/S0011-9164(96)00155-5

Guo, H., Yuan, P., Pavlovic, V., Barber, J., & Kim, Y. (2021). Ammonium sulfate production from wastewater and low-grade sulfuric acid using bipolar- and cation-exchange membranes. *Journal of Cleaner Production*, *285*. https://doi.org/10.1016/j.jclepro.2020.124888

Guo, X., Xiang, L., Sun, M., Wang, S., Ji, Z., Bi, J., & Zhao, Y. (2023). Selective electrodialysis process for the recovery of potassium from multicomponent solution systems. *Water Science and Technology*, *88*(5). https://doi.org/10.2166/wst.2023.269

Han, J. H., Hwang, K. sik, Jeong, H., Byeon, S. Y., Nam, J. Y., Kim, C. S., Kim, H., Yang, S. C., Choi, J. Y., & Jeong, N. (2019). Electrode system for large-scale reverse electrodialysis: water electrolysis, bubble resistance, and inorganic scaling. *Journal of Applied Electrochemistry*. https://doi.org/10.1007/s10800-019-01303-4

Huang, H., Yang, J., & Li, D. (2014). Recovery and removal of ammonia-nitrogen and phosphate from swine wastewater by internal recycling of struvite chlorination product. *Bioresource Technology*, *172*. https://doi.org/10.1016/j.biortech.2014.09.024

Huang, J., Kankanamge, N. R., Chow, C., Welsh, D. T., Li, T., & Teasdale, P. R. (2018). Removing ammonium from water and wastewater using cost-effective adsorbents: A review. In *Journal of Environmental Sciences (China)* (Vol. 63). https://doi.org/10.1016/j.jes.2017.09.009

Iskander, S. M., Brazil, B., Novak, J. T., & He, Z. (2016). Resource recovery from landfill leachate using bioelectrochemical systems: Opportunities, challenges, and perspectives. In *Bioresource Technology* (Vol. 201). https://doi.org/10.1016/j.biortech.2015.11.051

Jaime-Ferrer, J. S., Couallier, E., Viers, P., & Rakib, M. (2009). Two-compartment bipolar membrane electrodialysis for splitting of sodium formate into formic acid and sodium hydroxide: Modelling. *Journal of Membrane Science*, *328*(1–2). https://doi.org/10.1016/j.memsci.2008.10.058

Kang, H., Kim, E., & Jung, S. P. (2017). Influence of flowrates to a reverse electro-dialysis (RED) stack on performance and electrochemistry of a microbial reverse electrodialysis cell (MRC). *International Journal of Hydrogen Energy*, *42*(45). https://doi.org/10.1016/j.ijhydene.2017.06.187

Kim, Y., Walker, W. S., & Lawler, D. F. (2011). Electrodialysis with spacers: Effects of variation and correlation of boundary layer thickness. *Desalination*, *274*(1–3). https://doi.org/10.1016/j.desal.2011.01.076

Koivisto, E. S., Reuter, T., & Zevenhoven, R. (2023). Performance Optimization of Bipolar Membrane Electrodialysis of Ammonium Sulfate/Bisulfate Reagents for CO2 Mineralization. *ACS ES and T Water*, *3*(7). https://doi.org/10.1021/acsestwater.3c00028

Kroupa, J., Kinčl, J., & Cakl, J. (2015). Recovery of H2SO4 and NaOH from Na2SO4 by electrodialysis with heterogeneous bipolar membrane. *Desalination and Water Treatment*, *56*(12). https://doi.org/10.1080/19443994.2014.980972

Ledezma, P., Kuntke, P., Buisman, C. J. N., Keller, J., & Freguia, S. (2015). Source-separated urine opens golden opportunities for microbial electrochemical technologies. In *Trends in Biotechnology* (Vol. 33, Issue 4). https://doi.org/10.1016/j.tibtech.2015.01.007

Lee, H. J., Strathmann, H., & Moon, S. H. (2006). Determination of the limiting current density in electrodialysis desalination as an empirical function of linear velocity. *Desalination*, *190*(1–3). https://doi.org/10.1016/j.desal.2005.08.004

Li, F., Guo, Y., & Wang, S. (2022). Pilot-Scale Selective Electrodialysis for the Separation of Chloride and Sulphate from High-Salinity Wastewater. *Membranes*, *12*(6). https://doi.org/10.3390/membranes12060610

Li, P. F., Chen, Q. B., Wang, J., Xu, Y., Dong, L., & Wang, J. (2022). Developing a reclamation strategy for softening nanofiltration brine: A scaling-free conversion approach via continuous two-stage electrodialysis metathesis. *Science of the Total Environment*, *807*. https://doi.org/10.1016/j.scitotenv.2021.150374

Li, X., Wei, X., Yang, N., Wang, X., Wang, Q., & Wu, K. (2024). Process for Producing Lithium Iodide Cleanly through Electrodialysis Metathesis. *ACS Omega*. https://doi.org/10.1021/acsomega.4c00643

Li, Y., Shi, S., Cao, H., Wu, X., Zhao, Z., & Wang, L. (2016). Bipolar membrane electrodialysis for generation of hydrochloric acid and ammonia from simulated ammonium chloride wastewater. *Water Research*, *89*. https://doi.org/10.1016/j.watres.2015.11.038

Liu, H., & She, Q. (2024). Scaling-Enhanced Scaling during Electrodialysis Desalination. *ACS ES and T Engineering*, *4*(5). https://doi.org/10.1021/acsestengg.3c00549

Liu, Y., Dai, L., Ke, X., Ding, J., Wu, X., Chen, R., Ding, R., & Van der Bruggen, B. (2022). Arsenic and cation metal removal from copper slag using a bipolar membrane electrodialysis system. *Journal of Cleaner Production*, *338*. https://doi.org/10.1016/j.jclepro.2022.130662

Liu, Y., Wu, X., Wu, X., Dai, L., Ding, J., Ye, X., Chen, R., Ding, R., Liu, J., Jin, Y., & Van der Bruggen, B. (2023). Recovery of nickel, phosphorus and nitrogen from electroless nickel-plating wastewater using bipolar membrane electrodialysis. *Journal of Cleaner Production*, *382*. https://doi.org/10.1016/j.jclepro.2022.135326

Mafé, S., Ramírez, P., & Alcaraz, A. (1998). Electric field-assisted proton transfer and water dissociation at the junction of a fixed-charge bipolar membrane. *Chemical Physics Letters*, *294*(4–5). https://doi.org/10.1016/S0009-2614(98)00877-X

Mani, K. N. (1991). Electrodialysis water splitting technology. *Journal of Membrane Science*, *58*(2). https://doi.org/10.1016/S0376-7388(00)82450-3

Min, K. J., Kim, J. H., Oh, E. J., Ryu, J. H., & Park, K. Y. (2021). Flow velocity and cell pair number effect on current efficiency in plating wastewater treatment through electrodialysis. *Environmental Engineering Research*, *26*(2). https://doi.org/10.4491/eer.2019.502

Nosova, E., Achoh, A., Zabolotsky, V., & Melnikov, S. (2022). Electrodialysis Desalination with Simultaneous pH Adjustment Using Bilayer and Bipolar Membranes, Modeling and Experiment. *Membranes*, *12*(11). https://doi.org/10.3390/membranes12111102

Omran, K. A., Goher, M. E., & El-Shamy, A. S. (2023). Factors Affecting Electrodialysis Unit Performance in the Removal of Copper from Wastewaters and Aquatic Environment Treatment. *Egyptian Journal of Aquatic Biology and Fisheries*, *27*(3). https://doi.org/10.21608/ejabf.2023.298889

Pourcelly, G. (2002). Electrodialysis with bipolar membranes: Principles, optimization, and applications. *Russian Journal of Electrochemistry*, *38*(8). https://doi.org/10.1023/A:1016882216287

Raissouni, I., Marraha, M., & Azmani, A. (2007). Effect of some parameters on the improvement of the bipolar membrane electrodialysis process. *Desalination*, *208*(1–3). https://doi.org/10.1016/j.desal.2006.03.584

Rodrigues, M., De Mattos, T. T., Sleutels, T., Ter Heijne, A., Hamelers, H. V. M., Buisman, C. J. N., & Kuntke, P. (2020). Minimal Bipolar Membrane Cell Configuration for Scaling up Ammonium Recovery. *ACS Sustainable Chemistry and Engineering*, *8*(47). https://doi.org/10.1021/acssuschemeng.0c05043

Shen, J., Huang, J., Liu, L., Ye, W., Lin, J., & Van der Bruggen, B. (2013). The use of BMED for glyphosate recovery from glyphosate neutralization liquor in view of zero discharge. *Journal of Hazardous Materials*, *260*. https://doi.org/10.1016/j.jhazmat.2013.06.028

Shi, L., Hu, Y., Xie, S., Wu, G., Hu, Z., & Zhan, X. (2018). Recovery of nutrients and volatile fatty acids from pig manure hydrolysate using two-stage bipolar membrane electrodialysis. *Chemical Engineering Journal*, *334*. https://doi.org/10.1016/j.cej.2017.10.010

Simons, R. (1993). Preparation of a high performance bipolar membrane. *Journal of Membrane Science*, *78*(1–2). https://doi.org/10.1016/0376-7388(93)85243-P

Sonu Vinay, Barber John, Ramanan Harikrishnan, & Sridharan Varshneya. (2016). *Electrodialysis spacer and stack*.

Sotres, A., Cerrillo, M., Viñas, M., & Bonmatí, A. (2015). Nitrogen recovery from pig slurry in a two-chambered bioelectrochemical system. *Bioresource Technology*, *194*. https://doi.org/10.1016/j.biortech.2015.07.036

Strathmann, H. (1995). Chapter 6 Electrodialysis and related processes. *Membrane Science and Technology*, *2*(C). https://doi.org/10.1016/S0927-5193(06)80008-2

Van Geluwe, S., Braeken, L., Robberecht, T., Jans, M., Creemers, C., & Van Der Bruggen, B. (2011). Evaluation of electrodialysis for scaling prevention of nanofiltration membranes at high water recoveries. *Resources, Conservation and Recycling*, *56*(1). https://doi.org/10.1016/j.resconrec.2011.09.001

van Linden, N., Bandinu, G. L., Vermaas, D. A., Spanjers, H., & van Lier, J. B. (2020). Bipolar membrane electrodialysis for energetically competitive ammonium removal and dissolved ammonia production. *Journal of Cleaner Production*, *259*. https://doi.org/10.1016/j.jclepro.2020.120788

van Linden, N., Spanjers, H., & van Lier, J. B. (2019). Application of dynamic current density for increased concentration factors and reduced energy consumption for concentrating ammonium by electrodialysis. *Water Research*, *163*. https://doi.org/10.1016/j.watres.2019.114856

Walker, W. S., Kim, Y., & Lawler, D. F. (2014). Treatment of model inland brackish groundwater reverse osmosis concentrate with electrodialysis-Part I: Sensitivity to superficial velocity. *Desalination*, *344*. https://doi.org/10.1016/j.desal.2014.03.035

Wang, D., Meng, W., Lei, Y., Li, C., Cheng, J., Qu, W., Wang, G., Zhang, M., & Li, S. (2020). The novel strategy for increasing the efficiency and yield of the bipolar membrane electrodialysis by the double conjugate salts stress. *Polymers*, *12*(2). https://doi.org/10.3390/polym12020343

Wang, S., Wu, X., Xu, S., Leng, Q., Jin, D., Wang, P., Dong, F., & Wu, D. (2023). Energetic evaluation of phenol wastewater treatment by reverse electrodialysis reactor using different anodes. *Journal of Environmental Management*, *329*. https://doi.org/10.1016/j.jenvman.2022.117089

Wu, H., & Vaneeckhaute, C. (2022). Nutrient recovery from wastewater: A review on the integrated Physicochemical technologies of ammonia stripping, adsorption and struvite precipitation. In *Chemical Engineering Journal* (Vol. 433). https://doi.org/10.1016/j.cej.2021.133664

Wu, X., Lv, Y., Sun, D., Zhang, Y., & Xu, S. (2023). Effects of electrode rinse solution on performance of hydrogen and electricity cogeneration system by reverse electrodialysis. *Energy Conversion and Management*, *287*. https://doi.org/10.1016/j.enconman.2023.117122

Xiang, S., Liu, Y., Zhang, G., Ruan, R., Wang, Y., Wu, X., Zheng, H., Zhang, Q., & Cao, L. (2020). New progress of ammonia recovery during ammonia nitrogen removal from various wastewaters. In *World Journal of Microbiology and Biotechnology* (Vol. 36, Issue 10). https://doi.org/10.1007/s11274-020-02921-3

Xie, M., Shon, H. K., Gray, S. R., & Elimelech, M. (2016). Membrane-based processes for wastewater nutrient recovery: Technology, challenges, and future direction. In *Water Research* (Vol. 89). https://doi.org/10.1016/j.watres.2015.11.045

Yan, H., Wang, Y., Wu, L., Shehzad, M. A., Jiang, C., Fu, R., Liu, Z., & Xu, T. (2019). Multistage-batch electrodialysis to concentrate high-salinity solutions: Process optimisation, water transport, and energy consumption. *Journal of Membrane Science*, *570–571*. https://doi.org/10.1016/j.memsci.2018.10.008

Yan, T., Ye, Y., Ma, H., Zhang, Y., Guo, W., Du, B., Wei, Q., Wei, D., & Ngo, H. H. (2018). A critical review on membrane hybrid system for nutrient recovery from wastewater. In *Chemical Engineering Journal* (Vol. 348). https://doi.org/10.1016/j.cej.2018.04.166

Yang, D., Liu, H., & She, Q. (2023). Mixed cation transport behaviours in electrodialysis during simultaneous ammonium enrichment and wastewater desalination. *Desalination*, *545*. https://doi.org/10.1016/j.desal.2022.116155

Yang, J., Ul Afsar, N., Chen, Q., Fu, R., Liu, Z., Ge, L., & Xu, T. (2024). Treatment of simulated brominated butyl rubber wastewater using monovalent anion perm-selective membranes through selective electrodialysis. *Separation and Purification Technology*, *344*, 127293. https://doi.org/10.1016/J.SEPPUR.2024.127293

Yasri, N. G., & Gunasekaran, S. (2017). Electrochemical technologies for environmental remediation. In *Enhancing Cleanup of Environmental Pollutants* (Vol. 2). https://doi.org/10.1007/978-3-319-55423-5_2

Ye, Y., Ngo, H. H., Guo, W., Liu, Y., Chang, S. W., Nguyen, D. D., Liang, H., & Wang, J. (2018). A critical review on ammonium recovery from wastewater for sustainable wastewater management. In *Bioresource Technology* (Vol. 268). https://doi.org/10.1016/j.biortech.2018.07.111

Zhang, G., Wang, Q., Guan, W., Zeng, L., Li, Q., Cao, Z., Xiao, L., & Zhou, Q. (2019). Batch preparation of ammonium isopolymolybdate solution from ammonium molybdate solutions using bipolar membrane electrodialysis. *Separation and Purification Technology*, *209*. https://doi.org/10.1016/j.seppur.2018.09.015

Zhou, Y., Yan, H., Wang, X., Wang, Y., & Xu, T. (2016). A closed loop production of water insoluble organic acid using bipolar membranes electrodialysis (BMED). *Journal of Membrane Science*, *520*. https://doi.org/10.1016/j.memsci.2016.08.011

Zoungrana, A., & Çakmakci, M. (2021). Optimization of the reverse electrodialysis power output through the ratio of the feed solutions salinity. *IET Renewable Power Generation*, *15*(4). https://doi.org/10.1049/rpg2.12066

# 8. Appendix

## A. Calibration of pump

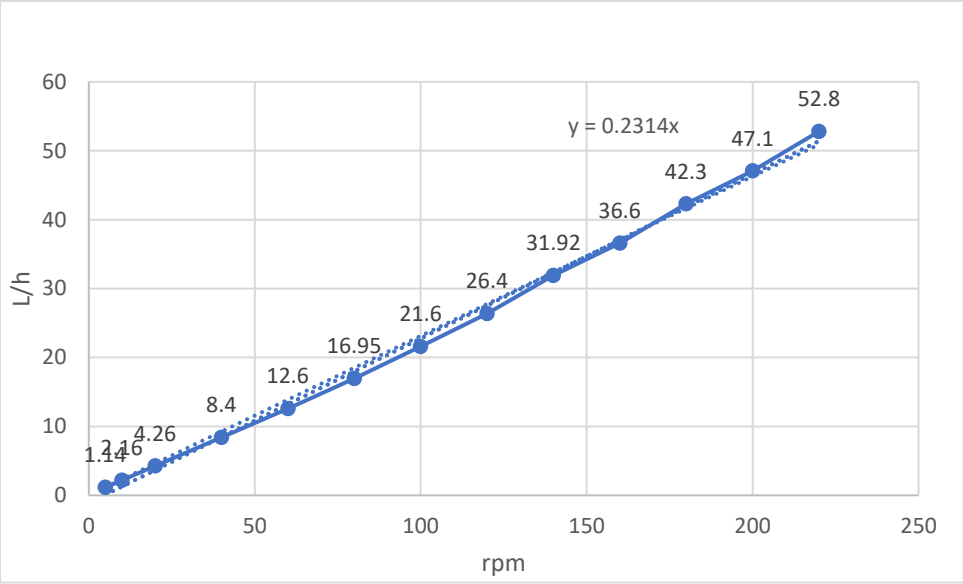


*Figure A. 1Pump Calibration*

## B. Current Density

### B.1 $NH_4^+$ concentration over time

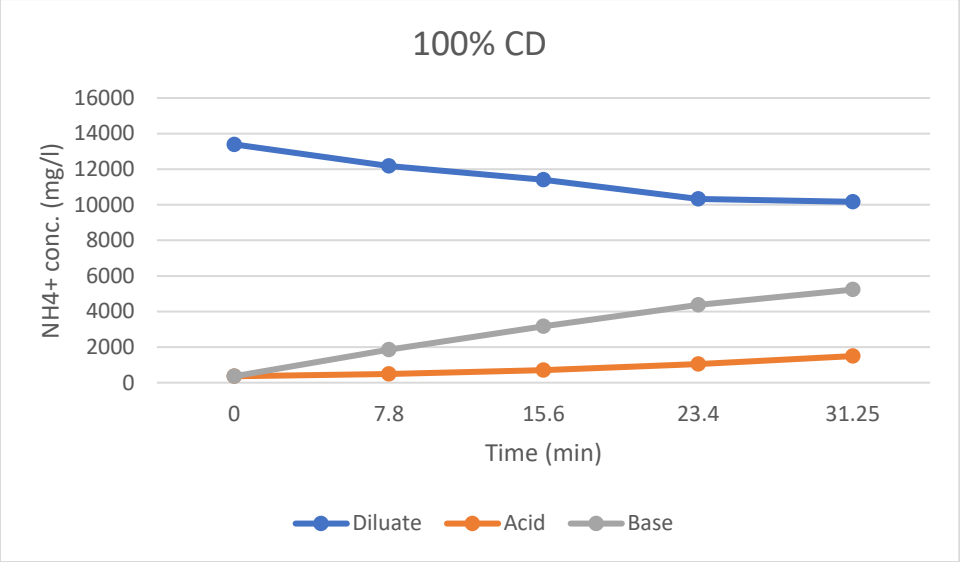


*Figure B.1. 1 100% current density: Average $NH_4^+$ mass distribution over experimental time of 31 mins 15 sec (i.e., 31.25 mins)*

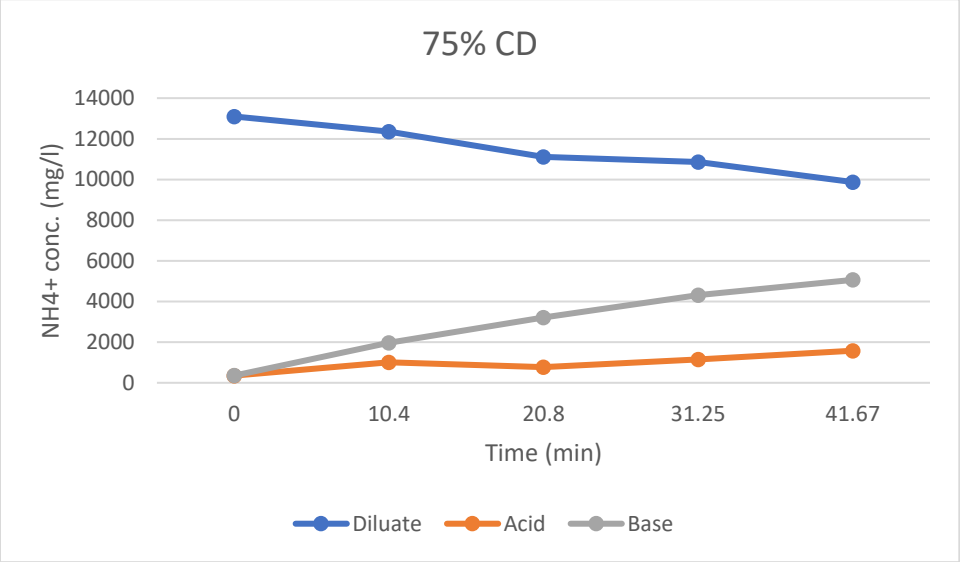


*Figure B.1. 2 75% current density: Average $NH_4^+$ mass distribution over experimental time of 41 mins 40 sec (i.e., 41.67 mins)*

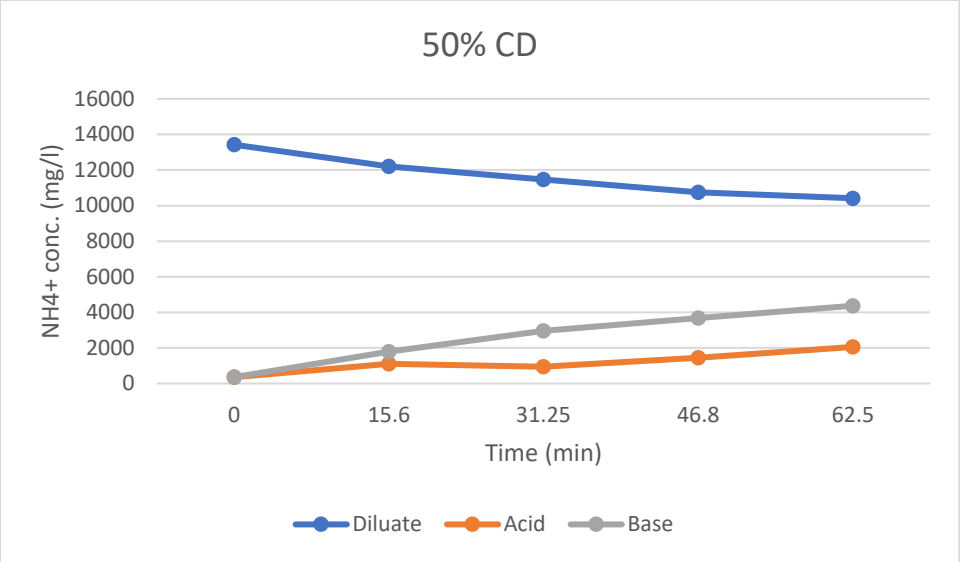


*Figure B.1. 3 50% current density: Average $NH_4^+$ mass distribution over experimental time of 1 hour 2 mins 30 sec (i.e., 62.5 mins)*

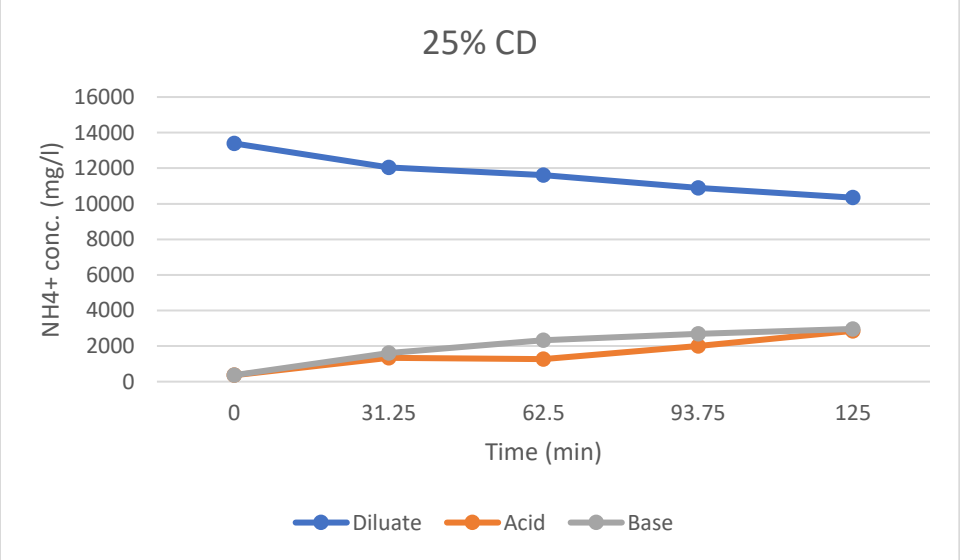


*Figure B.1. 4 25% current density: Average $NH_4^+$ mass distribution over experimental time of 2 hours 5 mins (i.e., 125 mins)*

## B.2 pH and EC graphs over time

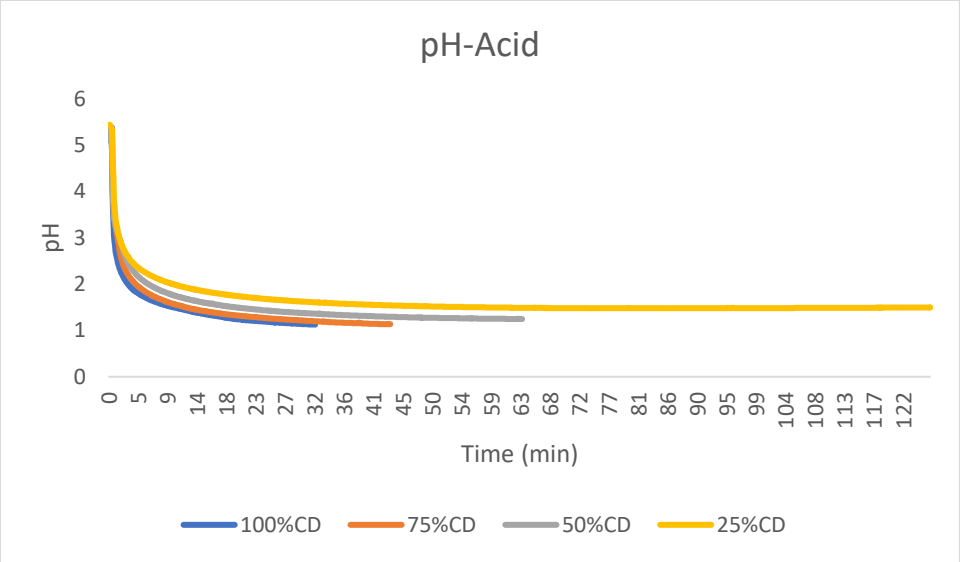


*Figure B.2. 1 Average pH of Acid over time for varied current densities*

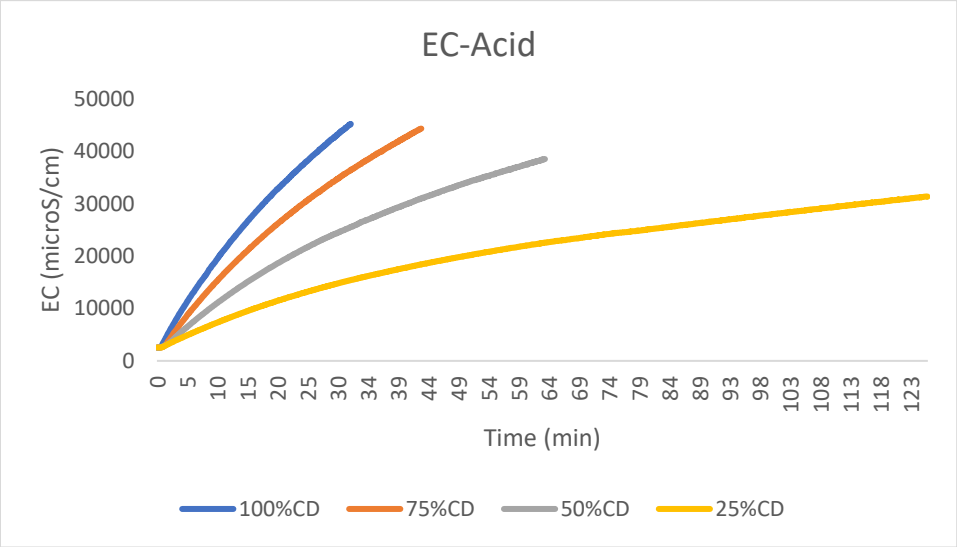


*Figure B.2. 2 Average electrical conductivity (µS/cm) of Acid over time for varied current densities*

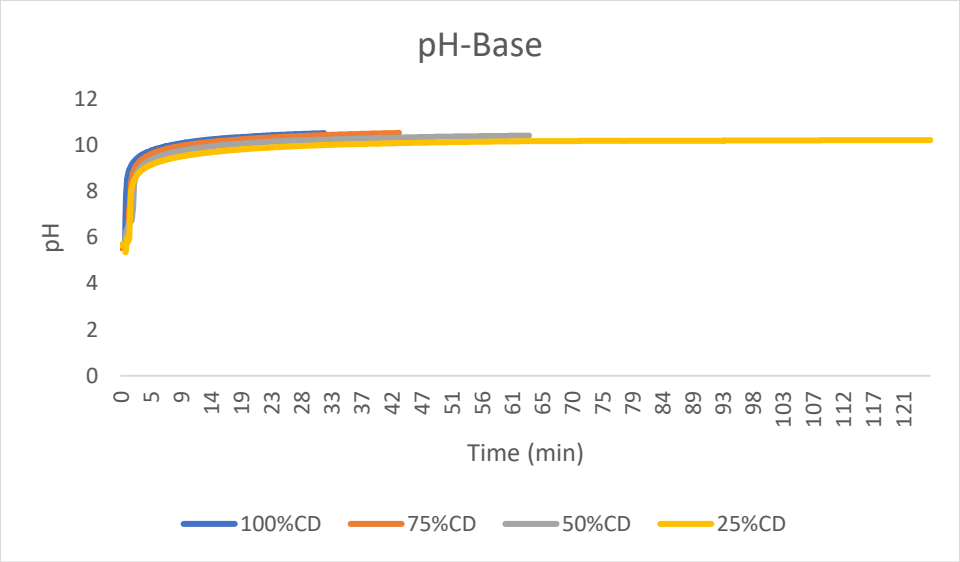


*Figure B.2. 3 Average pH of Base over time for varied current densities*

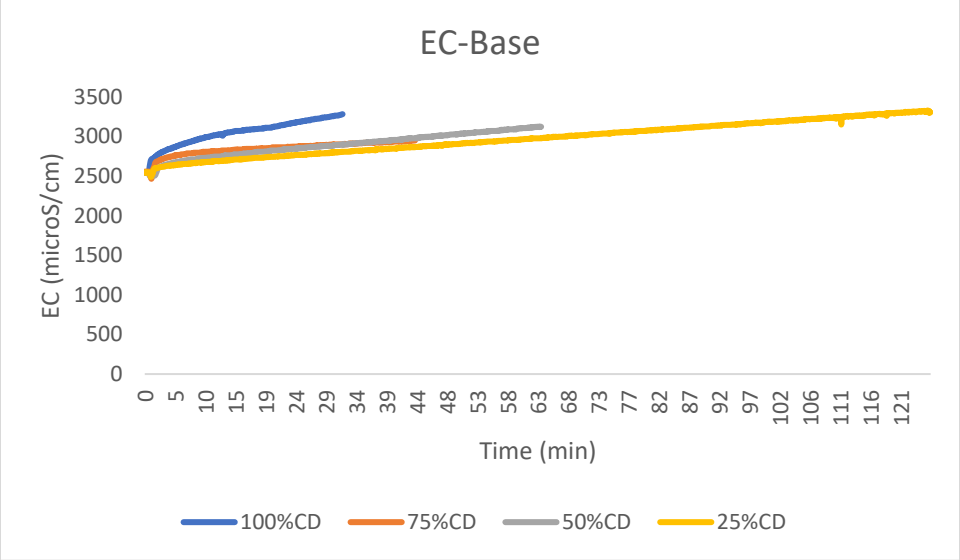


*Figure B.2. 4 Average electrical conductivity (µS/cm) of Base over time for varied current densities*

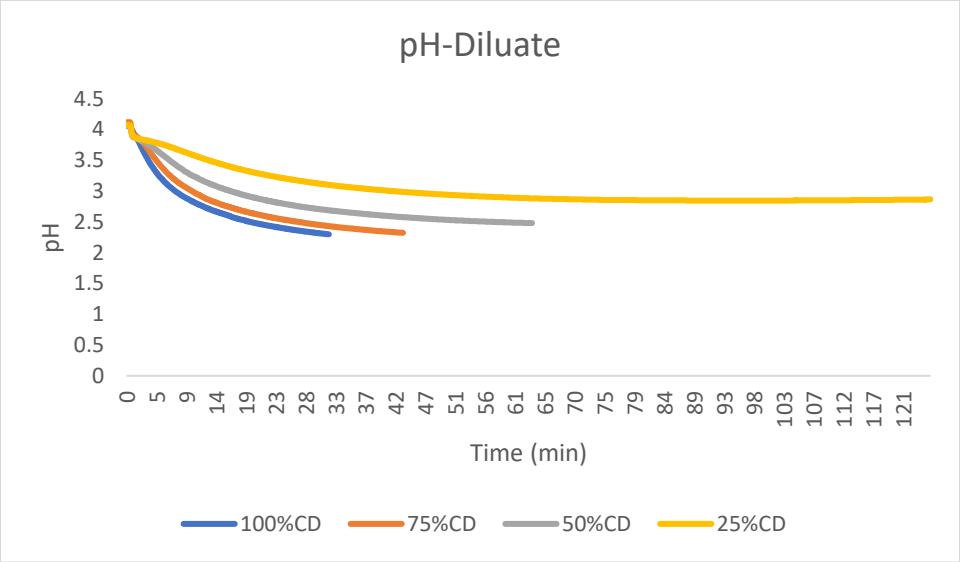


*Figure B.2. 5 Average pH of Diluate over time for varied current densities*

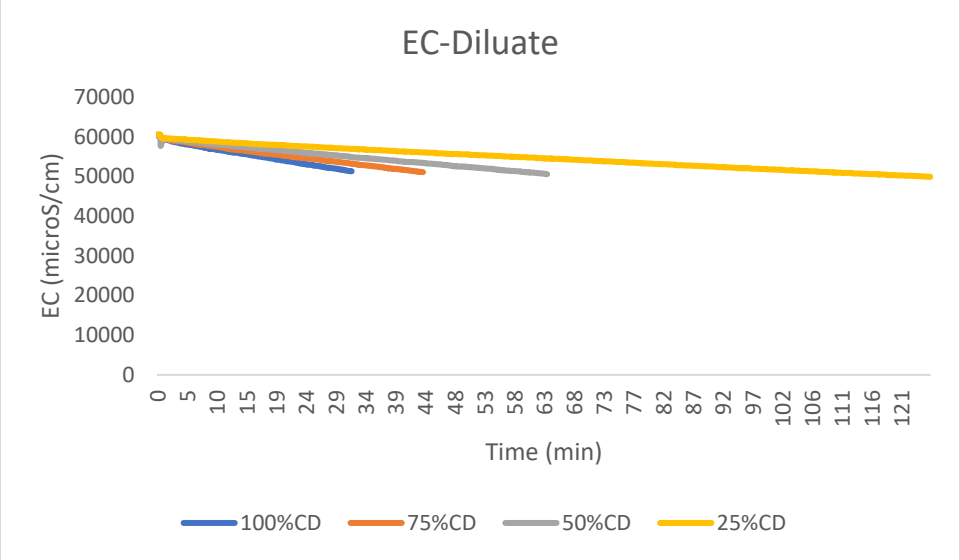


*Figure B.2. 6 Average electrical conductivity (µS/cm) of Diluate over time for varied current densities*

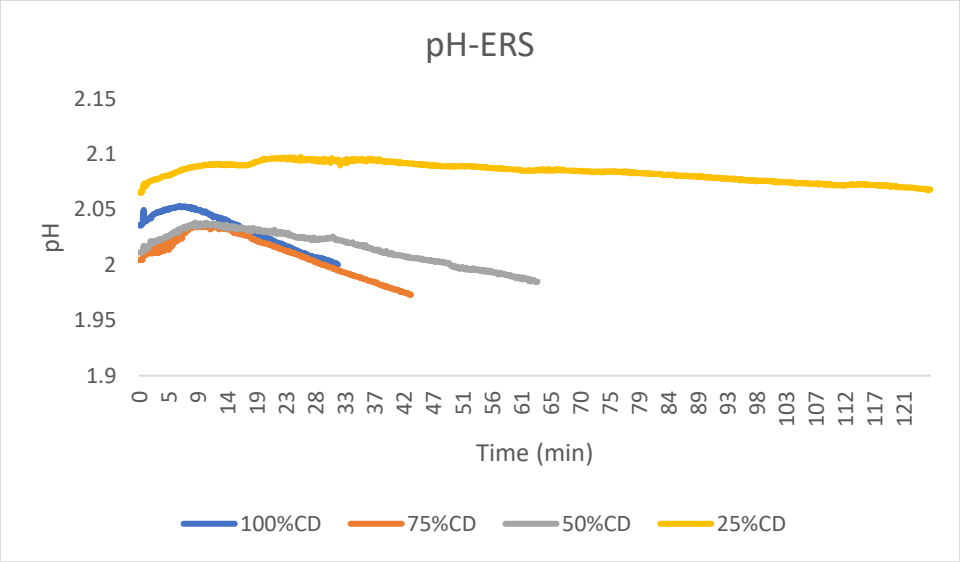


*Figure B.2. 7 Average pH of ERS over time for varied current densities*

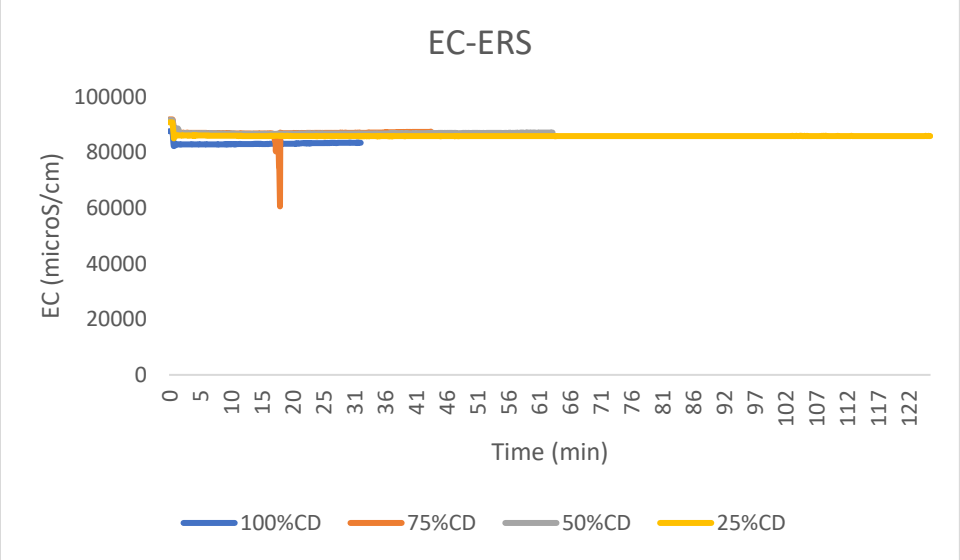


*Figure B.2. 8 Average electrical conductivity (µS/cm) of ERS over time for varied current densities*

## C. Flow rate

### C.1 $NH_4^+$ concentration over time

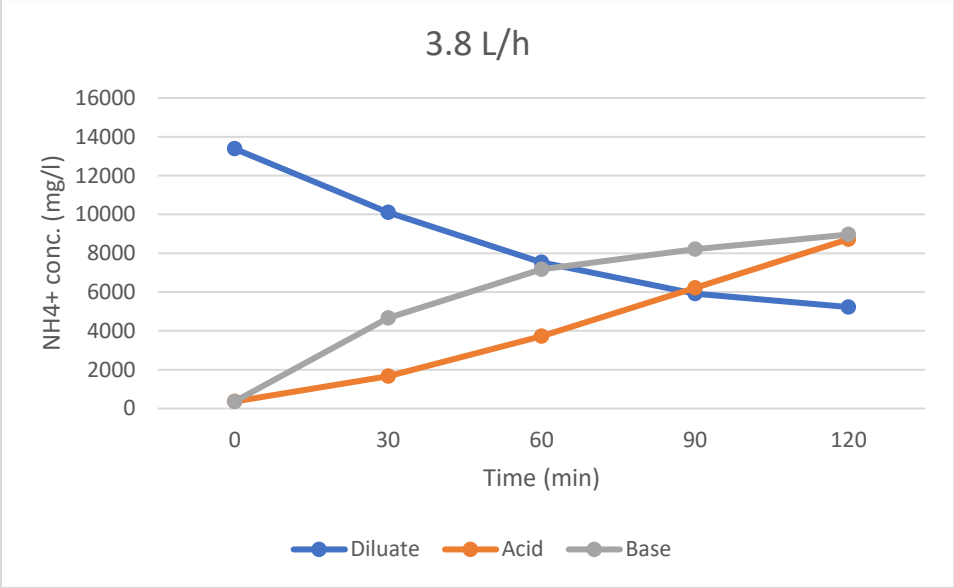


*Figure C.1. 1 3.8 L/h flow rate: Average $NH_4^+$ mass distribution over an experimental time of 120 minutes.*

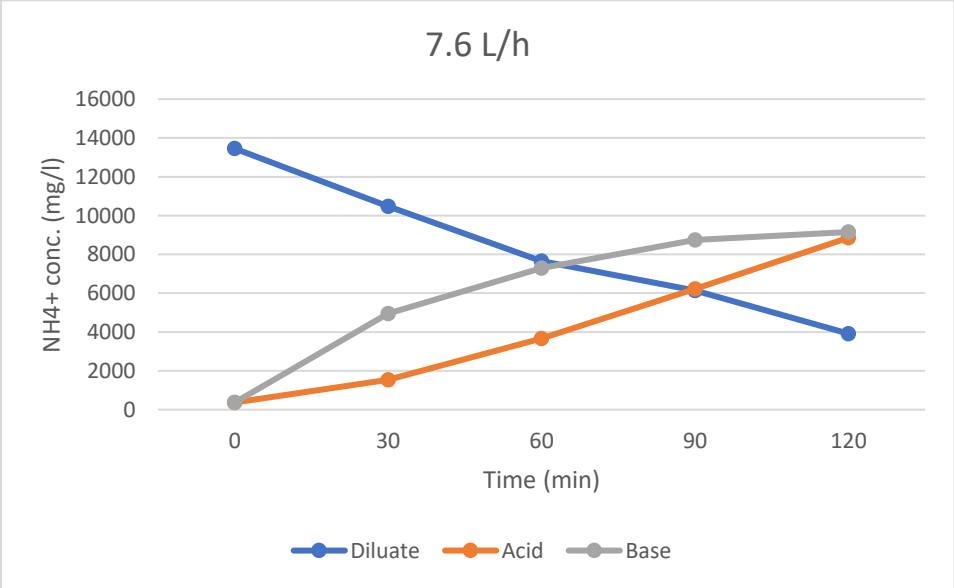


*Figure C.1. 2 7.6 L/h flow rate: Average $NH_4^+$ mass distribution over an experimental time of 120 minutes.*

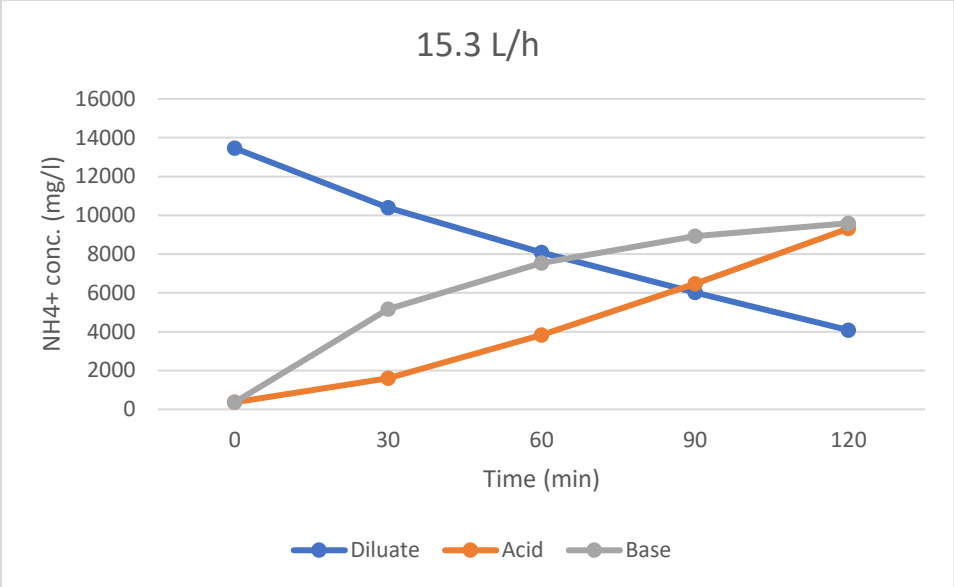


*Figure C.1. 3 15.3 L/h flow rate: Average $NH_4^+$ mass distribution over an experimental time of 120 minutes.*

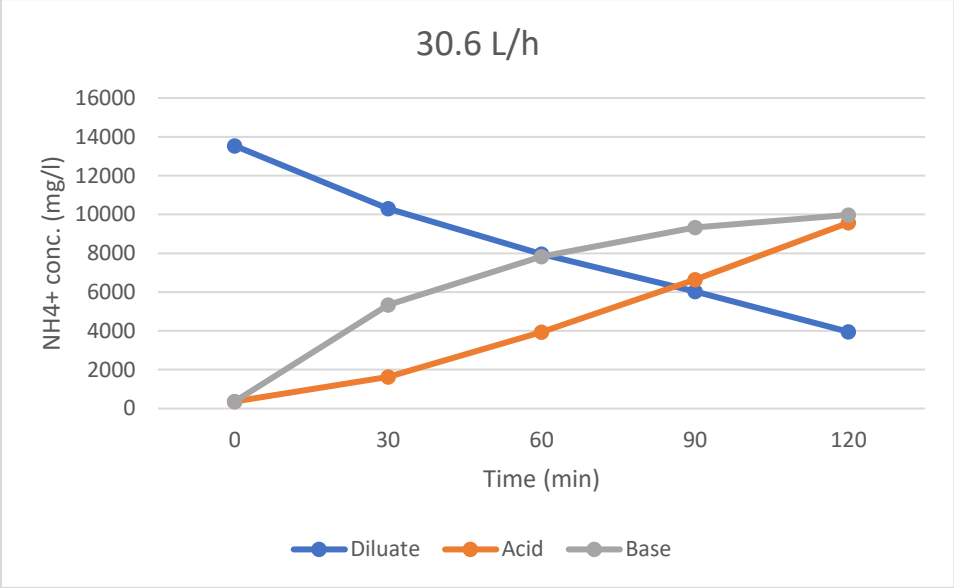


*Figure C.1. 4 30.6 L/h flow rate: Average $NH_4^+$ mass distribution over an experimental time of 120 minutes.*

## C.2 pH and EC graphs over time

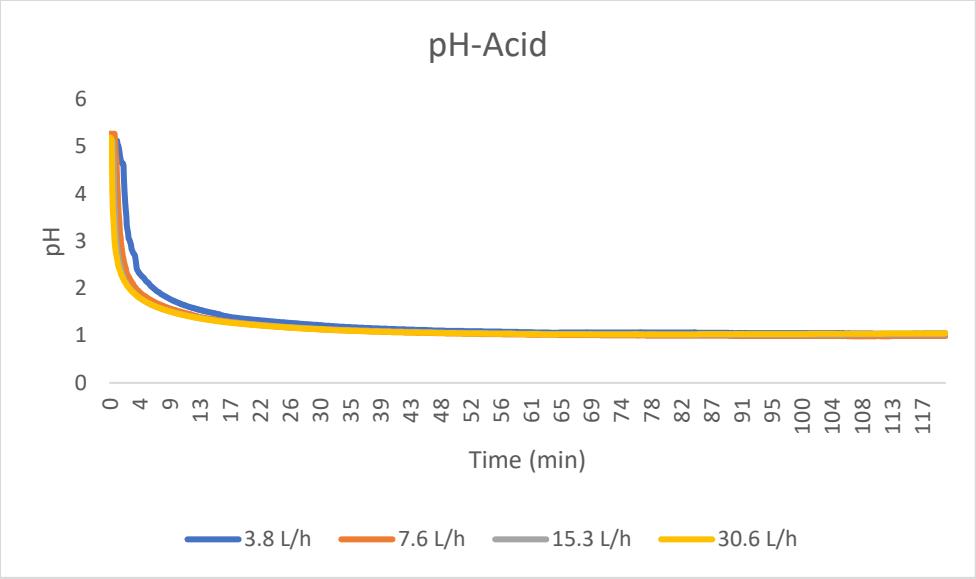


*Figure C.2. 1 Average pH of Acid over time for varied flow rates where 3.8 L/h, 7.6 L/h, 15.3 L/h, and 30.6 L/h flow rates correspond to 0.5, 1, 2, and 4 cm/s crossflow velocities.*

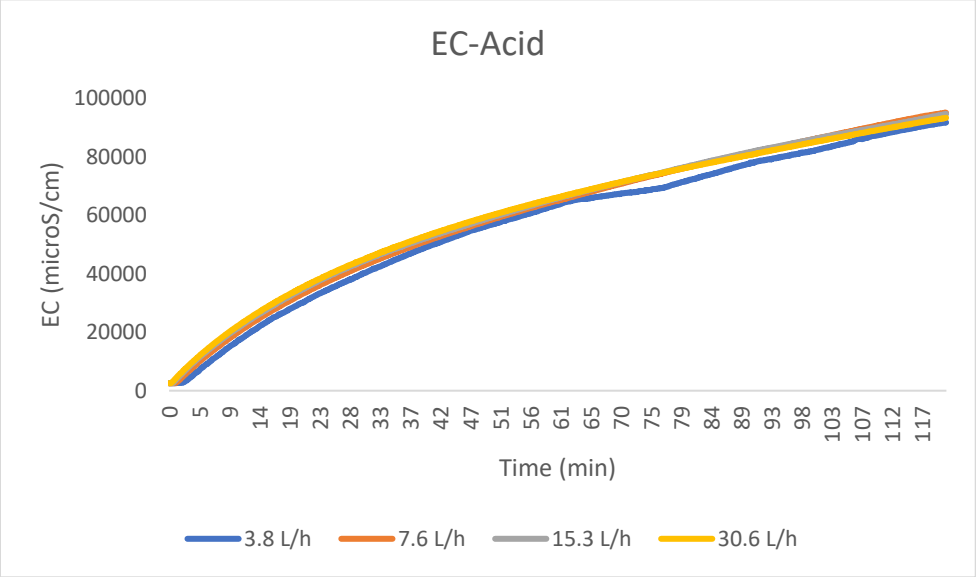


*Figure C.2. 2 Average electrical conductivity (µS/cm) of Acid over time for varied flow rates where 3.8 L/h, 7.6 L/h, 15.3 L/h, and 30.6 L/h flow rates correspond to 0.5, 1, 2, and 4 cm/s crossflow velocities.*

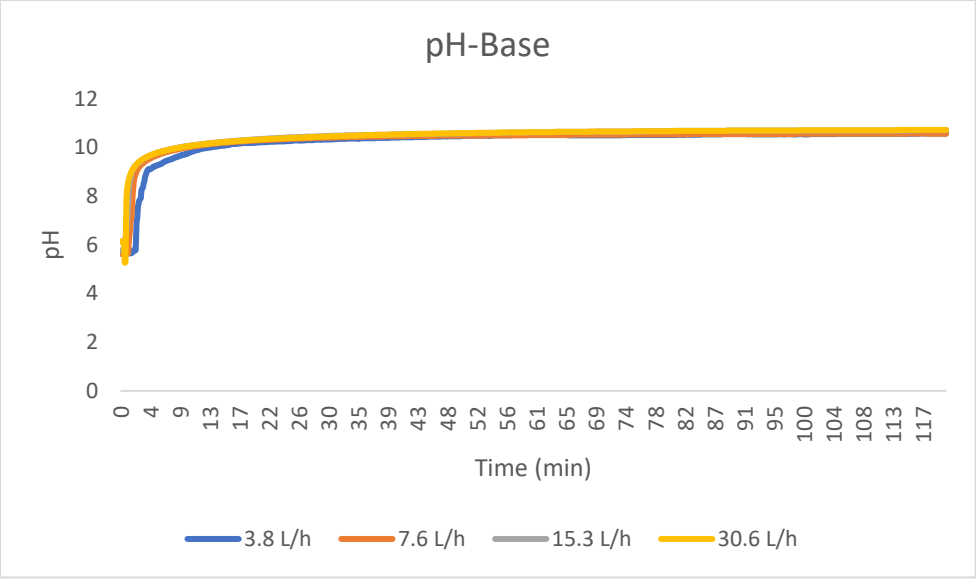


*Figure C.2. 3 Average pH of Base over time for varied flow rates where 3.8 L/h, 7.6 L/h, 15.3 L/h, and 30.6 L/h flow rates correspond to 0.5, 1, 2, and 4 cm/s crossflow velocities.*

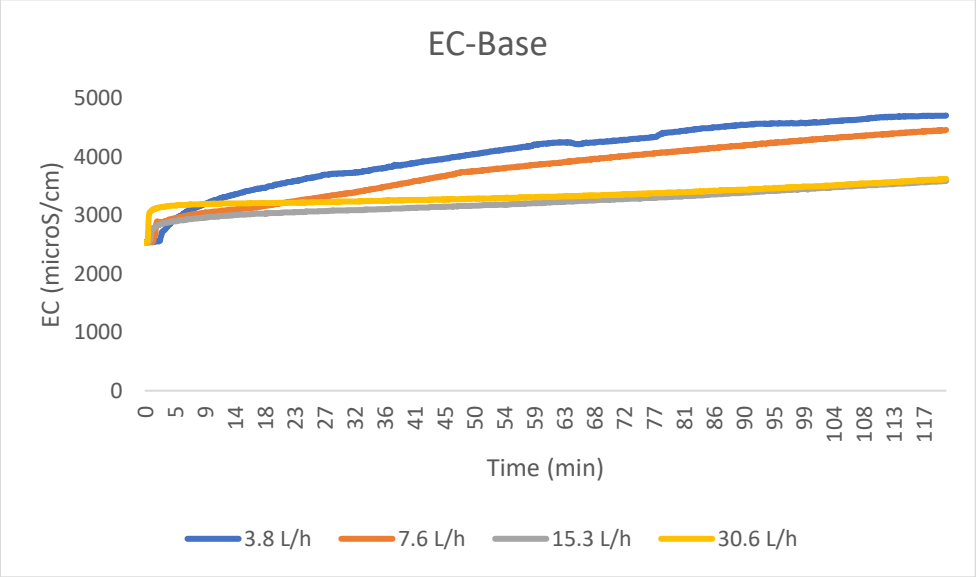


*Figure C.2. 4 Average electrical conductivity (µS/cm) of Base over time for varied flow rates where 3.8 L/h, 7.6 L/h, 15.3 L/h, and 30.6 L/h flow rates correspond to 0.5, 1, 2, and 4 cm/s crossflow velocities.*

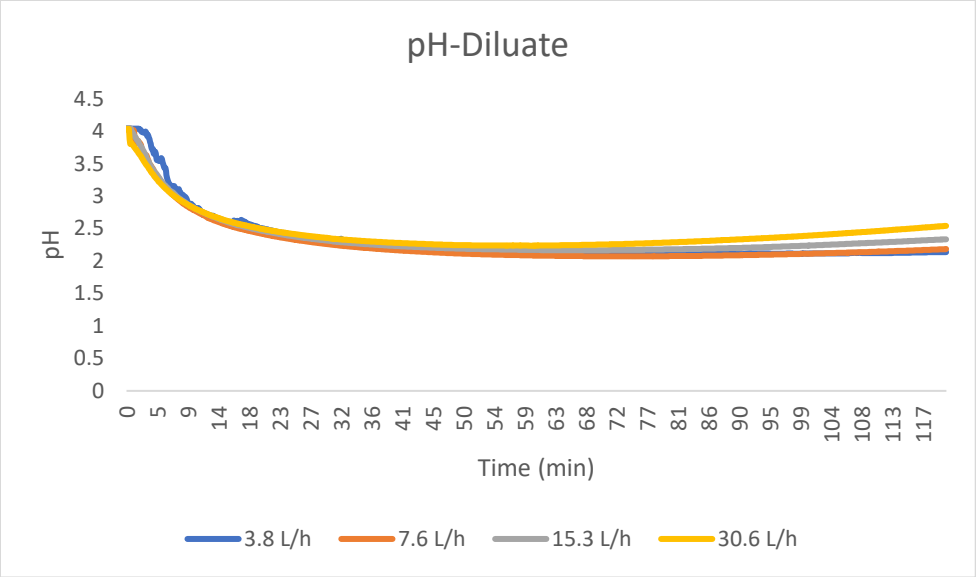


*Figure C.2. 5 Average pH of Diluate over time for varied flow rates where 3.8 L/h, 7.6 L/h, 15.3 L/h, and 30.6 L/h flow rates correspond to 0.5, 1, 2, and 4 cm/s crossflow velocities.*

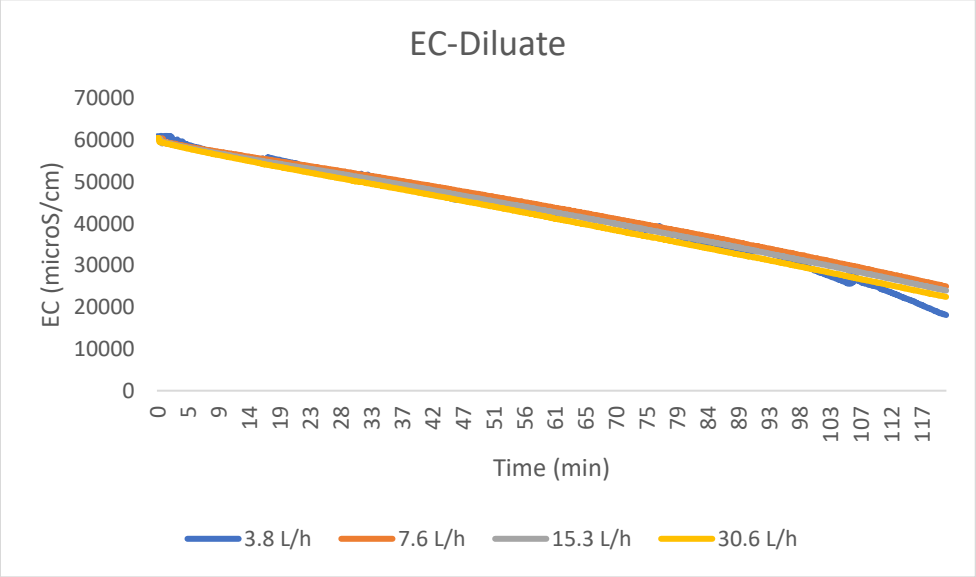


*Figure C.2. 6 Average electrical conductivity (µS/cm) of Diluate over time for varied flow rates where 3.8 L/h, 7.6 L/h, 15.3 L/h, and 30.6 L/h flow rates correspond to 0.5, 1, 2, and 4 cm/s crossflow velocities.*

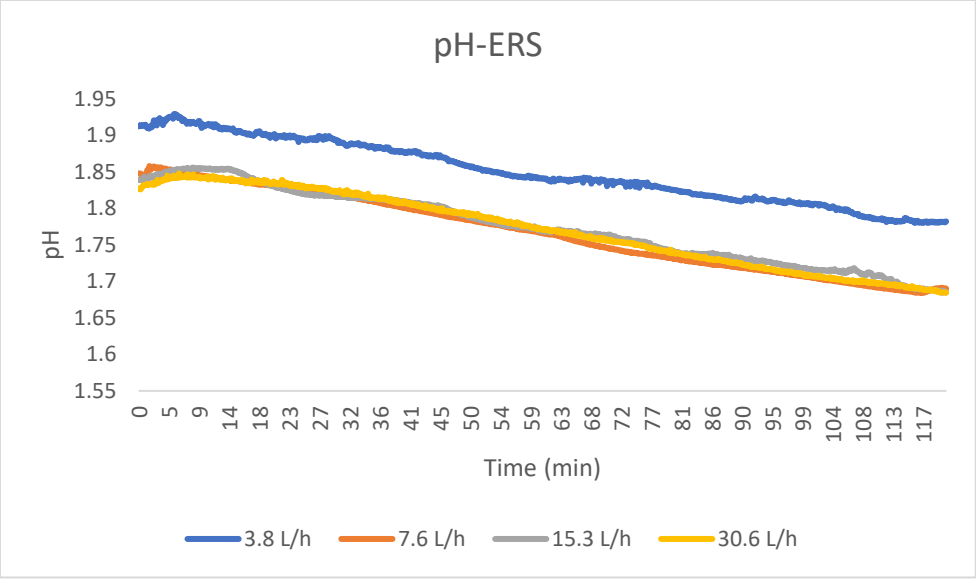


*Figure C.2. 7 Average pH of ERS over time for varied flow rates where 3.8 L/h, 7.6 L/h, 15.3 L/h, and 30.6 L/h flow rates correspond to 0.5, 1, 2, and 4 cm/s crossflow velocities.*

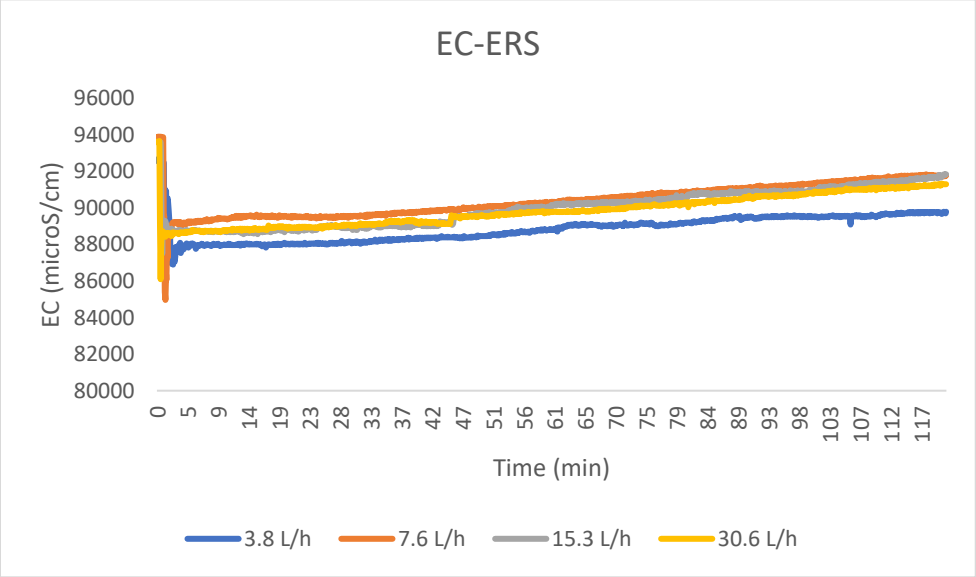


*Figure C.2. 8 Average electrical conductivity (µS/cm) of ERS over time for varied flow rates where 3.8 L/h, 7.6 L/h, 15.3 L/h, and 30.6 L/h flow rates correspond to 0.5, 1, 2, and 4 cm/s crossflow velocities.*

## D. Base Volume

### D.1 $NH_4^+$ concentration over time

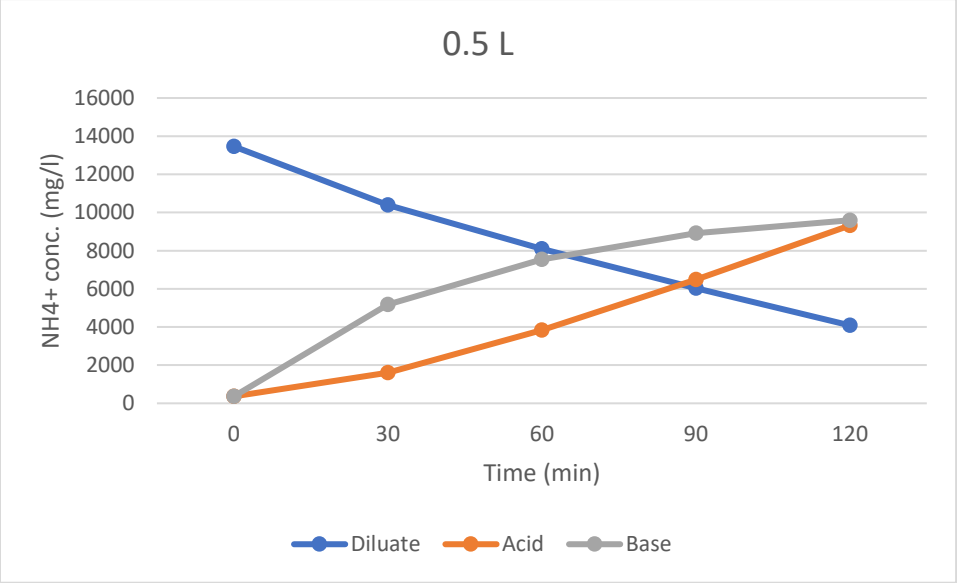


*Figure D.1. 1 0.5 L Base volume: Average $NH_4^+$ mass distribution over an experimental time of 120 minutes.*

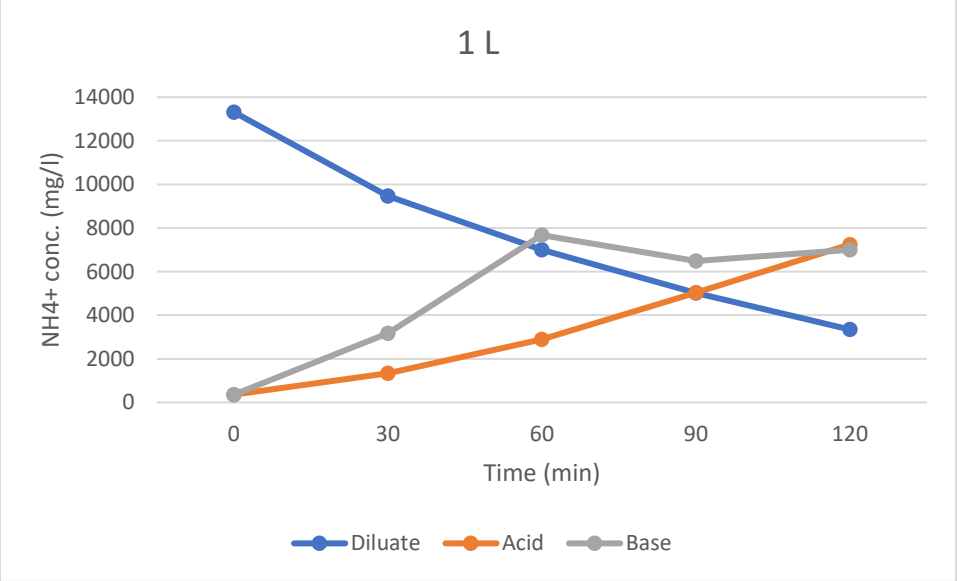


*Figure D.1. 2 1 L Base volume: Average $NH_4^+$ mass distribution over an experimental time of 120 minutes.*

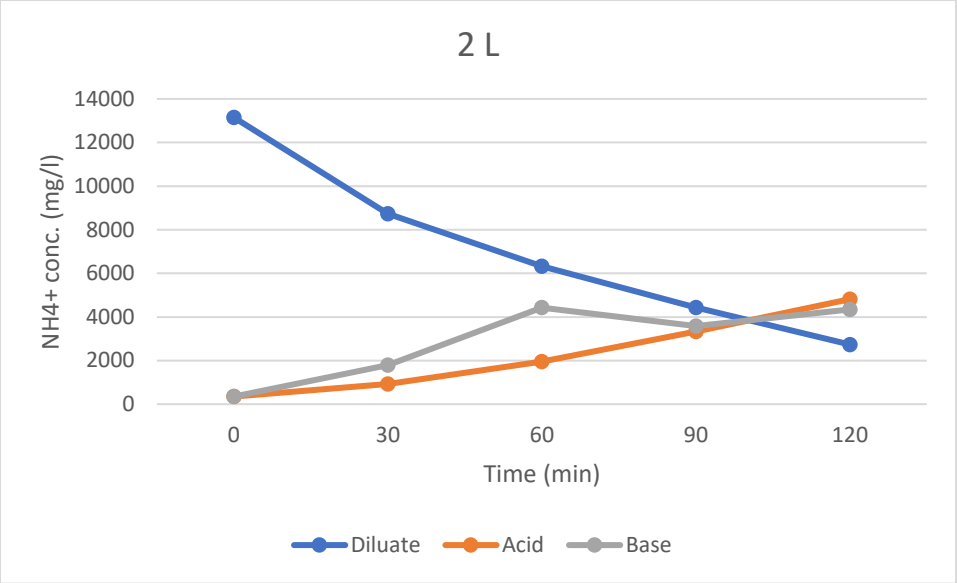


*Figure D.1. 3 2 L Base volume: Average $NH_4^+$ mass distribution over an experimental time of 120 minutes.*

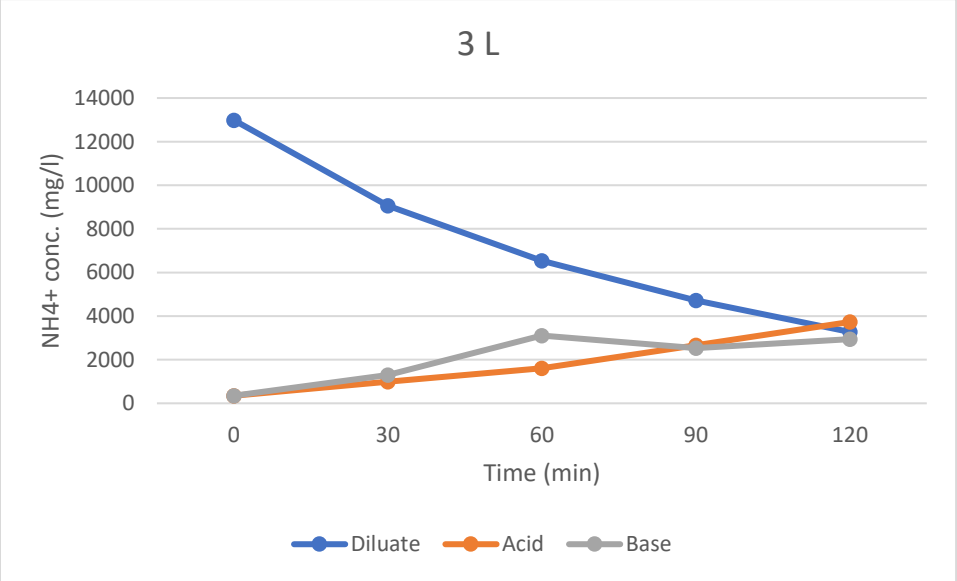


*Figure D.1. 4 3 L Base volume: Average $NH_4^+$ mass distribution over an experimental time of 120 minutes.*

## D.2 pH and EC graphs over time

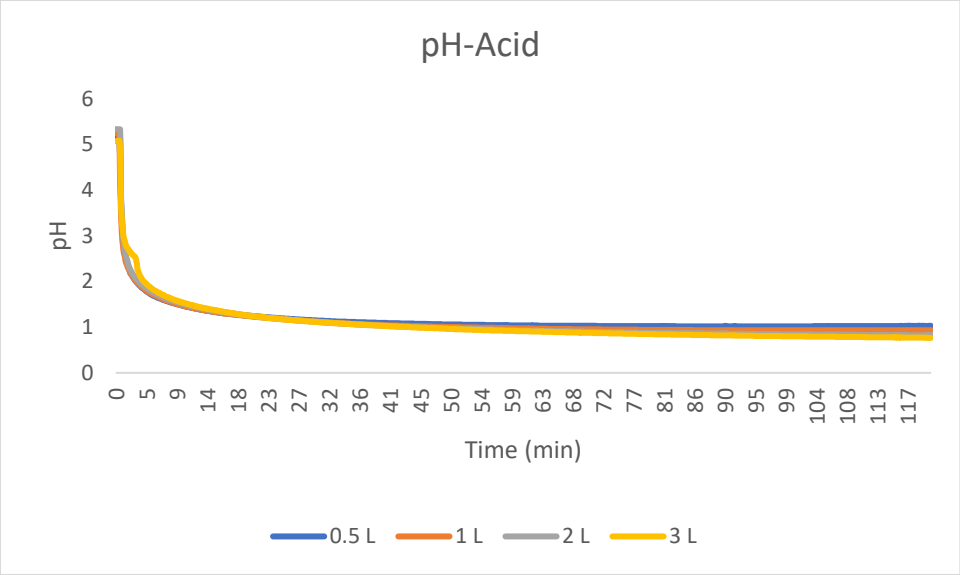


*Figure D.2. 1 Average pH of Acid over time for varied base volumes*

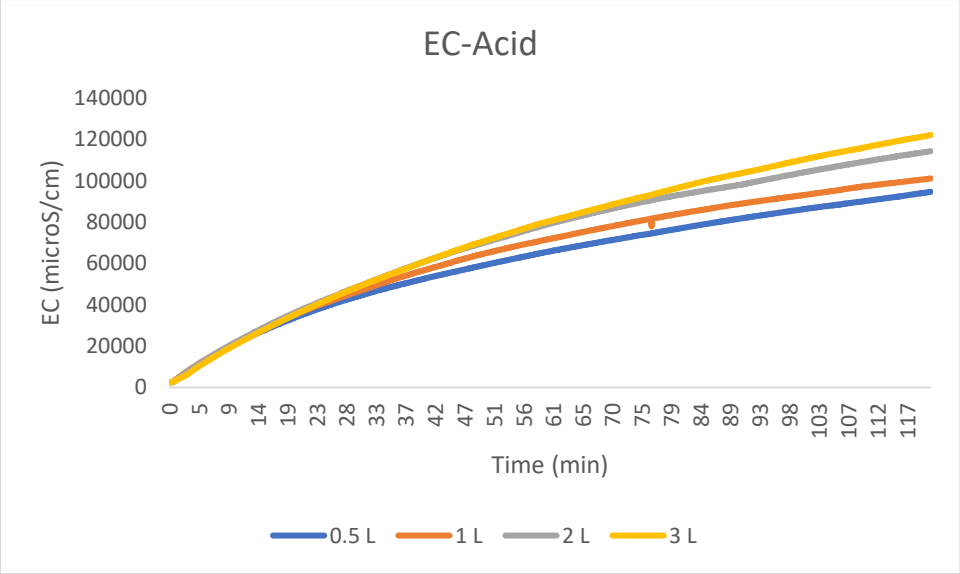


*Figure D.2. 2 Average electrical conductivity (µS/cm) of Acid over time for varied base volumes*

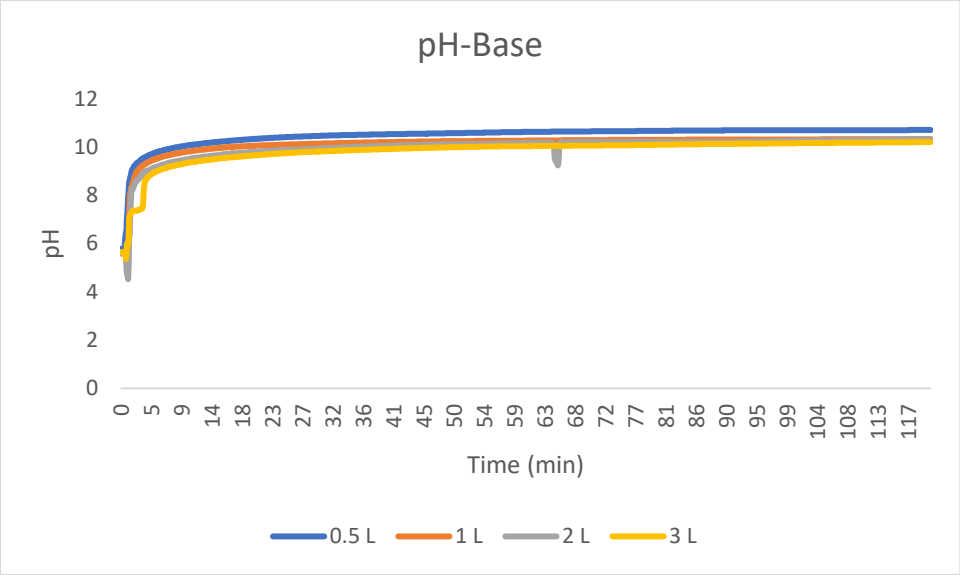


*Figure D.2. 3 Average pH of Base over time for varied base volumes*

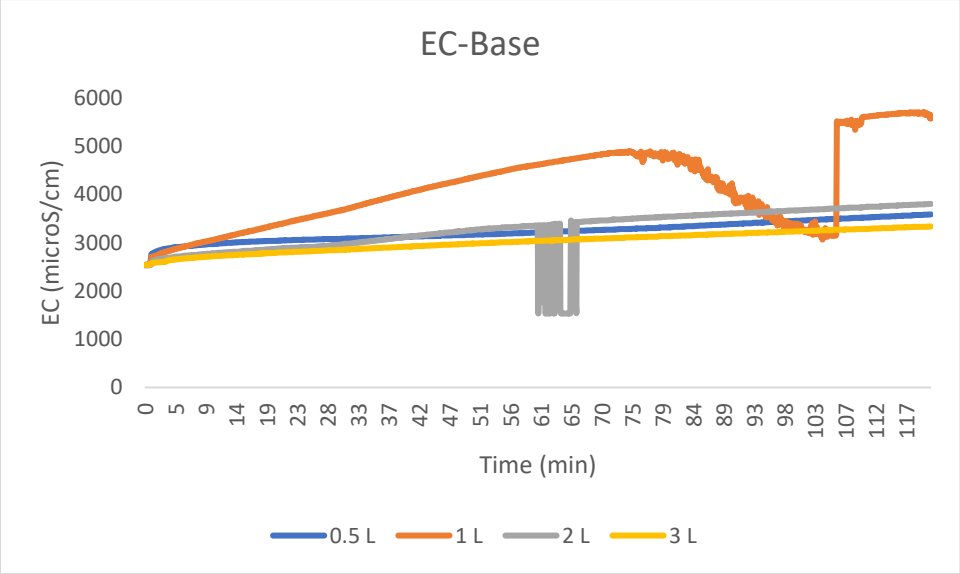


*Figure D.2. 4 Average electrical conductivity (µS/cm) of Base over time for varied base volumes*

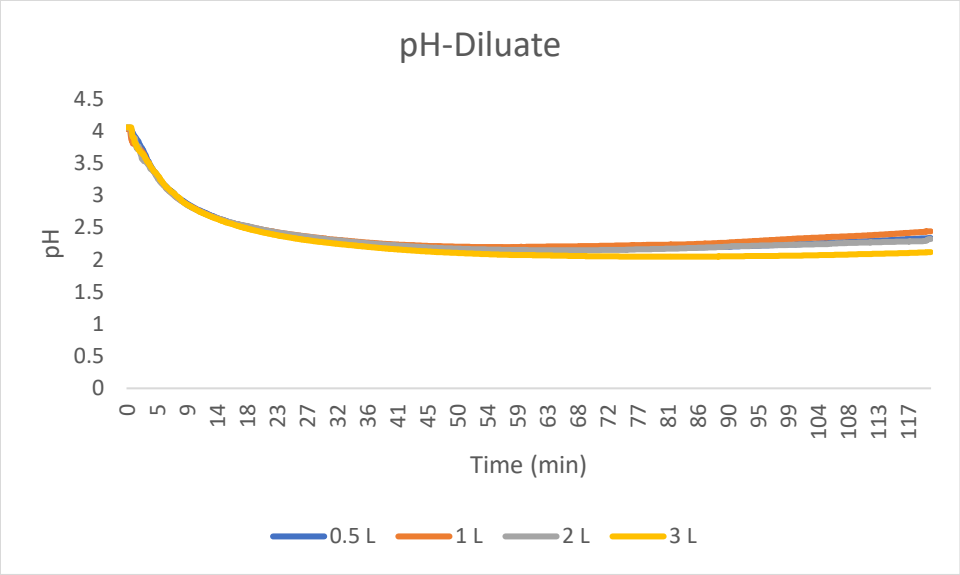


*Figure D.2. 5 Average pH of Diluate over time for varied base volumes*

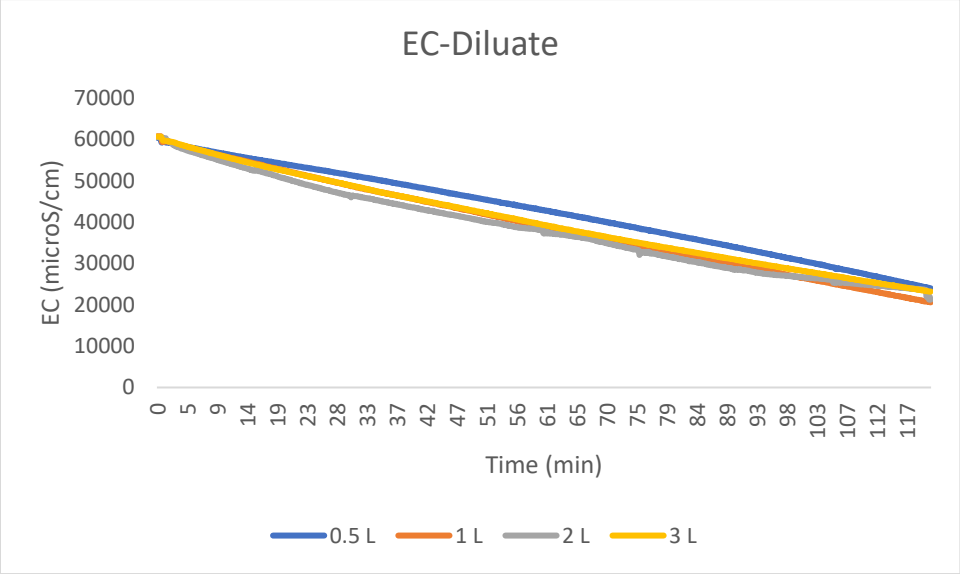


*Figure D.2. 6 Average electrical conductivity (µS/cm) of Diluate over time for varied base volumes*

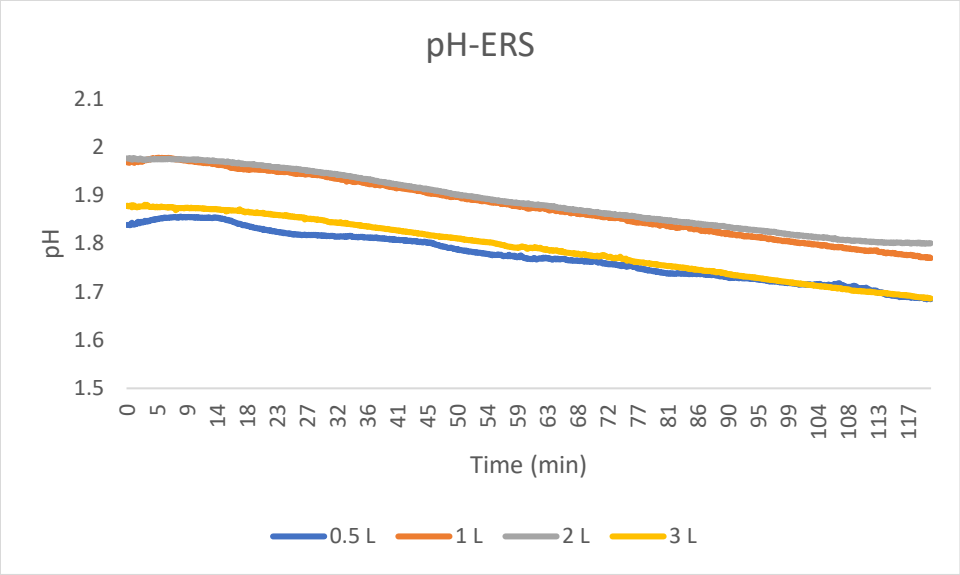


*Figure D.2. 7 Average pH of ERS over time for varied base volumes*

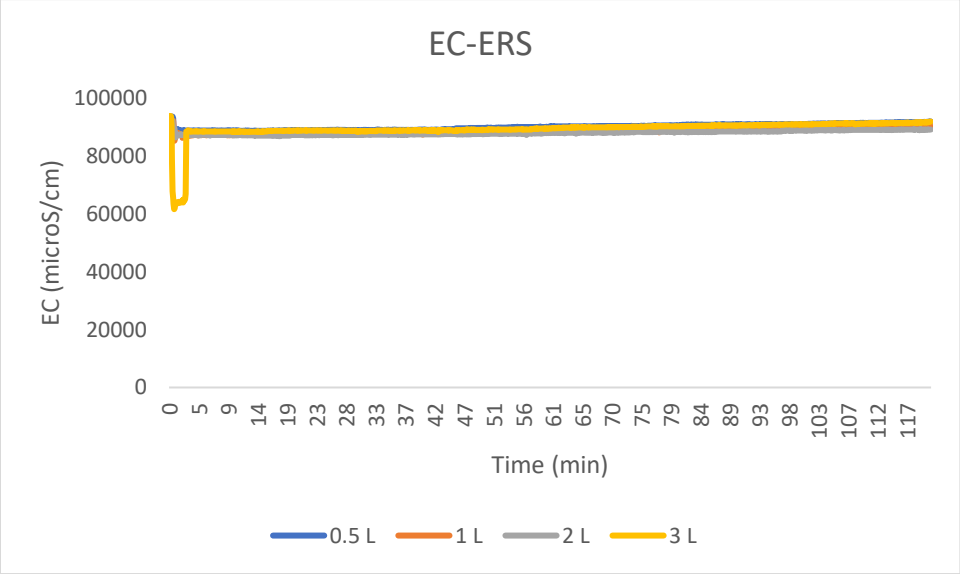


*Figure D.2. 8 Average electrical conductivity (µS/cm) of ERS over time for varied base volumes*

## E. Different BPMED Cell Configuration

### E.1 $NH_4^+$ concentration over time

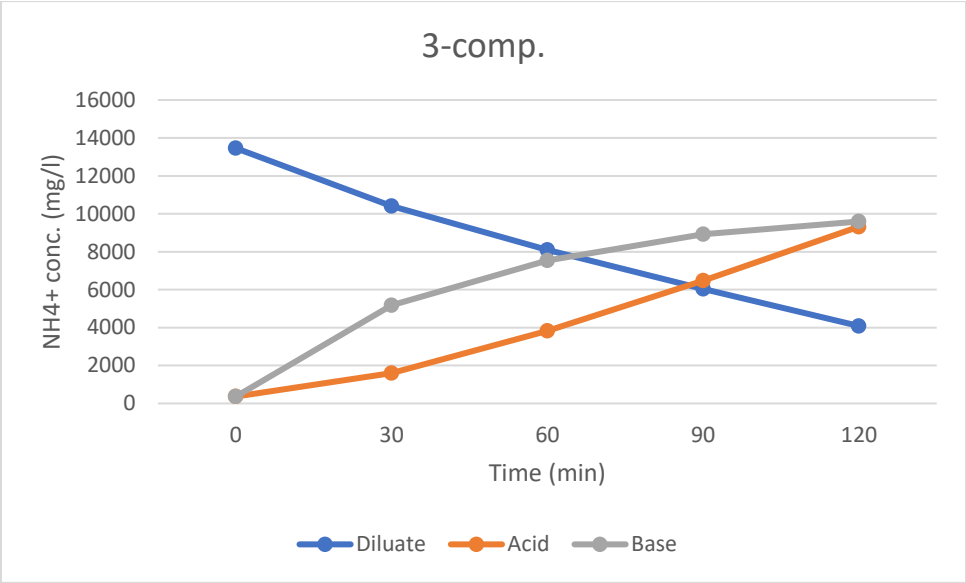


*Figure E.1. 1 3-compartment BPMED cell: Average $NH_4^+$ mass distribution over an experimental time of 120 minutes.*

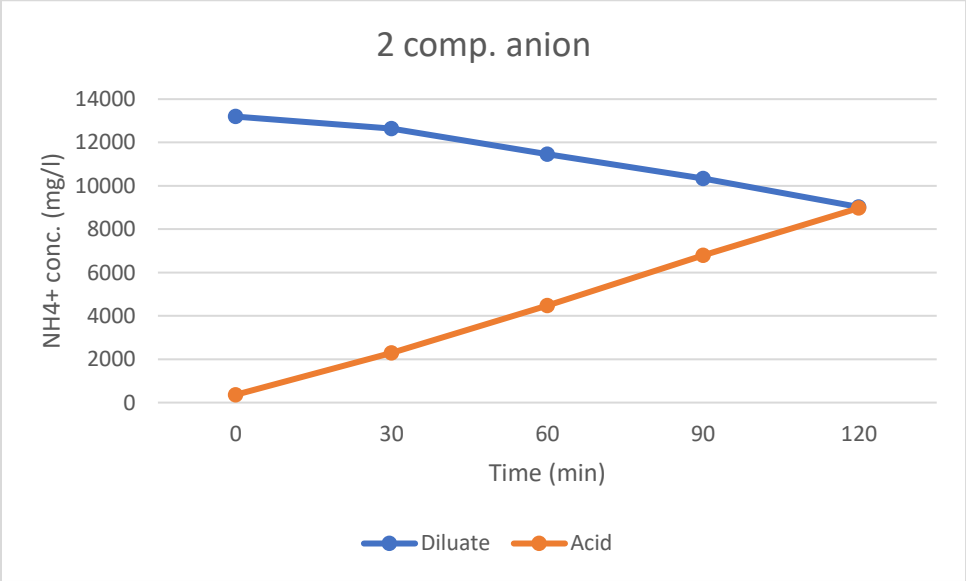


*Figure E.1. 2 2-compartment anion cell: Average $NH_4^+$ mass distribution over an experimental time of 120 minutes.*

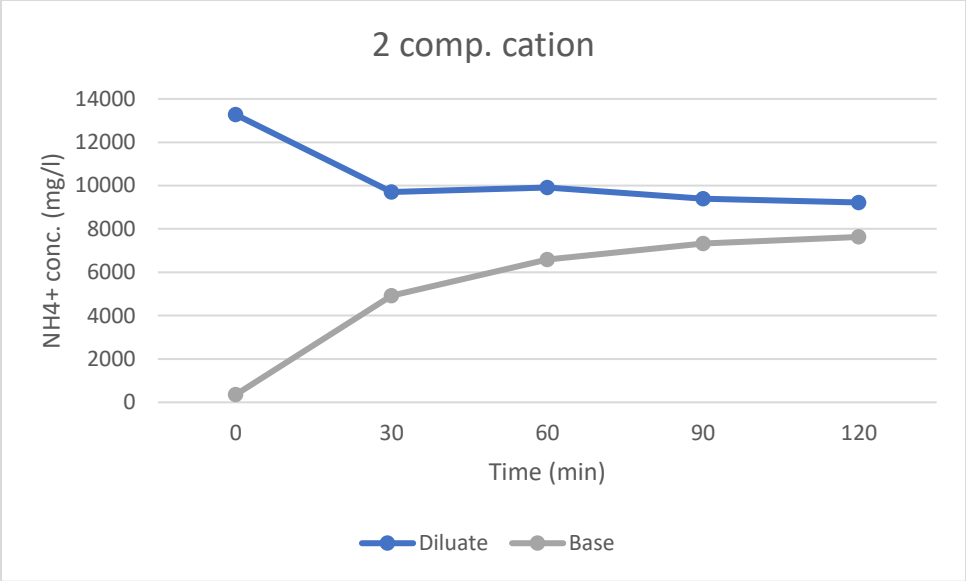


*Figure E.1. 3 2-compartment cation cell: Average $NH_4^+$ mass distribution over an experimental time of 120 minutes.*

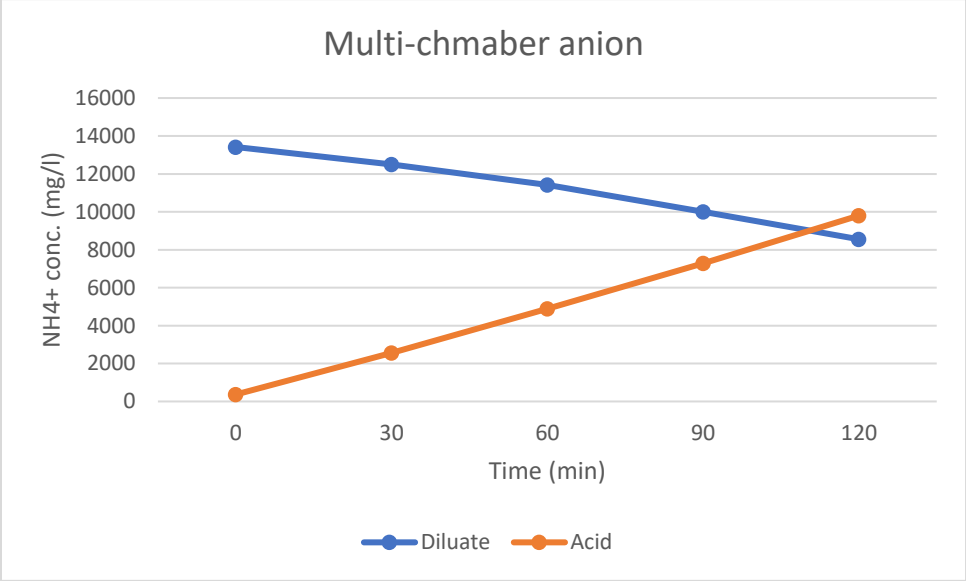


*Figure E.1. 4 Multi-chamber anion cell: Average $NH_4^+$ mass distribution over an experimental time of 120 minutes*

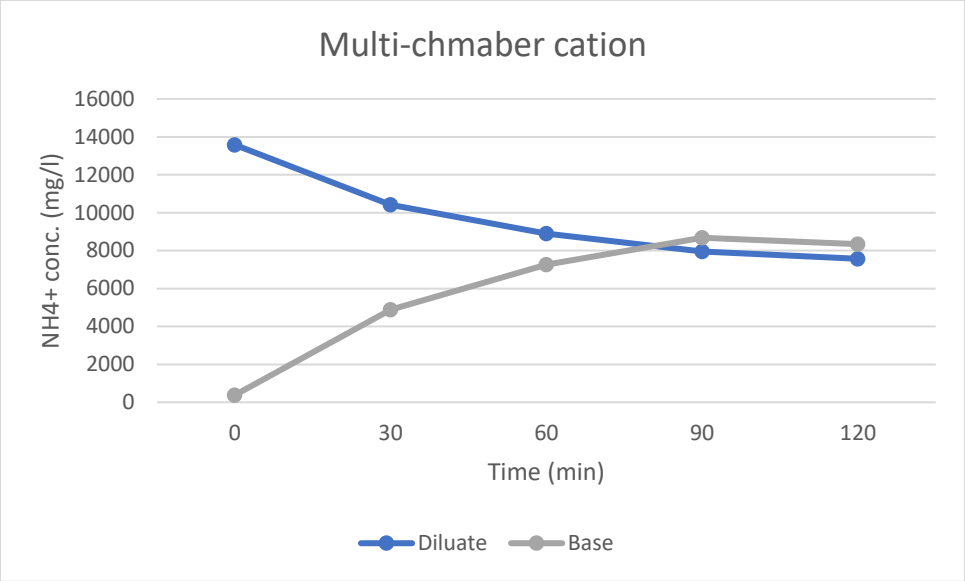


*Figure E.1. 5 Multi-chamber cation cell: Average $NH_4^+$ mass distribution over an experimental time of 120 minutes*

## E.2 pH and EC graphs over time

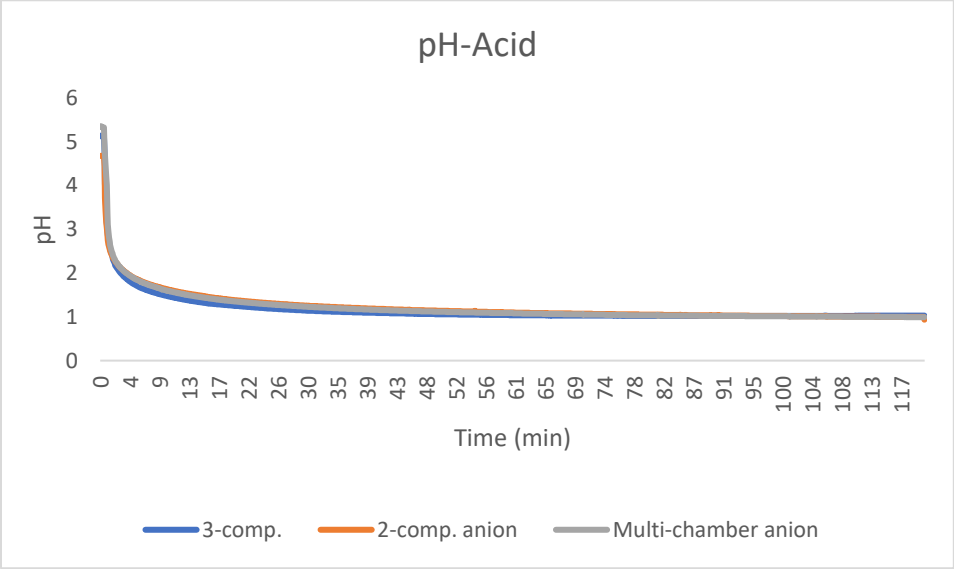


*Figure E.2. 1 Average pH of Acid over time for different BPMED cell configurations*

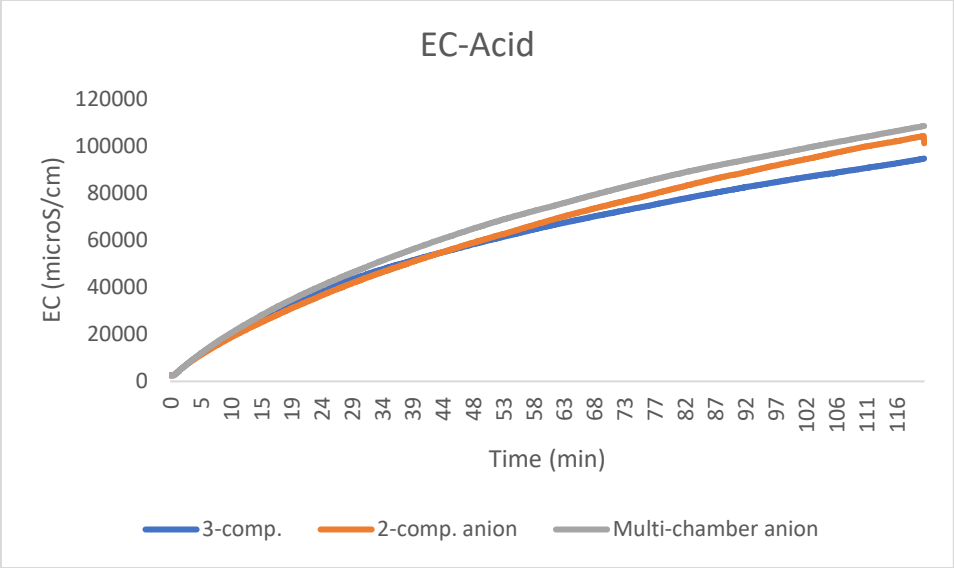


*Figure E.2. 2 Average electrical conductivity (µS/cm) of Acid over time for different BPMED cell configurations*

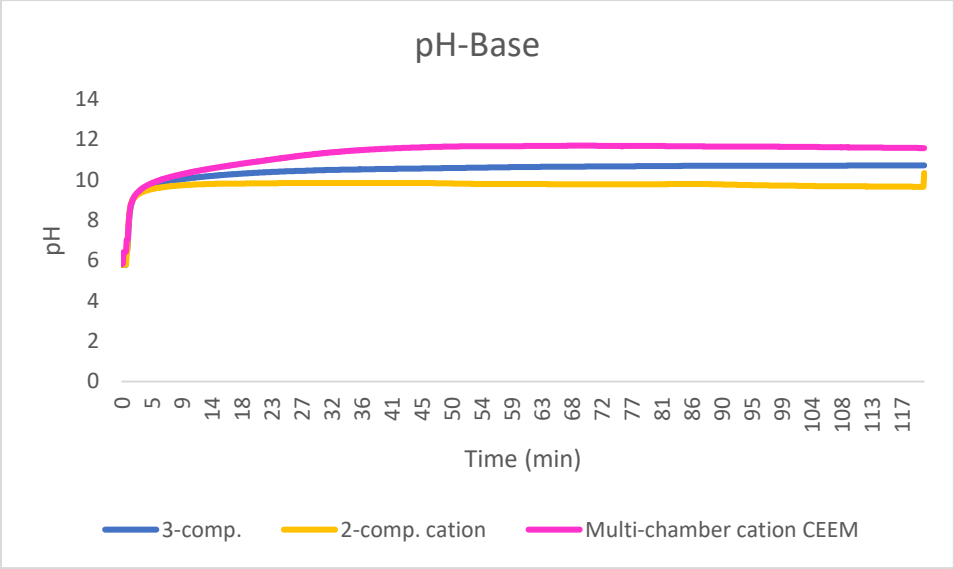


*Figure E.2. 3 Average pH of Base over time for different BPMED cell configurations*

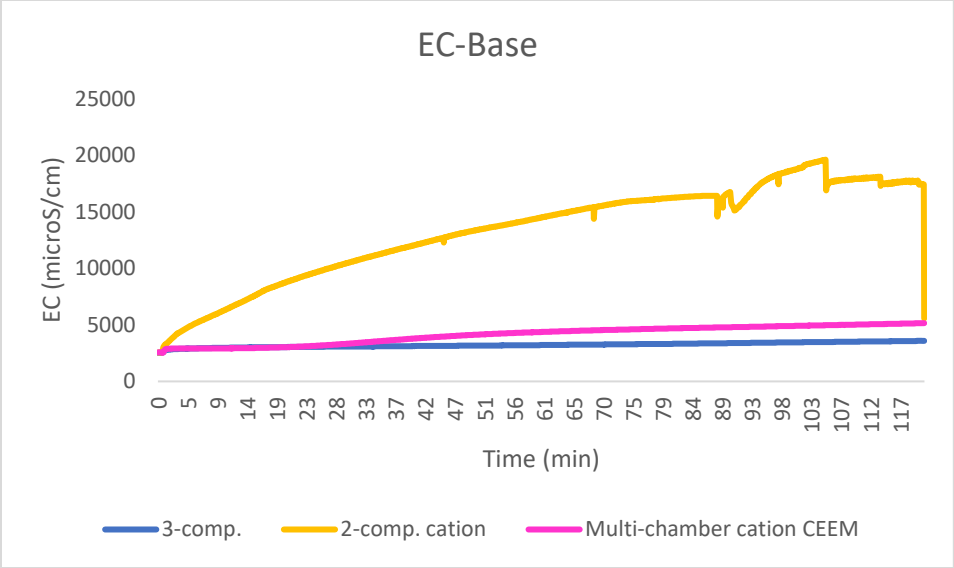


*Figure E.2. 4 Average electrical conductivity (µS/cm) of Base over time for different BPMED cell configurations*

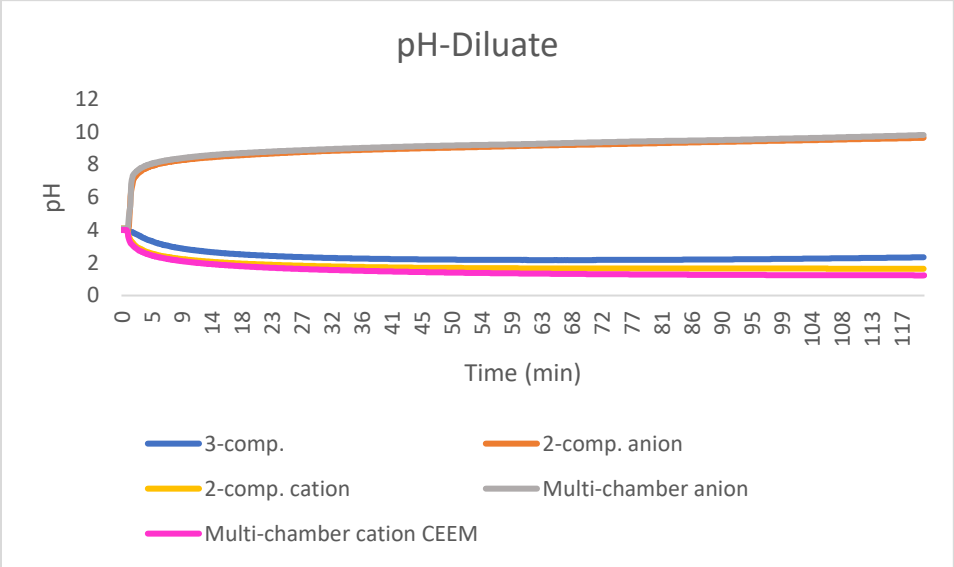


*Figure E.2. 5 Average pH of Diluate over time for different BPMED cell configurations*

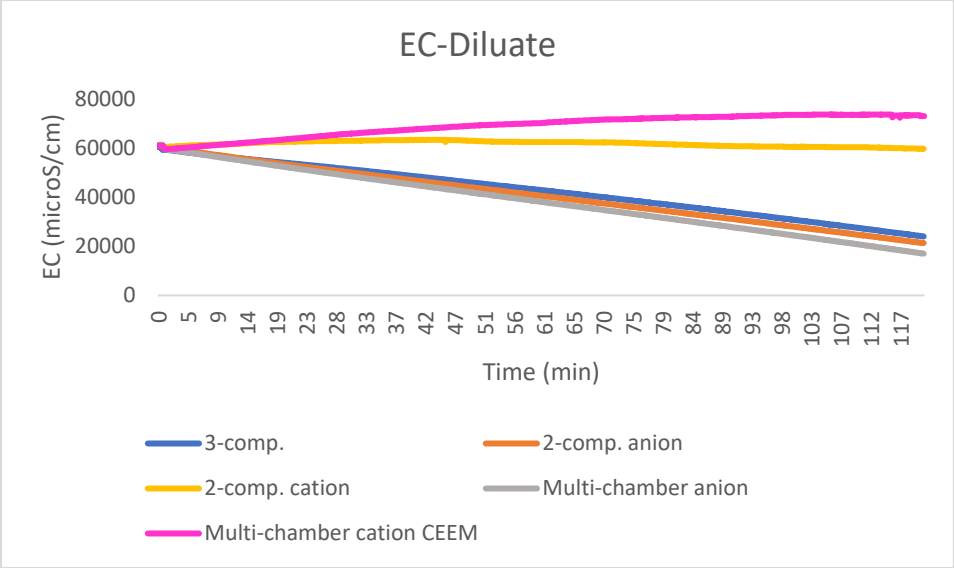


*Figure E.2. 6 Average electrical conductivity (µS/cm) of Diluate over time for different BPMED cell configurations*

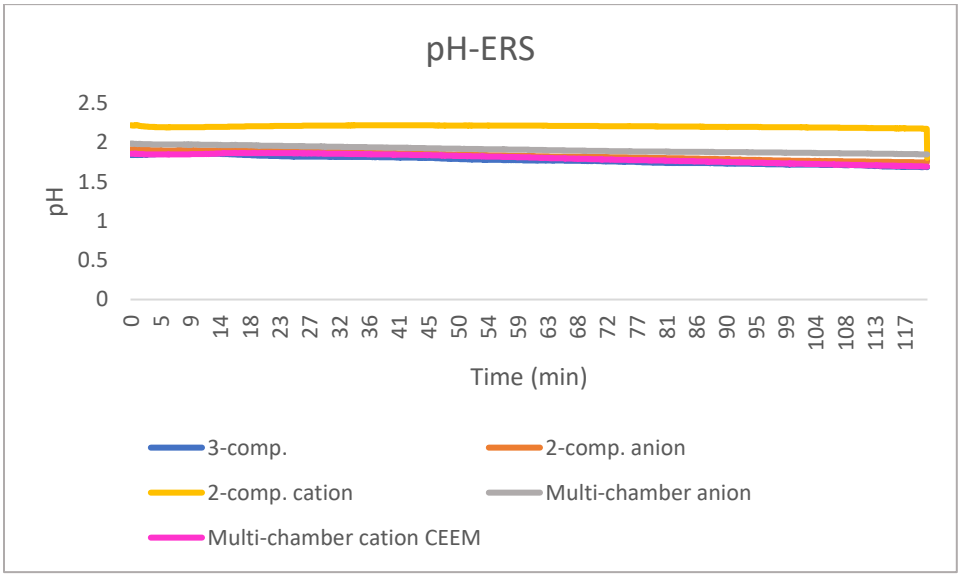


*Figure E.2. 7 Average pH of ERS over time for different BPMED cell configurations*

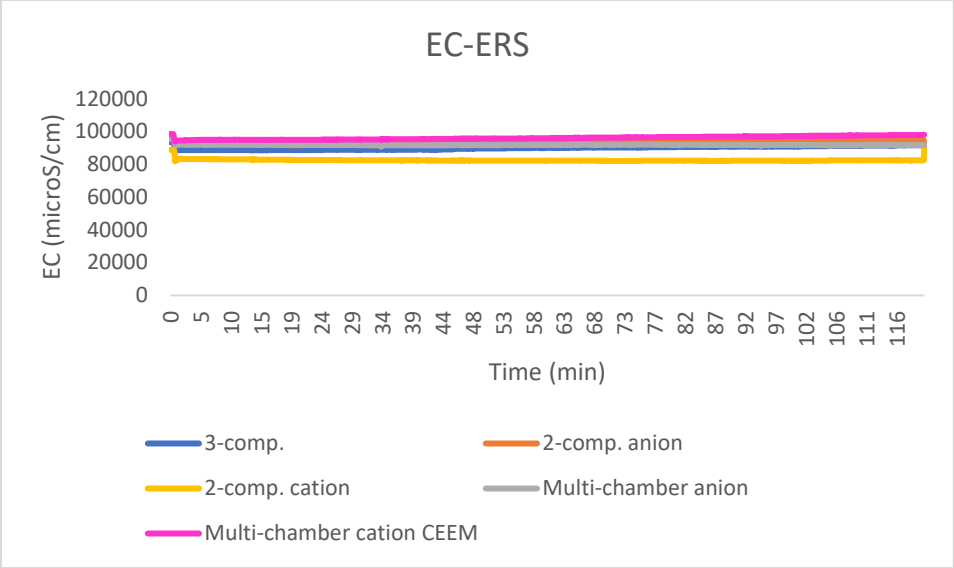


*Figure E.2. 8 Average electrical conductivity (µS/cm) of ERS over time for different BPMED cell configurations*

## E.3 Purity of ammonium in the base

$$P_{NH4+} = \frac{C_{b,NH4+}(t)}{C_{b,NH4+}(t) + C_{b,SO4-}(t)} . 100\%$$

Here, $P_{NH4+}$ = Purity of ammonium in the base (in %)

$C_{b,NH4+}$ (t) = the concentration of ammonium in the base solution at time t=120 mins (in mol/L)

$C_{b,SO4-}$ (t) = the concentration of sulfate in the base solution at time t=120 mins (in mol/L)

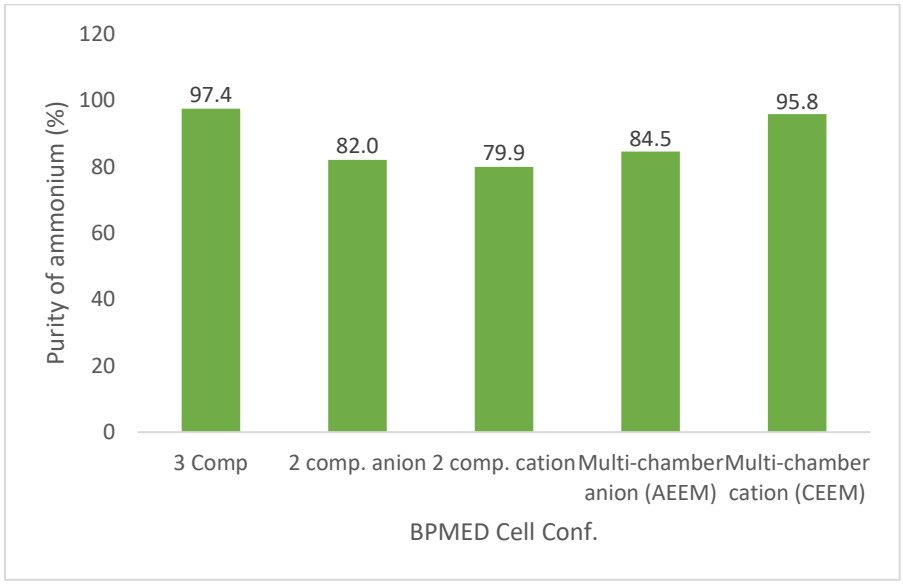


*Figure E.3. 1 Average purity of ammonium in the base for different BPMED cell configurations (%)*

## F. Feed Volume

### F.1 $NH_4^+$ concentration over time

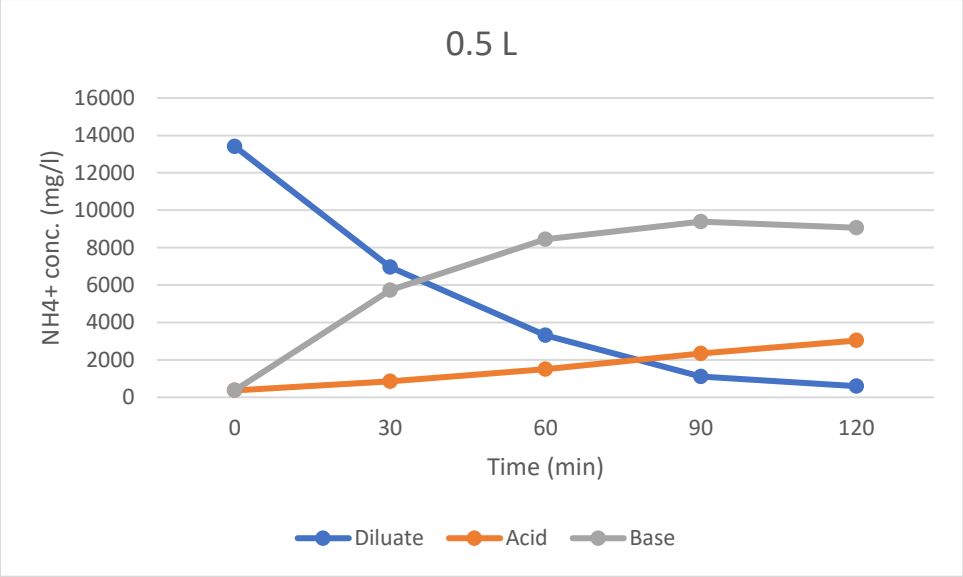


*Figure F.1. 1 0.5 L Feed volume: Average $NH_4^+$ mass distribution over an experimental time of 120 minutes.*

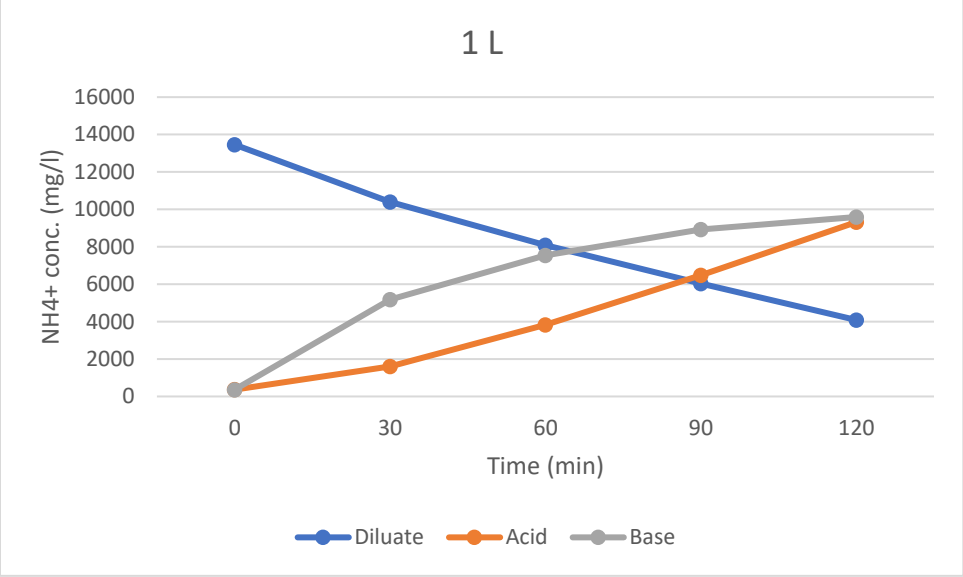


*Figure F.1. 2 1 L Feed volume: Average $NH_4^+$ mass distribution over an experimental time of 120 minutes.*

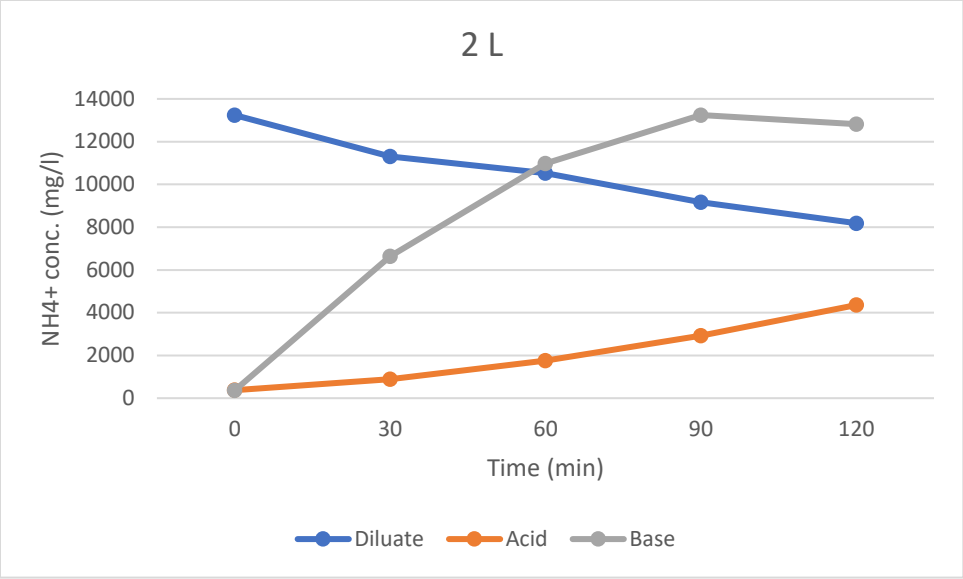


*Figure F.1. 3 2 L Feed volume: Average $NH_4^+$ mass distribution over an experimental time of 120 minutes.*

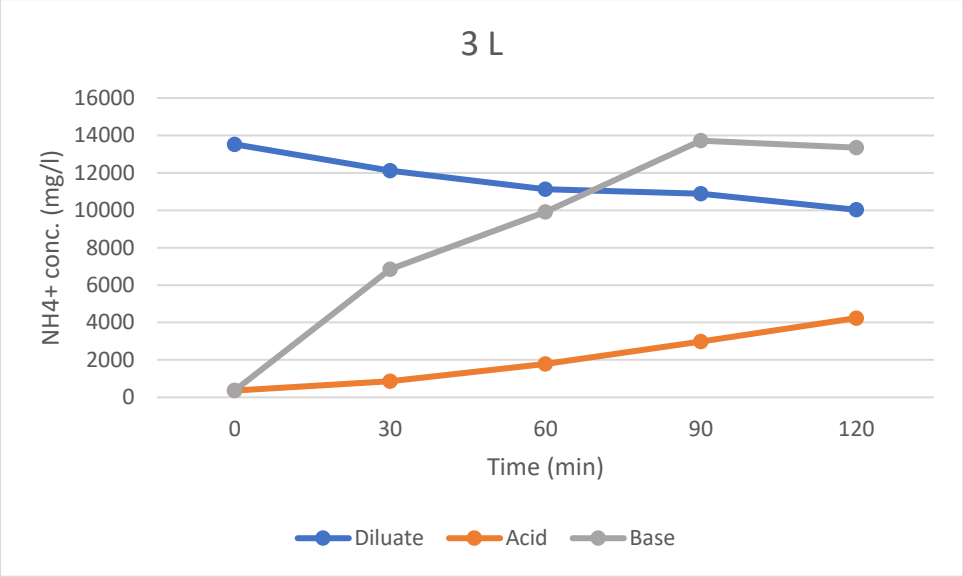


*Figure F.1. 4 3 L Feed volume: Average $NH_4^+$ mass distribution over an experimental time of 120 minutes.*

## F.2 pH and EC graphs over time

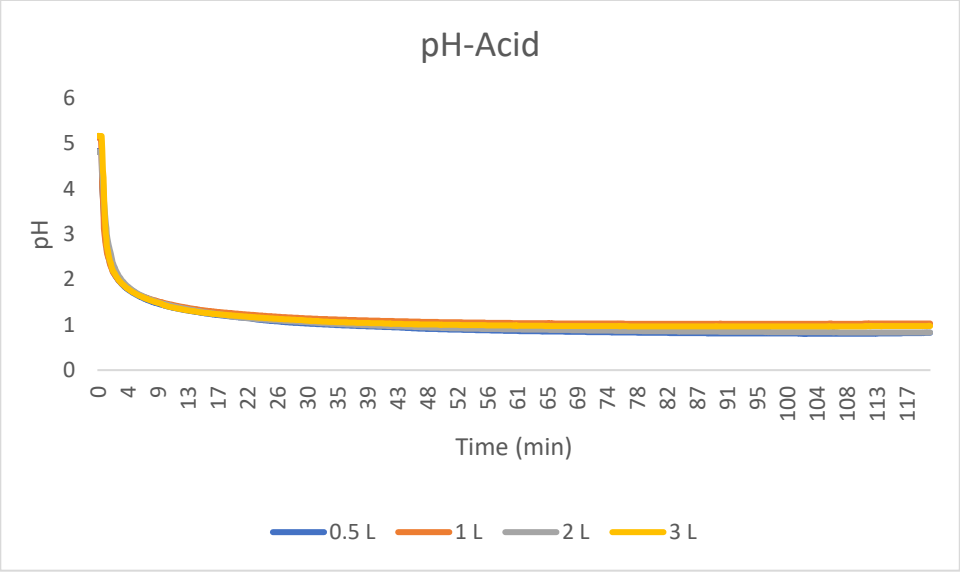


*Figure F.2. 1 Average pH of Acid over time for varied feed volumes*

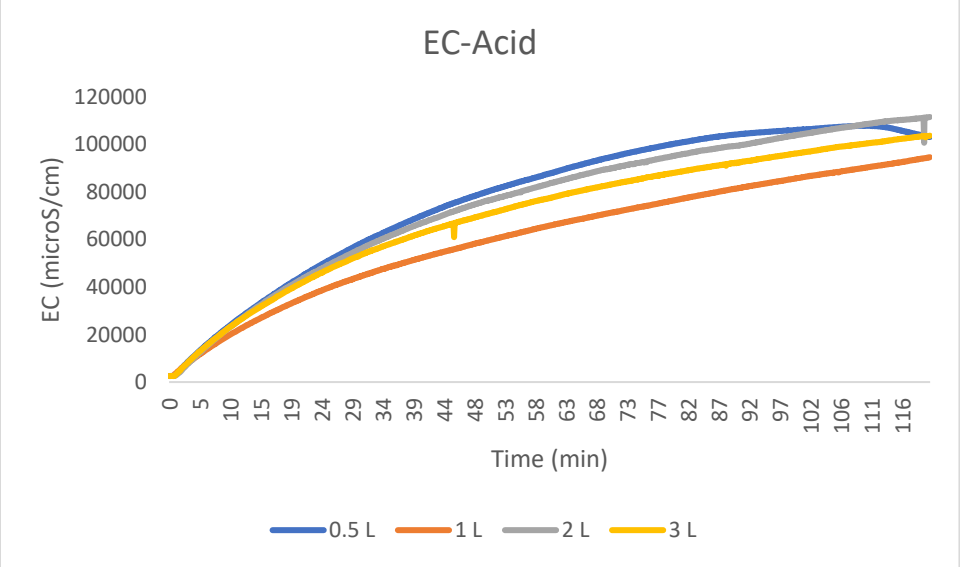


*Figure F.2. 2 Average electrical conductivity (µS/cm) of Acid over time for varied feed volumes*

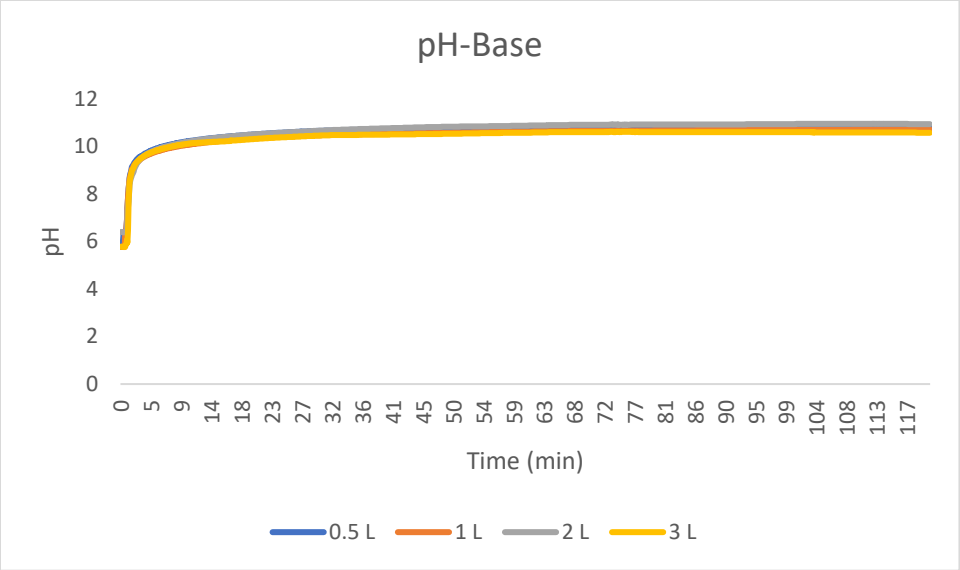


*Figure F.2. 3 Average pH of Base over time for varied feed volumes*

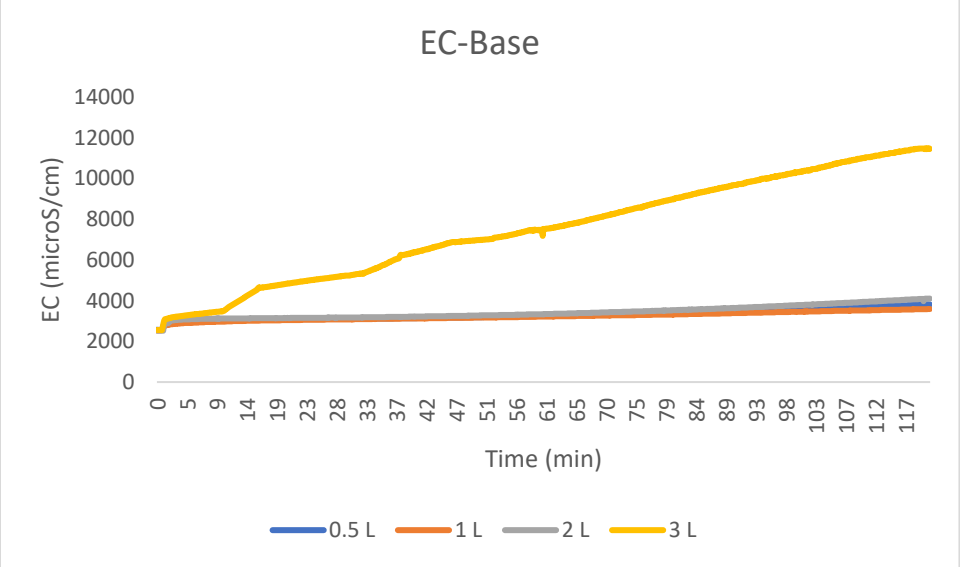


*Figure F.2. 4 Average electrical conductivity (µS/cm) of Base over time for varied feed volumes*

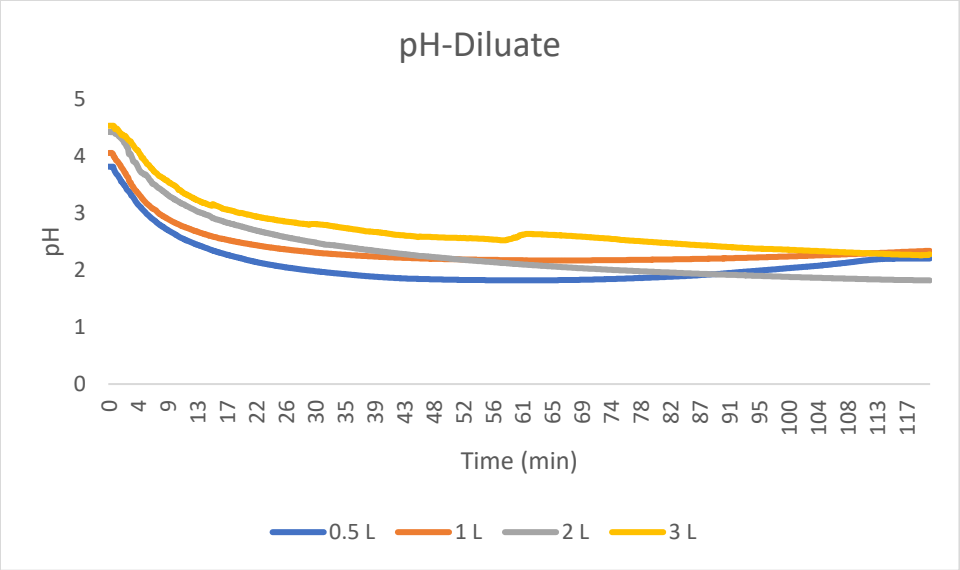


*Figure F.2. 5 Average pH of Diluate over time for varied feed volumes*

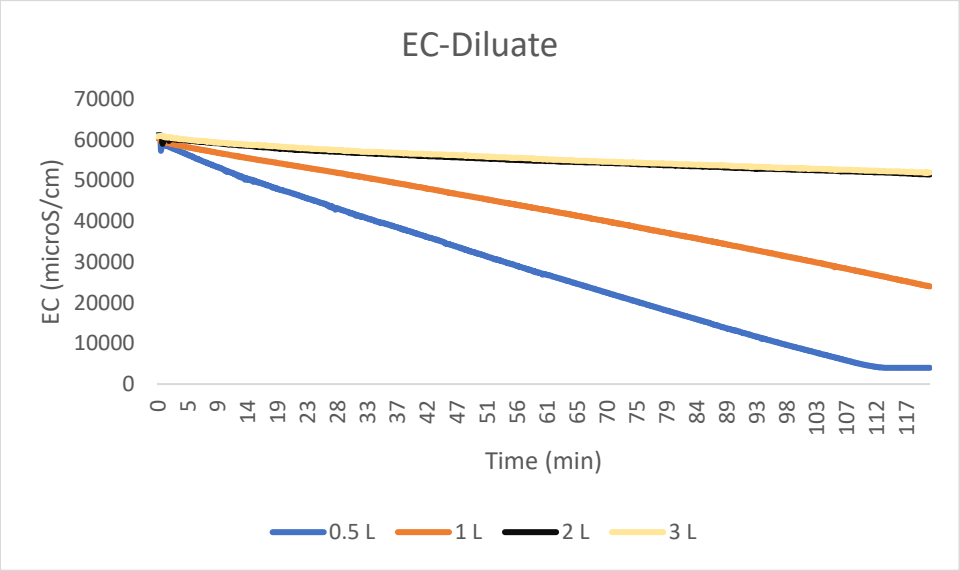


*Figure F.2. 6 Average electrical conductivity (µS/cm) of Diluate over time for varied feed volumes*

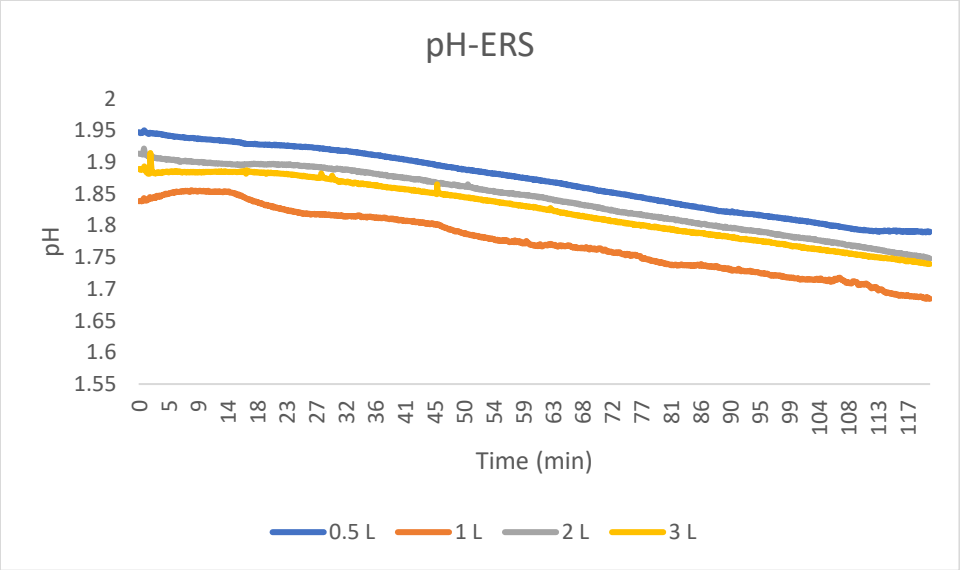


*Figure F.2. 7 Average pH of ERS over time for varied feed volumes*

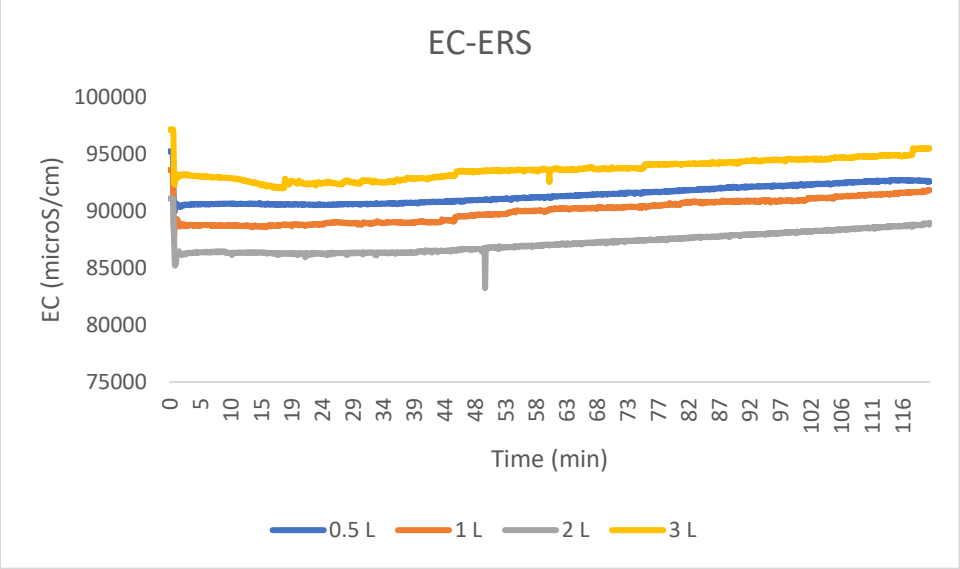


*Figure F.2. 8 Average electrical conductivity (µS/cm) of ERS over time for varied feed volumes*

## G. Optimum Experiment

### G.1 $NH_4^+$ concentration over time

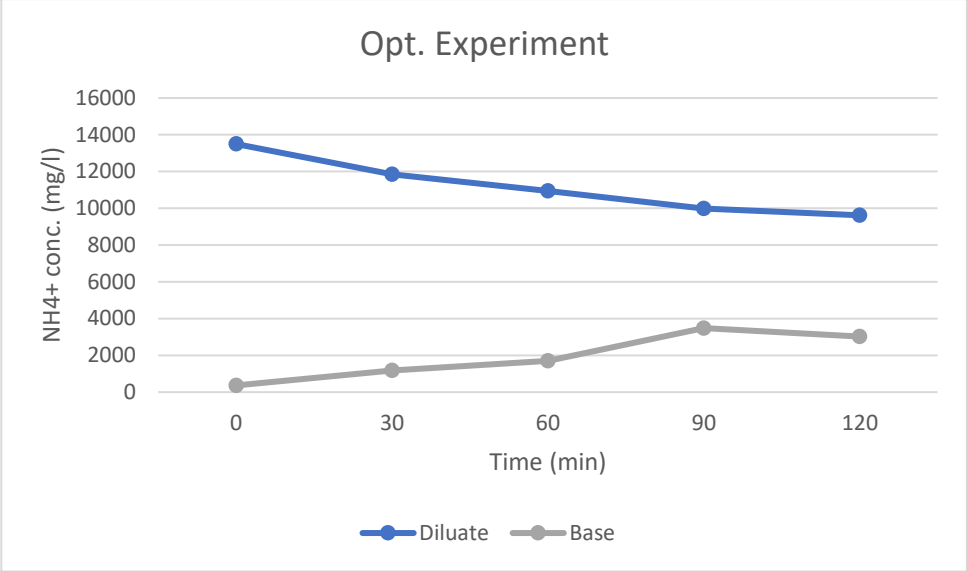


*Figure G. 1 Optimum Experiment: Average $NH_4^+$ mass distribution over an experimental time of 120 minutes.*

### G.2 pH and EC graphs over time

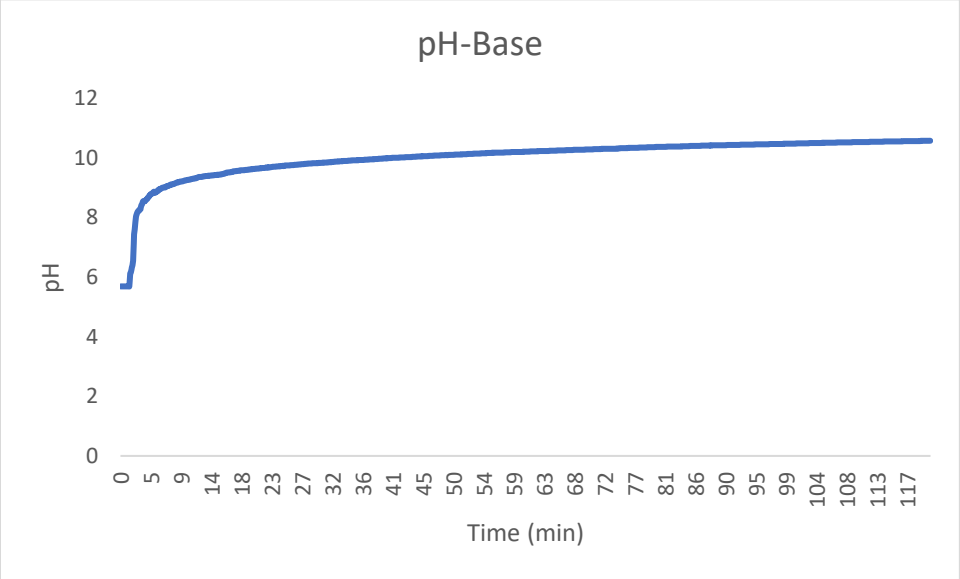


*Figure G.2. 1 Average pH of Base over time for optimum experiment*

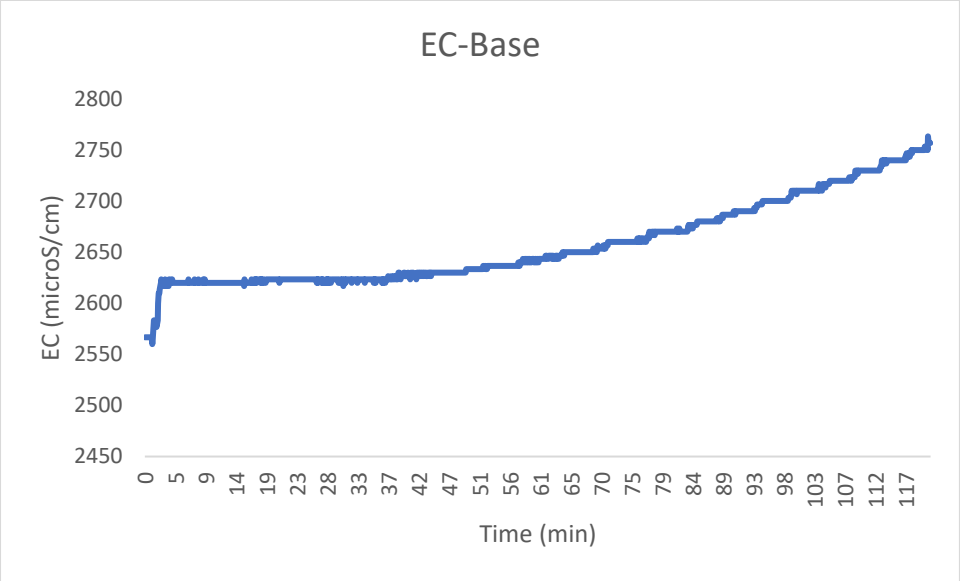


*Figure G.2. 2 Average electrical conductivity (µS/cm) of Base over time for optimum experiment*

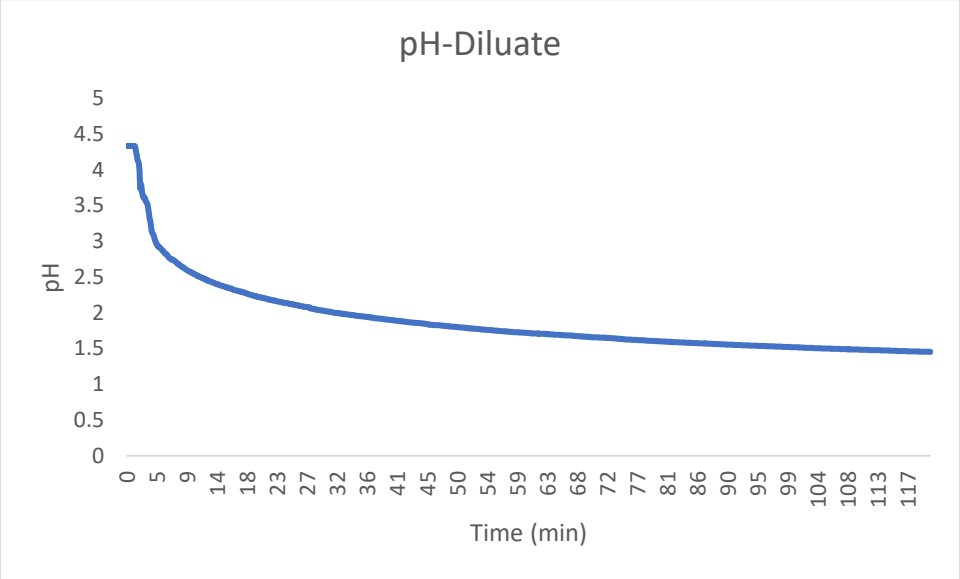


*Figure G.2. 3 Average pH of Diluate over time for optimum experiment*

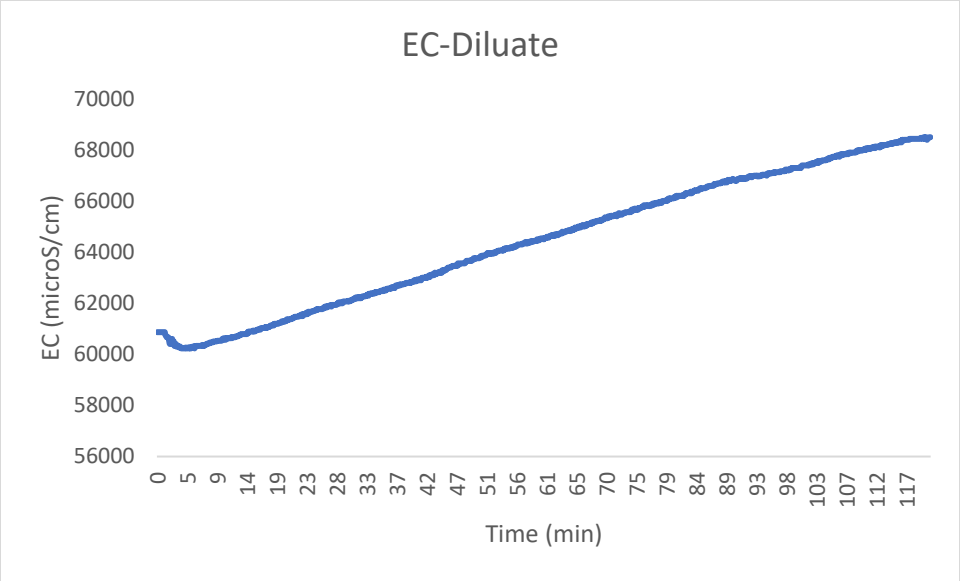


*Figure G.2. 4 Average electrical conductivity (µS/cm) of Diluate over time for optimum experiment*

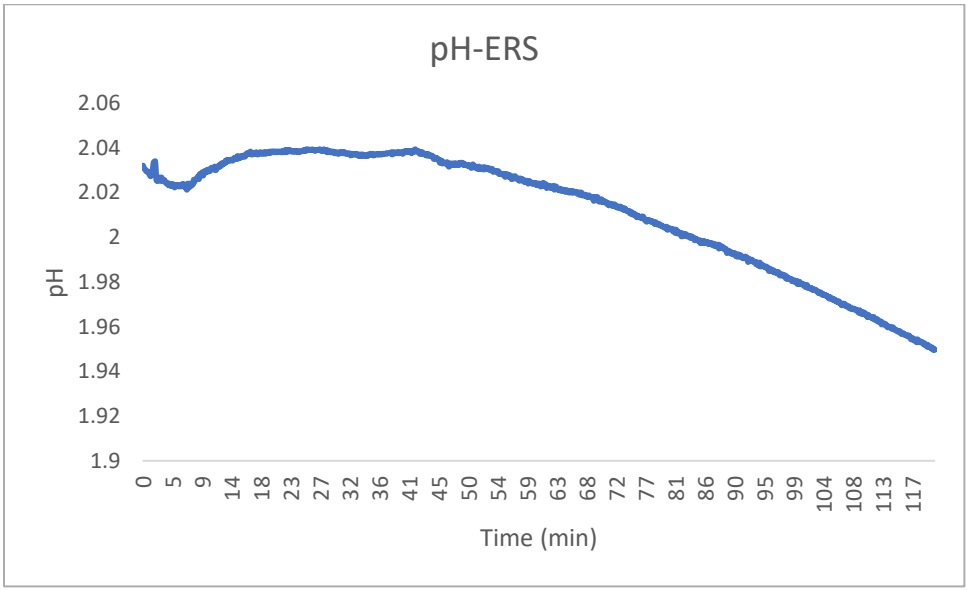


*Figure G.2. 5 Average pH of ERS over time for optimum experiment*

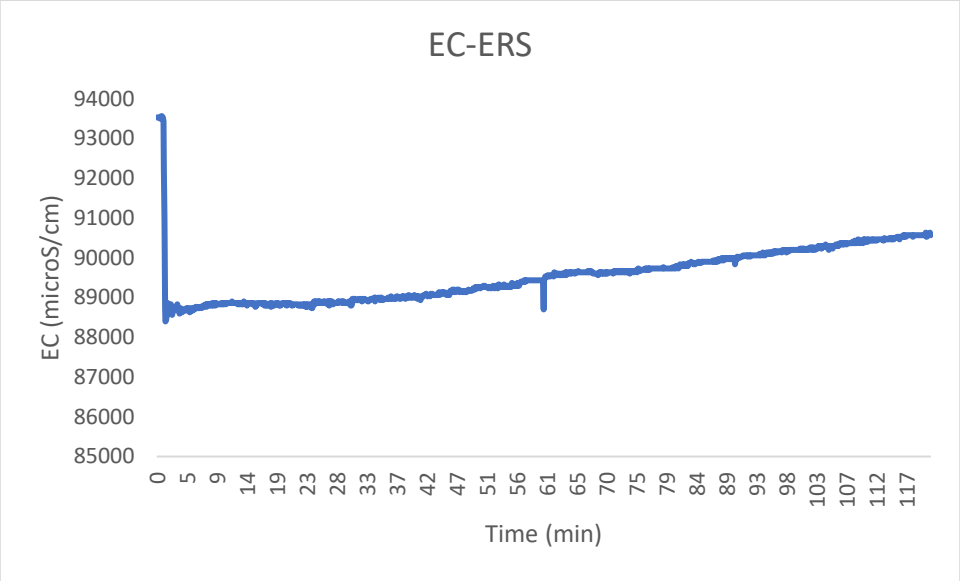


*Figure G.2. 6 Average electrical conductivity (µS/cm) of ERS over time for optimum experiment*